

SEMMELWEIS EGYETEM
DOKTORI ISKOLA

Ph.D. értekezések

2819.

PÁZMÁNY RITA

Celluláris és molekuláris biofizika
című program

Programvezető: Dr. Kellermayer Miklós, egyetemi tanár
Témavezető: Dr. Jedlovszky-Hajdú Angéla, egyetemi docens

POROUS POLY(AMINO ACID) BASED ELECTROSPUN FIBROUS SCAFFOLDS FOR TISSUE ENGINEERING

Ph.D. thesis

Pázmány Rita

born Rita Varga

Doctoral School of Theoretical and Translational Medicine
Semmelweis University



Supervisor: Angéla Jedlovszky-Hajdú Ph.D.

Official reviewers: Adrienn Kazsoki Ph.D.
Ferenc Ender Ph.D.

Head of the Complex Examination Committee: Alán Alpár, MD, D.Sc.

Members of the Complex Examination Committee: László Cervenák, Ph.D.
Mihály Kovács, D.Sc.

Budapest
2022

Table of Contents

List of Abbreviations	5
1 Introduction	6
1.1 Clinical need for tissue engineering.....	6
1.2 Short story of tissue engineering	7
1.3 Strategies and approaches in tissue engineering.....	10
1.4. Extracellular matrix (ECM), and ECM analogue scaffolds.....	12
1.4 Requirements for tissue engineering scaffolds	13
1.5 Scaffold materials	15
1.6 Scaffolding techniques.....	17
1.6.1 Electrospinning	18
1.7 Storage conditions and long-term preservation of scaffolds.....	22
2 Objectives	23
3 Materials and Methods [RP1][103], [RP2][134]	24
3.1 List of materials	24
3.2 Synthesis of Polysuccinimide (PSI).....	24
3.3 Fabrication of PSI nanofibers by electrospinning.....	25
3.4 Post-electrospinning processing.....	25
3.4.1 Compressing.....	25
3.4.2 Crosslinking	26
3.4.3 Hydrolysis	26
3.4.4 Ultrasonication	27
3.4.5 Freeze-drying	27
3.5 Attenuated Total Reflectance Fourier Transform Infrared (ATR-FTIR) Spectroscopy	28

3.6	Scanning Electron Microscopy (SEM)	29
3.7	Mechanical characterization	29
3.8	Degradation.....	30
3.9	Cell studies.....	30
3.9.1	Cell culture.....	30
3.9.2	Cell viability assay on the surface of scaffolds (2D samples)	30
3.9.3	Indirect cytotoxicity assay (3D samples).....	31
3.9.4	Multiphoton microscopy	32
4	Results.....	34
4.1	Poly(amino acid) based fibrous scaffolds with tuneable <i>in vivo</i> biodegradation (2D) [RP1] [103]	34
4.1.1	Cell viability on the surface of the compressed scaffolds.....	34
4.2	Ultrasound induced, easy-to-store porous poly(amino acid) based electrospun scaffolds (3D) [RP2] [134].....	36
4.2.1	Preparation of scaffolds and the effect of ultrasonication.....	36
4.2.2	Attenuated Total Reflectance Fourier Transform Infrared (ATR-FTIR) Spectroscopy.....	38
4.2.3	Scanning electron microscopy (SEM)	39
4.2.4	Mechanical analysis and degradation	40
4.2.5	Cell studies.....	44
5	Discussion	47
5.1	Poly(amino acid) based fibrous scaffolds with tuneable <i>in vivo</i> biodegradation [RP1] [103].....	47
5.1.1	Cell viability on the surface of the compressed scaffolds.....	47
5.2	Ultrasound induced, easy-to-store porous poly(amino acid) based electrospun scaffolds [RP2] [134]	49
5.2.1	Characterization of ultrasonicated samples.....	49

5.2.2	Mechanical analysis and degradation	51
5.2.3	Cell studies.....	53
6	Conclusions	54
7	Summary	56
8	References.....	57
9	Bibliography of the candidate’s publications – related to the thesis	77
10	Bibliography of the candidate’s publications – not related to the thesis.....	78
11	Acknowledgements	79
12	Statement of Originality.....	80

List of Abbreviations

2D	Two-dimensional
3D	Three-dimensional
ATR-FTIR	Attenuated Total Reflectance Fourier Transform Infrared Spectroscopy
CHAp	Carbonated hydroxyapatite
DAB	1,4-Diaminobutane
ECM	Extracellular matrix
FDA	The United States Food and Drug Administration
MEM	Minimal Essential Media
PASP	Poly(aspartic acid)
PASPDAB	Poly(aspartic acid) crosslinked with 1,4-Diaminobutane
PCL	Polycaprolactone
PGA	Poly(glycolic acid)
PLA	Poly(lactic acid)
PLGA	Poly(lactic-co-glycolic acid)
PLLA	Poly(L-lactic acid)
PSI	Polysuccinimide
PSIDAB	Polysuccinimide crosslinked with 1,4-Diaminobutane
SEM	Scanning Electron Microscopy
US	Ultrasonication
UV	Ultraviolet radiation

1 Introduction

1.1 Clinical need for tissue engineering

The past four decades have seen the fast-flowing development of tissue engineering, in which research and clinical application focus on treatments to initiate the regeneration, replacement, or repair of aged, diseased, or injured cells or tissues [1]. This area is an interdisciplinary field of research that employs the knowledge of engineers, scientists, and physicians to create biological substitutes that can mimic tissues [2].

The first treatments in ancient history were based on implanting non-living materials such as gold and sea shells to mimic the function of a missing tooth [3]. Although these solutions improved people's quality of life, the regeneration of the tissue was limited, because the implants were not biologically active, and their structure was far from that of the original living tissue. The development of medicine enabled the possibility of utilizing cells in therapy by replacing tissues, or even entire organs via allogeneic transplantation (from different individuals of the same species) (Figure 1). Transplant medicine made rapid progress, become a widely practiced method, and has had an undeniable impact on humanity. However, the main limitation of its application is the limited number of available suitable donated organs. This and the risk of organ rejection brought engineered tissues into the focus [4],[5],[6].

The first engineered tissue-based therapies were applied for skin replacement, because of their relatively low risk, simple structure, and the fact that this tissue does not require extensive vascularization. The gold standard for deep cutaneous wounds is autologous split-thickness skin grafts, using donor sites from the patient remaining to harvest skin graft material (autologous transplantation – from the same individual) [7]. To cover larger areas of the wound, it is possible to create a uniformly perforated skin graft mesh. However, this method may result in limited mobility due to graft construction and a crocodile skin-like appearance of the scar [8] (Figure 1).

As an alternative to the shortage of donors in transplantation, xenotransplantation (from different species) is also investigated (Figure 1). On January 7, 2022, the first person who received a heart transplant from a genetically modified pig survived the operation and extended his life by two months [9]. The organ used was from a pig that

had ten genetic modifications made using the CRISPR-Cas9 genome editing method to make it less likely to be attacked by the human immune system.

The use of artificial organs or parts of organs, such as mechanical heart valves (prostheses), is durable and often lasts a lifetime; however, due to the tendency of blood clot formation, it requires lifelong take of blood thinners [10] (Figure 1).

The aim of tissue engineering is to develop a native-like functional tissue, based on the cells of the patient, that can replace the failing organ and can last a lifetime [11]. This strategy is believed to overcome the mentioned limitations.

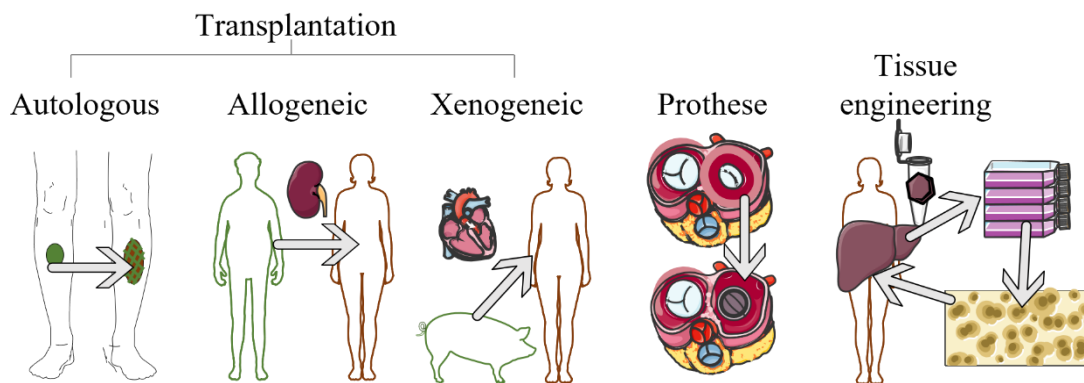


Figure 1 The figure depicts some of the numerous strategies for replacing or regenerating injured, aged, or failing tissues or organs. Parts of the figure were drawn using pictures from Servier Medical Art.

The early success of tissue engineering regarding skin regeneration induced great enthusiasm and led to high expectations and unrealistic extrapolations about bedside and utilization. However, such methods turned out to be far more complicated when it came to their real-life application. Although there are numerous commercialized tissue-engineered medical products, they are not widely adopted in clinical practice. Significant challenges remain, but the optimism for potential solutions is very high. The dream of engineered tissues or even organs is to become a widely available therapy and to have a real and positive impact on people's lives.

1.2 Short story of tissue engineering

The history of the first tissue-engineered products began in different laboratories of Green [12], Bell [13], Yannas [14], and Vacanti [15] at different times, but all of them were crucial for the nowadays well-known tissue-engineering field. These research groups took various approaches and developed medical products out of skin and cartilage grafts [16]. Since then, a wide range of laboratory investigations, animal studies, and

clinical trials were conducted and demonstrated the fascinating opportunity of creating a new scaffold.

In 1975, Howard Green and James G. Rheinwald at Harvard Medical School described the technique of an *in vitro* protocol to culture keratinocytes of the skin epidermis, starting with single cells harvested from the patient [12]. In 1983, using small patches of skin removed from two (5 and 7 years old) burn victims who had suffered third-degree burns over 97 percent of their bodies, the laboratory-grown epidermal layer grafted onto their bodies by Dr. Nicholas O'Connor helped to save their lives [17]. Based on this technology, the first cell-based tissue-engineered product used in living cell therapy was commercialized as Epicel [18–20] (Figure 2).

The work of J. G. Vacanti and R. Langer – who defined “tissue engineering” in 1993 [1] - focused on the construction of artificial devices for culturing cartilage tissue [1]. Instead of the time-consuming copying of complex biological structures using natural substances, they used biocompatible synthetic matrices that had better supply, reproducibility, and lower costs. Employing polymer sciences, the research group was able to manipulate the chemical structure of the scaffold and earned desirable mechanical and biological properties [1],[15]. In 1996, C. Vacanti and his team created a scaffold from a synthetic nonwoven mesh of poly(glycolic acid) (PGA) and shaped it into the form of a human auricle. To create a cartilage structure, the implants were seeded with bovine chondrocytes and subcutaneously implanted in 10 athymic (immunodeficient) mice to culture. The “auriculosaurus”, also known as the earmouse induced considerable media attention and led to unrealistic extrapolations of tissue engineering [21] (Figure 2).

Creating tissue-engineered bladders is more complex and remodelling their functions is even more challenging. The main issue is having enough porosity to allow cell ingrowth while maintaining mechanical strength and a barrier function against urine, which is toxic to the surrounding tissues [22]. In 2006, Atala *et al.* were the first to successfully implant tissue-engineered autologous into seven patients, biodegradable bladder-shaped scaffolds made of collagen or a collagen-PGA composite [23] (Figure 2).

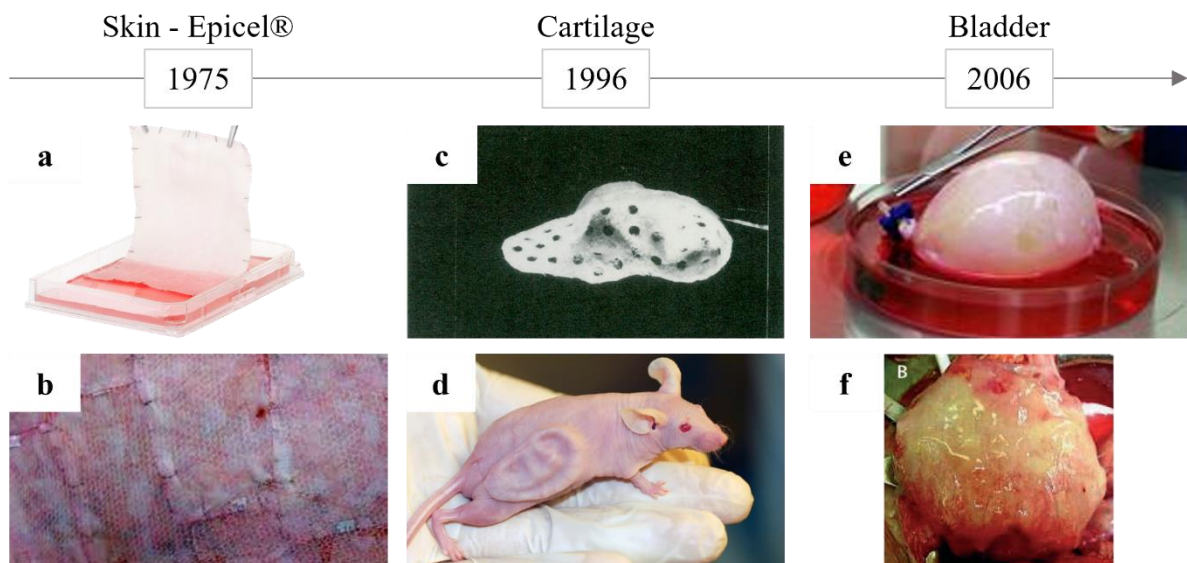


Figure 2 Historical milestones of tissue engineering: Skin grafts for regeneration of burned victims (a and b)[24]. First tissue-engineered auricle scaffold (c [21]), implanted under the skin of a mouse (d [25]). One of the first implanted tissue engineered products, a bladder (e [26]), and this engineered bladder is anastomosed to the native bladder with sutures (f [23]).

The tissue-engineered liver is one of the first attempts to create a fully functional organ to be transplanted, use as an extracorporeal device, or provide an *in vitro* model for drug testing [27]. Hepatic (liver) tissue engineering is based on seeding adult hepatocytes or stem cell-derived hepatocyte-like cells into a three-dimensional (3D) structure capable of ensuring their survival and maintaining their functional phenotype [28]. Constructs for liver regeneration went under many laboratory investigations, cell and animal studies, and also clinical trials, however, the translation the mainstream clinical application has yet to be successful [27].

Tissue engineering received widespread media publicity, and yielded high expectations, and unhelpful background noises as well. In 2000, Time magazine identified tissue engineer as “The Hottest Job” (the hottest career option) for the future, and it was predicted that body parts would be grown in Petri dishes [29],[30]. Due to the enormous time pressure from the media, the initial schemes for tissue engineering were oversimplified (regarding for example immune responses, or the need for vascular system), and the first medical products did not behave as originally intended [16]. In the last two decades, with the incorporation of advances in molecular and cellular biology and the tools of nanotechnology and engineering, several technologies have been

developed that may facilitate future breakthroughs [8]. Nevertheless, tissue-engineered medical products still have not reached mainstream bedside utilization [31],[32].

1.3 Strategies and approaches in tissue engineering

There are numerous strategies to improve the regeneration of tissues, restore its original function, and over the years, more and more approaches have been developed.

The most direct one is the utilization of cells as a therapeutic agent. In this case, autologous (from the same individual) or allogeneic (from different individual of the same species) cells are injected into, sprayed, or placed onto the damaged area. Possible cell types are undifferentiated stem cells, or tissue-specific differentiated cells. If there are not enough suitable cells left for autologous transplantation, stem cells allow the possibility of regenerating damaged areas. The stem cells can be implanted before their differentiation, or after *in vitro* manipulation. The utilization of aerosol vehicles for delivering epithelial cells already showed promising results, the sprayed cells were able to attach to and proliferate on the wound bed, and were active in esthetical curing of larger burns [33],[34],[35] (Figure 3a).

Another approach is to implant a biodegradable scaffold to the damaged area alone, and the cells in the surrounding area can migrate in and populate the scaffold (Figure 3b). The acellular methods can use decellularized extracellular matrix (ECM) of native tissues or premade porous scaffolds from natural or synthetic materials. The decellularized ECM could be an ideal material providing mechanical support and adhesion site for cells to adhere and proliferate. However, copying its complex chemical composition and structure would be prohibitively expensive and time-consuming. Another main challenge is the limited supply of autologous tissues, and the immune reaction to allogeneic donors. Therefore, an approach of using artificial polymeric scaffolds gained ground, as they can mimic the native tissue both chemically and structurally. In many cases, these scaffolds have proven to be successful, and they are readily available in large quantities [36],[37]. In an ideal case, after implantation the cells can colonize the scaffold, and synthesize new ECM and the scaffold undergoes degradation. However, finding the appropriate material for each kind of tissue with tuneable properties is a current challenge for scientists.

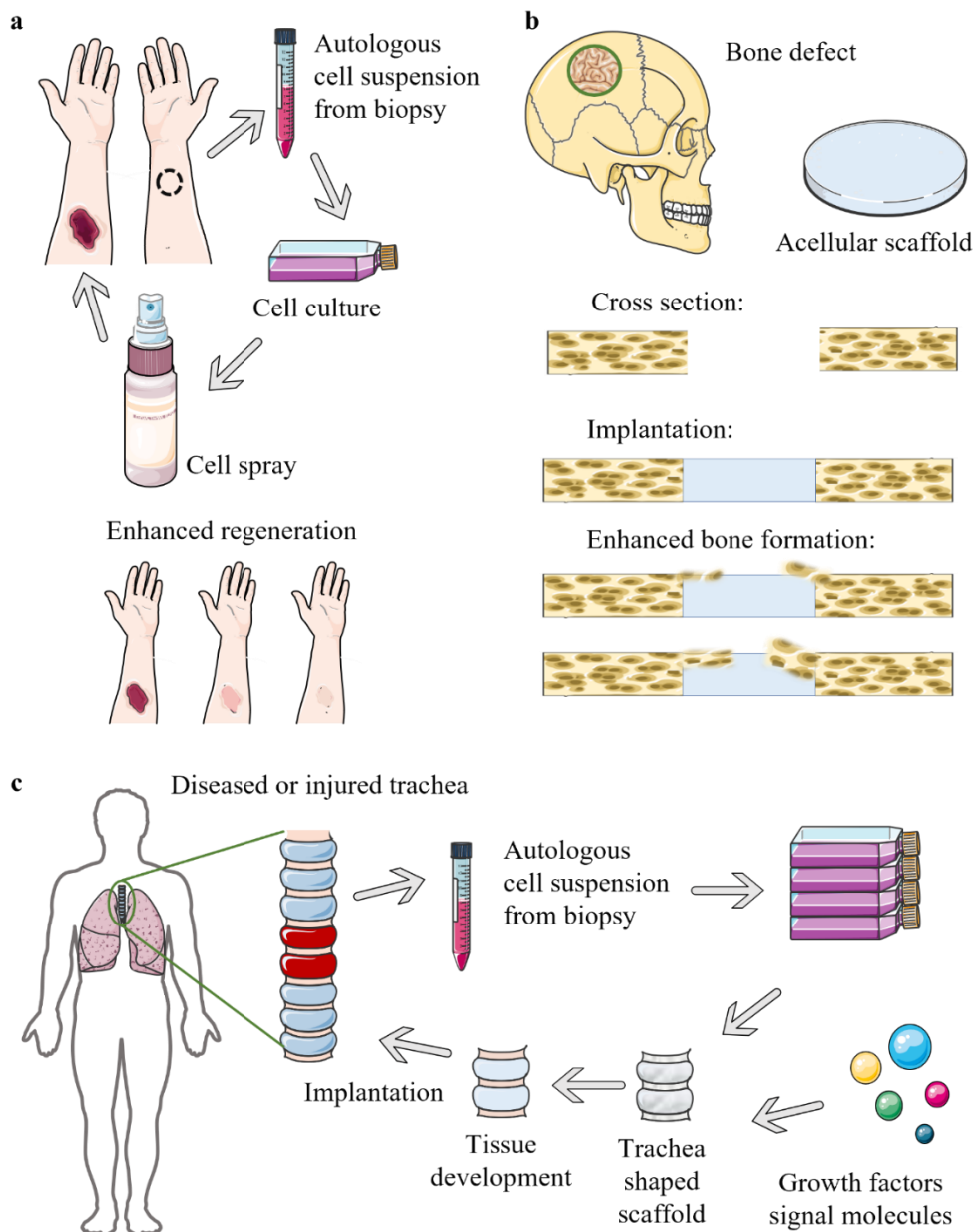


Figure 3 The three main approaches in tissue engineering. Cells can be injected, placed, or sprayed on the damaged area alone (a), or synthetic scaffolds can be implanted alone (b) (the project of Park et al.[38] inspired the image). Cells can be seeded in combination with growth factors and signal molecules on biodegradable scaffolds to function as an artificial tissue (c).

Parts of the figure were drawn by using pictures from Servier Medical Art.

Cells are also seeded in combination with growth factors and signal molecules on biodegradable scaffolds to function as an artificial tissue (Figure 3c). The cells can be seeded inside or on the top of the scaffolds after fabrication, or they can be encapsulated during fabrication. Cell sourcing is crucial in this method. Autologous cells do not induce immune response, however, their widespread adoption in clinical applications is limited

due to the shortage of cell availability and long culturing. Cells from allogeneic and xenogeneic sources are more abundant and can regenerate areas of massive loss, but they also carry the risk of graft rejection and infection. The cells need not only mechanical support for their normal function, but also growth factors and signal molecules, that have strong effect on cell differentiation, proliferation and penetration.

1.4. Extracellular matrix (ECM), and ECM analogue scaffolds

The human tissues are basically composed of two key components: cells and ECM. The ECM consists primarily of fibers with diameters between 50 and 500 nm which are highly organized into a 3D fiber network [39]. ECM gives not only most of the tissue volume but also forms the characteristic shape of tissues.

Although it was previously thought that ECM's primary function was to provide a structural framework for cells, our understanding of its diverse functions has grown. The ECM is a complex system that includes approximately 300 proteins and carbohydrates [40]. These components of the ECM are produced and assembled intracellularly and then secreted into the extracellular space via exocytosis [41]. These molecules interact with receptors of the cell surface and play a pivotal role in cell adhesion, proliferation, and migration. One of the main function of ECM is the scaffolding, when the cells adhere to many ECM molecules via many different molecules on the cell surface (*e.g.* integrin $\alpha1\beta1$, $\alpha2\beta1$, $\alpha10\beta1$, and $\alpha11\beta1$ bind to collagen [42]). The ECM molecules also regulate migration and proliferation of the cells.

Due to the complex structure and function of the ECM, it is challenging to copy the native form and create an artificial scaffold that can substitute the original (Figure 4a). The most exciting part of creating scaffolds is the regulation of the cell-ECM interactions, like enhancing cell adhesion and penetration into the scaffolds [43]. Researchers try to simplify and copy the main elements and functions. ECM analog scaffolds are produced from an extensive array of materials utilizing various fabrication techniques such as 3D printing [44] and electrospinning (Figure 4b) [45].

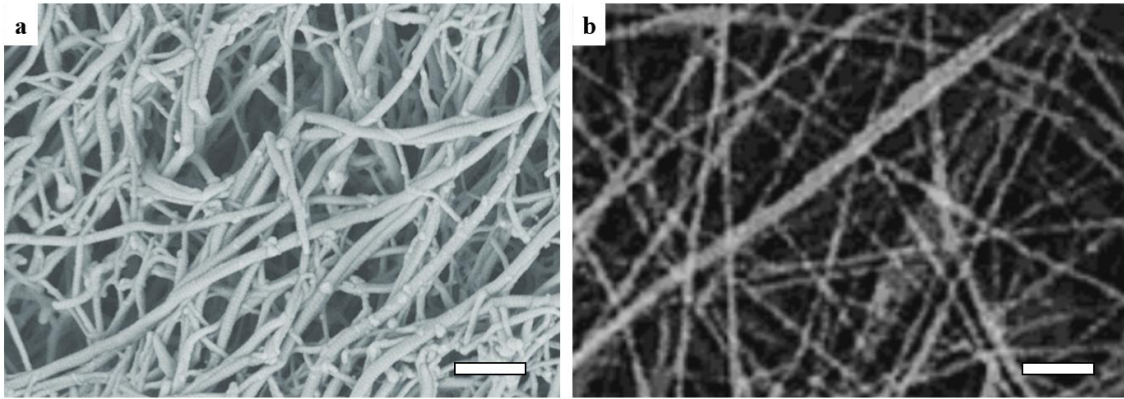


Figure 4 A scanning electron microscopy (SEM) image of human cartilage extracellular matrix and collagen fibers [46] (a). SEM image of calfskin type I collagen fibers prepared by electrospinning [47] (b). The scale bars indicate 1 μm .

1.4 Requirements for tissue engineering scaffolds

In order to create a successful tissue replacement, regardless of tissue type, a number of key considerations have to be taken into account [48].

A primary requirement for any type of successful implant is biocompatibility, indicating that neither the material nor its degradation products are cytotoxic, generate immunological overreaction, or cause rejection by the body [49]. However, a moderate inflammatory reaction can be elicited when a foreign object is implanted, although a constant immune response may indicate incompatibility [50],[51]. A scaffold with high biocompatibility enables cell attachment and proliferation on the surface.

Degradability is also an important factor of potential implants since the main principle of tissue engineering is to implant a scaffold, that is colonized by cells, the cells synthesize their own ECM, and at the same time the scaffold undergoes degradation (Figure 5). The proper degradation rate should match the cell growth, to give the cells the opportunity to proliferate, mature and replace the synthetic scaffold with their own [52]. One of the first use of biodegradable polymers in medical field was the synthetic absorbable suture called DexonTM made of PGA. The polymer degrades by hydrolysis, it loses about 50% of its mechanical strength after 2 weeks, and gets absorbed completely after accomplishing its mission in 4-6 months [53].

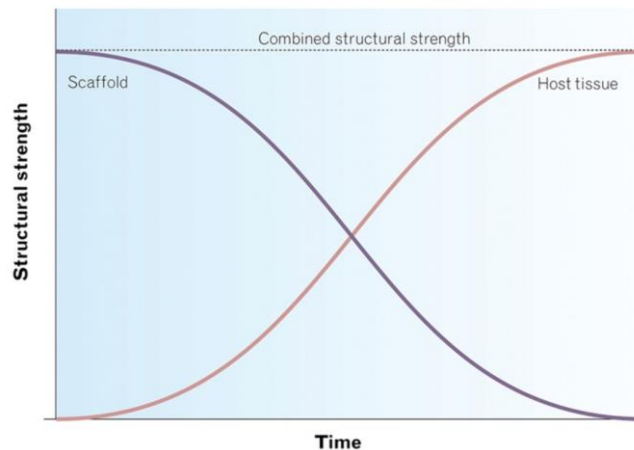


Figure 5 The tensile strength of a scaffold decreases, and its function is replaced by host tissues and their own ECM over time. Source: [54]

Mechanical properties of a scaffold ideally are consistent with those of the organ's intended to replace. One of the main functions of the scaffold is to provide shape and sufficient mechanical support for tissue growth. Scaffolds with carefully tailored load capacity and elasticity can enhance regeneration without the failure of the construct. The mechanical properties of the scaffold can be controlled by the altering the molecular weight of the base polymer [55], or by the changing copolymer composition [56].

Another crucial requirement to meet is the porous architecture of the artificial scaffolds. The adequate porosity (the pore fraction of the ECM) and pore interconnectivity of the scaffold allow for cell penetration, as well as the adequate diffusion of nutrients and metabolic waste products [57]. The infiltration of cells is related to the mean scaffold pore size and its distribution. The appropriate pore size for supporting colonization is in the range of 100 - 150 μm regarding most cell types, while pores with a diameter larger than 300 μm cannot be colonized completely [58],[59]., the scientists have to find a balance between the desired mechanical strength and the porosity to enhance the cellular infiltration, since these two properties seem to be inversely proportional [60].

To prevent the infection and graft-rejection, that may cause further complication, the scaffold needs to be sterilized before use. Sterilization of the scaffold must be safe, effective, and have a minimal impact on the structure and properties of the construct, furthermore, the sterilization process should not elicit hazardous reactions. Possible sterilization techniques include chemical agents like ethanol [61] and chlorine-dioxide [62]; irradiation like gamma [63], ultraviolet radiation (UV) [64], or E-beam [65]; heat

treatments like autoclaving [63]; and some novel techniques like treatment with supercritical carbon-dioxide [66] or plasma [67],[68].

Because of the numerous requirements to meet, large-scale manufacturing of these scaffolds and long-term preservation are the major challenges of this field. In the following three chapters, I would like to provide a short overview of the most commonly used scaffold materials, manufacturing techniques, and storage challenges that researchers have to face.

1.5 Scaffold materials

A large number of various polymers have been used as base polymers for tissue engineering. These biomaterials can be derived from both synthetic and natural sources.

Natural polymers for ECM analogues have the advantage of generally high biocompatibility, biodegradability, and bioactivity. Scaffolds engineered from materials, that are building up the ECM, like collagen, elastin and fibrinogen can retain some of their original biological functions, like enhancing the cellular attachment [69],[70]. Collagen is used for various medical application, like skin graft [71], treatment for spinal cord injury [72], wound dressing [73], scaffolds for cartilage repair [74]. Elastin is mainly utilized blended with collagen where the elasticity plays an important role by the function of the tissues, like blood vessels [75]. These proteins can be isolated from animal tissues (porcine and calf skin, tendon) in large quantities. The main disadvantages of the application of scaffold composed of these proteins are the possible negative immune response to the transmitted infectious agents and endotoxins, the batch-to-batch variability and the poor mechanical properties [43]. As an alternative to animal components, recombinant human collagen can be used [76].

The most common scaffold materials in clinical use are from synthetic origin. Synthetic scaffolds have many advantages as well as limitations over polymers of natural origin [77]. Their chemical and mechanical properties, degradation characteristics and architecture can be well controlled. Furthermore, the quality of the product is also constant from batch to batch even in large quantities. Polymers from the polyester family like poly(lactic acid) (PLA) [78], PGA [79], and its copolymer, poly(lactic-co-glycolic acid) (PLGA) [80] are widely utilized in scaffold fabrication not only because of their good biocompatibility, but they are FDA (United States Food and Drug Administration)

approved as well [81]. Common methods to modulate the degradation rate or mechanical properties of the scaffolds are to chemically modify polymers [82], use different polymers in combination [83],[84], or create copolymers (even with altering molar ratios [85],[86]). Although, these scaffolds from synthetic polyesters are customizable, reproducible, their degradation by hydrolysis yields weak acids, that can lower the local pH and have an adverse effect on cell viability [87]. Another polymer type gaining more and more attention is poly(amino acids). Due to their polypeptide backbone, they hold the potential to be degraded by proteases and peptidases [88]. In addition, they also possess the advantages of all synthetic polymers like low batch-to-batch variability and controllable physicochemical properties [89]. The application of polymers composed of lysine [90], glutamic acid [91],[92], aspartic acid [93], or alanine [94] building blocks (even in combination [95]) is well researched in the biomedical field.

In this current work, poly(aspartic acid) (PASP) was used as foundation to synthesize scaffolds. PASP is synthesized in a twostep method. First, its precursor, polysuccinimide (PSI) is synthesized by thermal polycondensation of L-aspartic acid in the presence of phosphoric acid catalyst [96]. PSI can be then hydrolyzed to form PASP in mild alkaline conditions (Figure 6). An advantage of the two step synthesis is that PSI can be easily modified at room temperature by primary amines and by that a wide variety of modified PSIs and PASPs with different chemical and physical properties could be synthesized. This opens the door for various biomedical applications in the future, like drug delivery [97],[98], surface coating [99], and scaffolding [88],[93],[100].

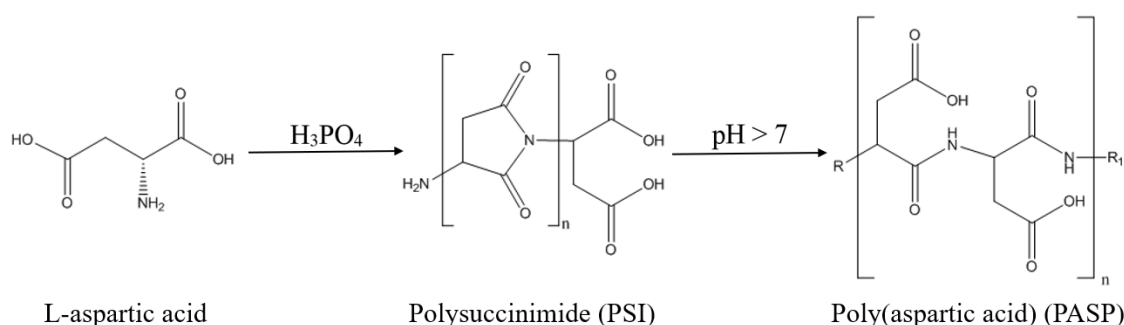


Figure 6 Synthesis of PSI and hydrolysis of PSI to PASP.

As scaffolding materials, hydrophilic polymers like PASP that can form hydrogels through crosslinks, show increasing popularity, they have been found to be useful in a

variety of biomedical applications. Moreover, because of high water content, and their mechanical properties are similar to the ECM [101].

Bulk hydrogels are found to be suitable for cell culturing, and being considered as potential materials for tissue engineering [101]. However, the restriction of the use of bulk hydrogels is the limited substrate-cell contact area, small mean pore size, and the missing fibrous structure of the ECM. Juriga *et al.* cultured human osteoblasts (MG-63) on PASP based bulk hydrogels and found that the cells were able to attach to, survive and proliferate on the scaffold (Figure 7a) [102]. Hydrogels are often used together with other techniques like particulate leaching, gas foaming, cryogelation, 3D printing and electrospinning (See Chapter 1.6), to improve the mechanical properties and/or porosity of the scaffold. Gyarmati *et al.* created supermacroporous PASP based scaffolds with cryogelation, that were suitable for *in vitro* cultivation of epithelial (Caco-2) cells [93]. To improve the mechanical properties of the bulk hydrogels, Molnar *et al.* used electrospinning technique to obtain PSI nanofibrous meshes, that could be crosslinked and hydrolyzed while retaining their fibrous structure (Figure 7b) [45], [103].

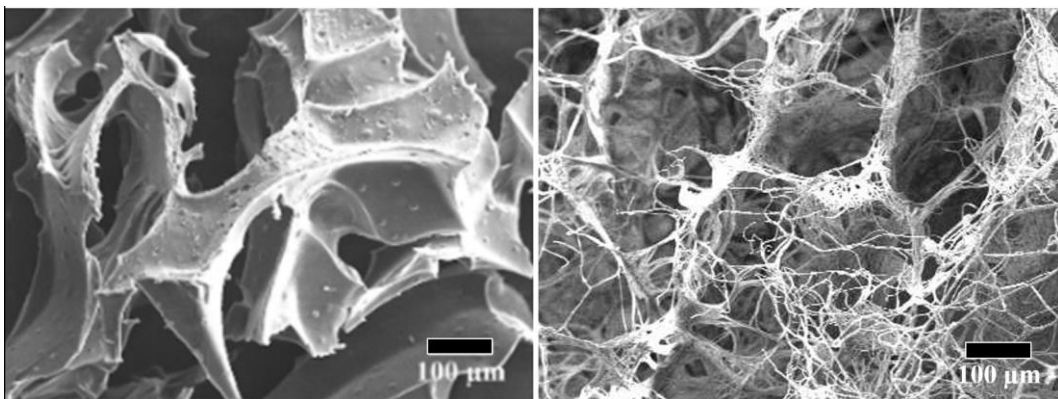


Figure 7 SEM micrographs of freeze dried PASP based bulk hydrogel (left, [104]) and PASPDAB based electrospun fibrous hydrogels (right).

1.6 Scaffolding techniques

To create scaffolds that are able to support cell growth and tissue regeneration, researchers developed various fabrication methods. To meet the requirements of scaffolds for biomedical application, all the relevant features including suitable mechanical properties and porosity, satisfying nutrient and waste transport, and many aspects have to be kept in view. In this chapter I will outline the most frequently used techniques, and lay emphasis on electrospinning, which is used as a fabrication technique in my work.

Particulate leaching technologies are one of the most commonly used methods to obtain 3D porous structure. Sola *et al.* used solutions of poly(methyl methacrylate) and polyurethane as base polymers and added sodium-chloride as porogen [105]. The average pore size was controlled by the size of the porogen, and the porosity by the polymer/porogen ratio. The solvent of the polymer was left to evaporate, and then the salt was removed by leaching in distilled water, resulting in a porous polymer-based scaffold.

Gas foaming is also extensively used to produce porous scaffolds, where incorporation of a blowing agent generating gas bubbles. Yusuf *et al.* used snail shells to synthesize carbonated hydroxyapatite (CHAp) and utilized a simple gas foaming technique to obtain porous structure for bone tissue engineering [106]. After mixing the CHAp with hydrogen peroxide solution, the samples were treated at 60°C to decompose the H₂O₂ solution (porogen) to form pores.

Three-dimensional structures of 3D printing polymers and metals have been investigated for a variety of biomedical applications like drug delivery [107], biosensors [108] and scaffolds [109]. Babilotte *et al.* used fused deposition modeling to create 3D porous scaffolds for bone tissue engineering using PLGA with hydroxyapatite nanoparticles, which yielded a highly accurate and low-cost 3D printed composite material, that enhanced osteodifferentiation [110].

1.6.1 Electrospinning

Electrospinning is a promising method for creating nano- to microfibrinous polymeric scaffolds with controlled properties. At the turn of the twentieth century J. F. Cooley and W. J. Morton were the first to patent electrospinning devices, which were primarily used in the textile industry. In the 1970s, the first record of a biomedical applications utilizing electrospinning technique were vascular prostheses and wound dressings published [111] and patented [112]. Since then, a wide range of natural and synthetic polymers have been used to synthesize electrospun scaffolds for drug delivery [113],[114] and tissue engineering such as skin [115], muscle [116], cartilage [117], tendon [118], bone [119], and nerve [120] regeneration. Electrospun fibers would be ideal materials for mimicking the ECM's fibrous micro- and nanoarchitecture.

The basic setup of electrospinning consists of a high voltage power supply, a syringe with a metal needle filled with a concentrated polymer solution (or melt [121])

and a grounded collector in front of the needle (Figure 8). By creating an electric field between the polymer solution delivered at a controlled flow rate and the collector, the electrospinning technique draws a polymer solution into a fiber. When a sufficiently high voltage is applied to a polymer solution, the charge exceeds the solution's surface tension, resulting in thread elongation. Due to the rapid evaporation of the solvent caused by its large surface area-to-volume ratio, this fiber is drying on its way to the collector. As a result, a nonwoven fiber is layered on top of another, forming a mesh that is deposited on the collector.

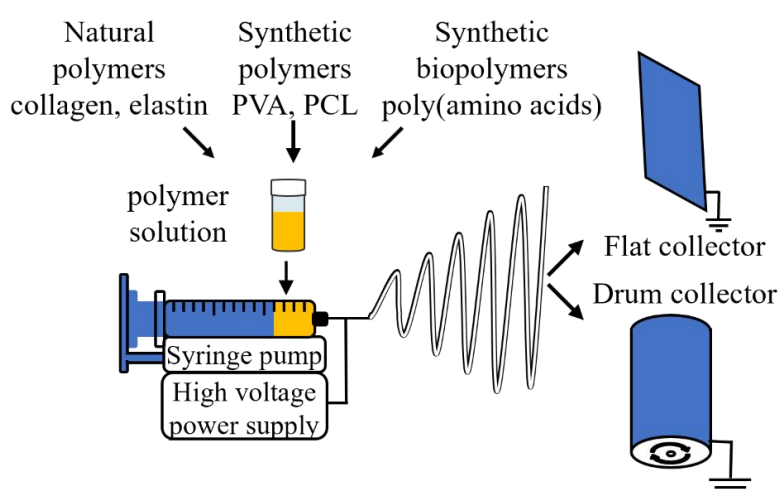


Figure 8 Basic setup of a conventional needle electrospinning device.

In the context of developing scaffolds that can provide an appropriate environment for tissue regeneration, the morphology, diameter, and porosity of the produced fibers and hereby corresponding meshes are of particular interest. Many parameters, such as polymer concentration and solvent selection, flow rate, applied voltage, humidity, needle size, and the distance between the needle and the collector, are involved in controlling the diameter of the polymer fiber. The production of fibers with diverse diameters is possible with careful optimization of these parameters. In general, by increasing the polymer concentration, the applied voltage and the flow rate are increasing the average fiber thickness due to the increased molecular chain entanglement and the decreased flight time. Increasing the distance between the needle and the collector, on the other hand, results in thinner fibers due to increased flight time. However, if the distance is increased beyond a critical value, it may cause instability resulting in beaded and fused fiber defects [122]. Dirk W. Schubert predicted scaling laws of universal validity based on fundamental physics to estimate fiber diameters and distributions using viscosity,

concentration, and surface tension of the polymer solution; the vapor pressure of the solvent, and the applied voltage [123]. Another approach for this purpose is to use modelling for prediction under certain conditions [124].

Numerous publications have recently appeared regarding electrospun fibrous structures using biopolymers, such as collagen [125] and gelatin [126], or synthetic polymers such as polycaprolactone (PCL) [127], polyvinylpyrrolidone [128] or synthetic biopolymers such as poly(L-lactic acid) (PLLA) [129], and polyamino acids [103] separately, or in combination [83].

Most of the time, researchers use monoaxial electrospinning [130], but coaxial [131] and multiaxial electrospinning, in which one or more needles are nested inside another, and receive a core-shell construct, have received widespread attention. To tune the properties of the scaffolds, researchers often use the monoaxial combination of different polymer solutions: co-electrospinning from two needles at the same time [62],[132], blend electrospinning by mixing them before spinning [133], or creating a multi-layer scaffold [134].

The conventional flat collector deposits randomly oriented fibers and in an inhomogeneous distribution, resulting in a mesh with a center thicker than the edges. Random fiber alignment and its inhomogeneity can be tailored using a rotating drum as a collector and adjusting the rotation speed. In the present work, I used randomly oriented fibrous meshes collected from a flat collector first [RP1] [103], then to produce scaffolds with uniform thickness [RP2] [135], I used a drum collector with a low rotating speed, which does not affect the alignment of the fibers (Figure 8).

Electrospinning extensively studied due to its potential applications for biomedical purposes. However, the production rate of a single needle laboratory-scale electrospinning device is usually rather low, around 0.01–2 g dry product per hour [136]. As a result, various approaches to develop electrospinning equipment for large-scale production were investigated, primarily by increasing the nanofiber jet through multiple needles, free-surface technologies, and hybrid methods that use an additional energy source [137]. Zs. K. Nagy *et al.* developed a high speed electrospinning method that fulfills the capacity requirements of the industry, achieved an output of 450 g drug-loaded polymer fiber per hour, which could be increased further by multiplying the high speed spinnerets [138].

Despite the many advantages of electrospinning, there are still some challenges to be overcome, before electrospun scaffolds can reach mainstream bedside utilization [139]. By creating polymer solutions, in most of the cases toxic and organic solvents are consumed. Those can also appear as residuals in the electrospun fibers and cause cytotoxicity after implantation. If the polymeric scaffolds are utilized without any post-electrospinning modification, for example when the human wound bed itself is used as a collector for skin regeneration, the residual solvent may cause graft rejection. Another challenge is the fact that the yielded mesh of randomly arrayed fibers is densely deposited, which results in low porosity and small pore sizes, that are too small for cellular ingrowth. This is limiting the cell migration through the scaffold, which is restricting their use in biomedical applications. To improve the porosity of the electrospun scaffolds, researchers developed various methods. In several approaches, the packing density is decreased due to the application of 3D printed scaffolds covered with electrospun fibers [140], special collectors [141], co-electrospinning techniques with sacrificial fibers [142], emulsion electrospinning [143] while creating fibers. Another approaches are the post-production processes such as gas foaming [144] and ultrasonication [145],[146],[147].

The current thesis studied the influence of ultrasonication on the macroscopical, chemical, mechanical, and toxicological properties of the electrospun scaffolds, as well as the permeability for cells (Figure 9).

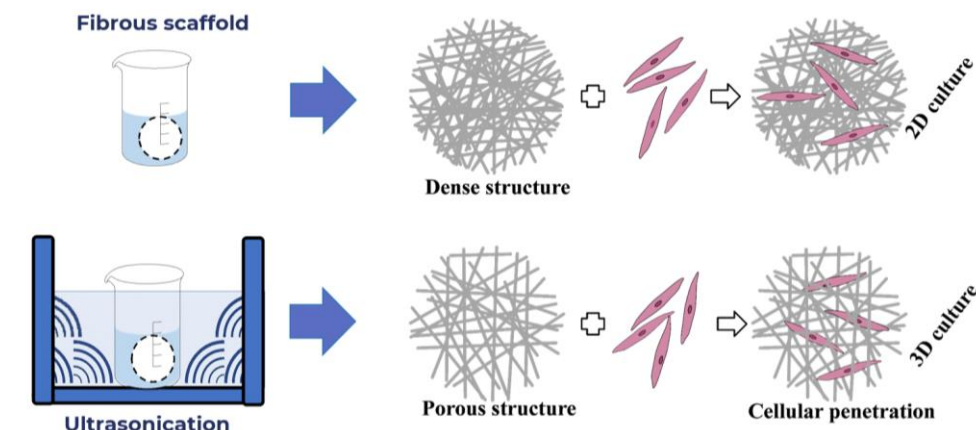


Figure 9 Electrospinning yields a mesh of randomly arrayed fibers, that is densely deposited, which results in low porosity and small pore sizes, that are too small for cellular ingrowth. Ultrasonication as a post electrospinning method can loosen the dense structure and enable the penetration of cells inside the scaffold and creating a 3D culture.

1.7 Storage conditions and long-term preservation of scaffolds

However, besides the advantages of hydrogels as scaffolds, they also introduce challenges concerning long-term preservation. They are susceptible to microbial spoilage due to their high water content [148]. Typically, tissue engineering products that are approved by the FDA are preserved by cryopreservation at -80°C for long term (Apligraf[®] [149], Dermagraft[®] [150]), but the transport of cryopreserved substances are expensive and challenging [151]. Another possible solution is drying the scaffolds, which reduces the water content to a minimal level where the deteriorative chemical reactions and the proliferation of bacteria are decreased or totally inhibited [148], then rehydrating them before use. Freeze-drying is a gentle technique, that is often applied in the case of heat-sensitive materials. However, both the drying [151] and the rehydrating process can affect the mechanical properties, although these effects are not revealed yet. Longer shelf life and cost effective, uniform manufacturing on larger scale are top priorities for tissue engineered scaffolds.

Having commercially available (off-the-shelf), easy to use tissue engineering products has gained popularity among scientists and doctors over the past few years, which would be a huge step towards mainstream applications involving implantable medical devices. This thesis studied freeze-drying as an alternative storage condition for electrospun fibrous hydrogels and its influence on the mechanical properties.

2 Objectives

The main objective of the thesis was the preparation of poly(aspartic acid) based fibrous scaffolds, that can be used in tissue engineering, creating a substrate for the cells to adhere to, grow and proliferate on.

At first, my aim was to produce two-dimensional (2D) poly(aspartic acid) based fibrous scaffolds with different chemical compositions, and investigate their interaction with cells.

The objective of the first part of the thesis:

1. To prepare polysuccinimide (PSI) fibrous scaffolds by electrospinning, compress them, crosslink the PSI chains (PSIDAB), and hydrolyze the scaffolds (PASPDAB), and to investigate the cell viability on the top of the scaffolds (PSIDAB and PASPDAB) and cell attachment on their surface.

Based on the results of the first part, my goal in the second part was to improve the cellular penetration and overall pore properties of the scaffolds. Another goal was to improve the storage conditions of fibrous hydrogels to extend their shelf life without compression and degradation.

The objectives of the second part of the thesis:

2. To use ultrasonication as a post-electrospinning technique to expand the fibrous PASPDAB hydrogel samples into the 3rd dimension.
3. To investigate the effect of ultrasonication on the fiber morphology, chemical structure, and the mechanical properties: the elongation, and the specific load capacity of the scaffolds.
4. To investigate the effect of ultrasonication on the cytotoxicity and to visualize the cellular penetration into the ultrasonicated scaffolds.
5. To examine freeze-drying as a possible storage condition and investigate the effect of freeze-drying and rehydrating on the mechanical properties.

3 Materials and Methods [RP1][103], [RP2][135]

3.1 List of materials

L-aspartic acid (99%), Phosphoric acid ($\geq 99.0\%$), 1,4-Diaminobutane (DAB, 99%), Imidazole ($\geq 99.5\%$), Paraformaldehyde (PFA, 95%), and Phosphate Buffered Saline (PBS) tablets were purchased from Sigma Aldrich (USA). N,N-Dimethylformamide (DMF, $\geq 99.5\%$), and anhydrous Ethanol (94-98%) were obtained from Reanal (Hungary). Citric acid monohydrate ($\geq 99.9\%$), Sodium-azide and Sodium-chloride (99.9%) were bought from VWR (USA). Minimum Essential Medium Eagle (M2279), Minimum Essential Medium without phenol red (51200-046), heat-inactivated Fetal Bovine Serum (FBS), Penicillin (10,000 U/ml) - Streptomycin (10,000 $\mu\text{g/ml}$), L-glutamine (200 mM), Non-Essential Amino Acids solution (NEAA), sterile Phosphate Buffered Saline (PBS) solution, and Vybrant DiD fluorescent vital dye were purchased from Thermo Fisher Scientific (Gibco, Invitrogen, USA). Chlorine Dioxide solution (3000 ppm) was purchased from Solvoxid (Hungary). The WST-1 cell proliferation reagent was obtained from Roche (Switzerland). Ultrapure water was provided by the Human Corporation ZeneerPower I Water Purification System (Republic of Korea). All chemicals were used without further purification.

3.2 Synthesis of Polysuccinimide (PSI)

PSI was synthesized through thermal polycondensation of L-aspartic acid in the presence of phosphoric acid as a catalyst at 180°C under vacuum using a previously described protocol [45].

Briefly, L-aspartic acid and crystalline phosphoric acid were mixed at a 1:1 mass ratio in a pear-shaped flask without any solvent. The mixture was gradually heated up to 180°C , while the pressure was gradually decreased to 5 mbar using a rotary vacuum evaporator system (130 rpm) (RV10, digital rotary evaporator, IKA, Germany). The duration of the synthesis was 8 hours. After the product reached room temperature, it was dissolved in N,N-dimethylformamide (DMF), then the solution was poured into ultrapure water and the precipitate was filtered and washed until the pH of the supernatant became neutral. After the final filtering, the PSI was oven-dried at 40°C for 2 days resulting in a white powder.

Based on the previous work of our research group, the viscosity-average molar mass of PSI is 28500 ± 3000 g/mol calculated by Kuhn-Mark-Houwink equation [45]. To determine the density of PSI, prior to using a pycnometer with anhydrous ethanol, a hydraulic press (EZ-Tools Hungary) was utilized to compress the pellets of the polymer powder.

3.3 Fabrication of PSI nanofibers by electrospinning

To fabricate PSI-based electrospun nanofibrous scaffolds, PSI was dissolved in DMF to produce a 25 w/w% solution. The polymer solution was loaded into a 5 mL syringe (Henke Sass Wolf) fitted with a metal blunt-ended 18G needle and it was electrospun directly on an aluminum foil-covered standing collector or drum collector (10 rpm; diameter = 10 cm) of the electrospinning system with a 20 cm needle tip-to-collector distance. A syringe pump (KDS100, KD Scientific, USA) was used to deliver the polymer solution to the needle tip at a constant feed rate of 1.0 ml/h. Electrospinning was conducted below 40 % humidity level, at the temperature of 22-26°C for 4 hours using a high-voltage DC power supply (73030P series, Genvolt, UK) at 12 kV. The resultant nanofibrous scaffold sheet was cut into adequate forms (circular: diameter 6 mm or 16 mm, prepared by commercially available hole punchers; rectangular: 2 x 2,5 cm, the longer side of the rectangle is parallel with the axis of rotation (when drum collector was used), prepared by a pair of scissors).

3.4 Post-electrospinning processing

The schematic representation of the preparation of different scaffolds and the chemical structures of the polymers obtained with the physical and chemical modifications can be found in Figure 10, Figure 11, and Figure 12. and the details of the reactions are listed below. The abbreviations of the samples and the explanations of commonly used features can be found in Table 1.

3.4.1 Compressing

In the first part of my work (Results section 4.1), standing collector was used and to make the samples mechanically durable and shelf-stable, nine layers were compressed together with a hydraulic press (1.2 MPa) (EZ-Tools Hungary). In the second part

(Results section 4.2), a rotating drum collector was used, and the samples were investigated without compression.

The schematic representation of the process of compressing and chemical modifications can be found in Figure 10 and Figure 11.

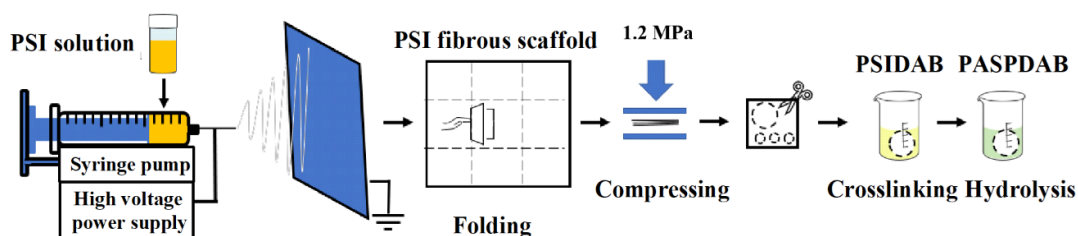


Figure 10 Schematic representation of the preparation of compressed scaffolds.

3.4.2 Crosslinking

The polymer chains were chemically crosslinked after the electrospinning process (post-electrospinning) by wet chemistry. Crosslinking was performed by submerging each scaffold in 0.5 M DAB in anhydrous ethanol for 3 hours, the same way as it was published previously [131]. After submersion, scaffolds were repeatedly washed with ultrapure water until neutral pH. A sample of each batch of the resultant scaffolds (PSIDAB) was subjected to a dissolution test in DMF to prove the existence of crosslinks (PSIDAB does not dissolve in DMF, but PSI does).

3.4.3 Hydrolysis

The hydrolysis of PSIDAB was conducted overnight in a mild alkali medium, in a water-based imidazole buffer at pH 8, where the ionic strength was 250 mM [152]. For 1 L of imidazole buffer (pH=8) 12.988 g imidazole, 1.728 g citric acid monohydrate and 11.466 g sodium-chloride was dissolved in ultrapure water. After the hydrolysis, the resultant hydrogel samples (PASPDAB) were washed with ultrapure water to remove the remaining salts. The chemical structures of the polymers obtained with the chemical modifications can be found in Figure 11.

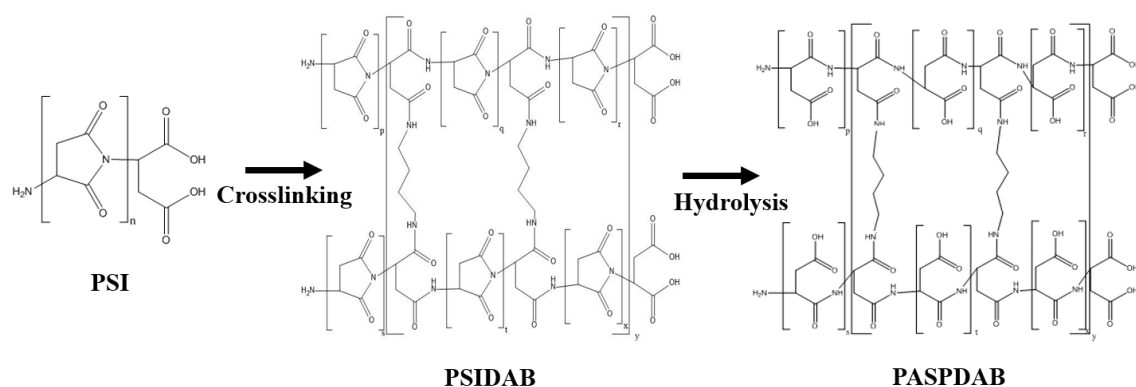


Figure 11 Chemical structures of the polymers obtained with the chemical modifications.

3.4.4 Ultrasonication

The PASPDAB samples were immersed into ultrapure water in a glass sample container at room temperature and ultrasonicated using a USC900THD ultrasonicator (VWR, Germany) with a power of 200 W. The duration of the treatment was in the range of 1 min to 120 min. For further characterization, PASPDAB scaffolds subjected to 60 min ultrasonication treatment were chosen.

3.4.5 Freeze-drying

The fibrous scaffolds were freeze-dried before some investigations (PSIDAB, PASPDAB, PASPDAB US). Before freeze-drying, the samples were washed thoroughly with ultrapure water, then were frozen at -20°C covered with ultrapure water. The freeze-drying was carried out using a Christ Alpha 1-4 LSC freeze-dryer (Germany) overnight (16 h). The thickness of the ultrasonicated samples was measured after freeze-drying on calibrated images using the ImageJ program (Open Source Software). The PASPDAB samples went under mechanical investigation after freeze-drying and followed by hydrating, these samples are hereafter referred to as “rehydrated”.

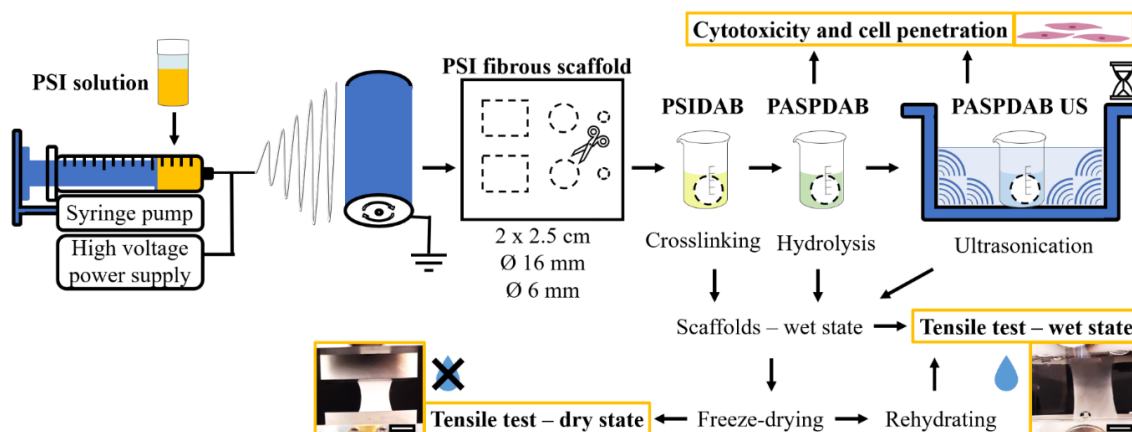


Figure 12 Schematic representation of the preparation and investigation of different scaffolds. The scale bars indicate 1 cm. The figure was adapted from [RP2] [135].

Table 1. List of abbreviations and explanations of commonly used features for electrospun fiber mats used

PSI	Polysuccinimide
PSIDAB	Polysuccinimide crosslinked with 1,4-Diaminobutane
PASPAB	Poly(aspartic acid) crosslinked with 1,4-Diaminobutane
PASPAB US	Poly(aspartic acid) crosslinked with 1,4-Diaminobutane – ultrasonicated for 1 hour
fresh	the samples were investigated immediately after preparation
rehydrated	the samples were investigated after freeze-drying and hydrating

3.5 Attenuated Total Reflectance Fourier Transform Infrared (ATR-FTIR) Spectroscopy

Attenuated Total Reflectance Fourier Transform Infrared spectroscopy (ATR-FTIR) was carried out to characterize the chemical structure of the samples using a JASCO 4700 (type A) FT/IR spectrophotometer equipped with a diamond ATR head. Samples were clamped directly against the diamond with consistent pressure. Infrared spectra were collected in the wavenumber range of $4000 - 400 \text{ cm}^{-1}$ at a spectral resolution of 2 cm^{-1} with 126 total numbers of scans, using H_2O , CO_2 , and ATR head subtraction. The background spectra were measured using clean and dry diamond crystal. PSI powder samples were examined oven-dried after synthesis. Electrospun PSI was measured dry, directly after electrospinning. The derivatives of PSI were examined after being washed with ultrapure water and freeze-dried for 18 h. The effect of the sterilization

with UV light exposition (1 hour) on the chemical structure of PASPDAB was also investigated.

3.6 Scanning Electron Microscopy (SEM)

Morphological investigations of the fibrous structure of the samples were carried out using a JSM 6380LA scanning electron microscope (JEOL, Japan). PSIDAB, PASPDAB, PASPDAB US samples were washed with ultrapure water and freeze-dried for 18 h before the examination, while PSI required no further treatment. Samples were fixed on an adaptor with a conductive sticker then they were sputter-coated with gold in 20-30 nm thickness using a JFC-1200 Sputter Coating System (JEOL, Japan). During the investigation of the samples by SEM, the applied accelerating voltage was 10 kV. For fiber diameter distribution analysis, 100 individual fibers were measured at 5000x magnification using the ImageJ program (Open Source Software). Shapiro-Wilk test for normality [153] and the following one-way ANOVA (Welch's correction) were performed using the GraphPad Prism 8.0.1 software (GraphPad Inc., USA).

3.7 Mechanical characterization

The mechanical properties of the samples were measured using a uniaxial mechanical testing machine (4952, Instron, USA). For this purpose, rectangular samples (2 cm x 2,5 cm) were cut from each scaffold (n=5). PSI scaffolds and freeze-dried samples were measured in a dry state at room temperature, below 30% humidity level. PSIDAB and PASPDAB samples were measured under physiological saline solution (150 mM, 25°C) immediately after the modification, or after washing with ultrapure water, freeze-drying, and rehydrating in saline solution. The specimens were assessed until rupture at a crosshead speed of 1 mm/min [126],[154].

From the recorded data, the extension and the regarding load were measured. The specific load capacity (maximal sustained load [N] divided by the area density [g/m²], Equation 1.) and the elongation were calculated (Equation 2.).

$$\text{Specific Load Capacity} \left[\frac{\text{Nm}^2}{\text{g}} \right] = \frac{\text{Maximal Sustained Load}[\text{N}]}{\text{Area Density} \left[\frac{\text{g}}{\text{m}^2} \right]} \quad \text{Eq. 1}$$

$$\text{Elongation} [\%] = \frac{\text{Deformation} [\text{mm}]}{\text{Initial length} [\text{mm}]} \cdot 100 \% \quad \text{Eq. 2}$$

One-way ANOVA analysis was performed on the Specific Load Capacities and the Elongation at breakpoint values using the GraphPad Prism 8.0.1 software (GraphPad Inc., USA).

3.8 Degradation

The degradation of the PASPDAB and PASPDAB US fibrous scaffolds was examined. Prior to the investigation, samples (n=5 in each group) were freeze-dried for 18 hours. Sample disks were 16 mm in diameter, with the weight of 2.7 ± 1.1 mg for the PASPDAB and 2.7 ± 1.3 mg for the PASPDAB US. The starting weights of the dry electrospun scaffolds were recorded as m_0 , and the samples were stored in 20 ml PBS for 1, 2, 3 and 4 months at RT. After that, the storing PBS solution was removed, and the samples were washed thoroughly with ultrapure water. Samples were freeze-dried for 18 h, and their dry weight was recorded as (m_t). The residual weight percentage was calculated using the following formula:

$$\text{Residual weight percentage [\%]} = \frac{m_t [\text{mg}]}{m_0 [\text{mg}]} \cdot 100 \% \quad \text{Eq. 3}$$

3.9 Cell studies

3.9.1 Cell culture

A human osteosarcoma cell line, MG-63, and human skin fibroblast cell line, 155BR (ECACC 90011809) was cultured as a subconfluent monolayer under standard conditions (37°C and 5% CO₂) in humidified atmosphere. The MG-63 cell line, that was used in the first part to optimize the protocols, cultured in Minimum Essential Medium supplemented with 10% fetal bovine serum (FBS), 2 mM L-glutamine, 1% non-essential amino acids (NEAA), 100 IU/ml penicillin and 100 µg/ml streptomycin. The 155BR cell line was cultured in Minimum Essential Medium supplemented with 15% FBS, 2 mM L-glutamine, 1% NEAA, 100 IU/ml penicillin and 100 µg/ml streptomycin.

3.9.2 Cell viability assay on the surface of scaffolds (2D samples)

Disks of an average diameter of 6 mm were cut from the compressed electrospun scaffolds (PSIDAB and PASPDAB). To minimize the probability of a bacterial or fungal

infection, the samples were stored in sterile-filtered PBS containing sodium azide. Before introducing the disks to the cells, the scaffold samples were sterilized in a 300 ppm chlorine-dioxide solution (in PBS) for 10 min and they were incubated in the completed medium for 1 hour. First, the gel disks were placed into the wells of low cell binding 96 well microplates (flat bottom, Nunc, Denmark). The surface of the low binding plates is not suitable for cells to attach to, and it was used to ensure, that the cells can only adhere on the scaffolds. After that, the MG-63 cells (adherent cell line) were seeded onto the gel disks at a concentration of 20 000 cells/well in 200 μ l medium/well and incubated for 24 or 72 hours at 37°C.

Cell viability was evaluated by a colorimetric assay using a commercially available cell proliferation reagent (WST-1). The WST-1 reagent was diluted with uncompleted MEM solution (lacking phenol red) in a ratio of 1:20. After washing the wells with PBS to remove the non- attached and slightly attached cells, 200 μ l of WST-1 solution was added to each well and the cells were incubated at 37°C for 4 h. The absorbance of the supernatant was measured at 450 nm with a reference wavelength of 655 nm using a microplate reader (Model 3550, Bio-Rad Laboratories, Japan).

3.9.3 Indirect cytotoxicity assay (3D samples)

Cytotoxicity tests were carried out as described in our previous studies[100],[103], with slight modifications. Circular samples of PASPDAB and PASPDAB US with a diameter of 6 mm ($m = 0.81 \pm 0.07$ mg) were cut from each scaffold. The sterility of the test samples was ensured by 60 minutes of UV light exposition. The *in vitro* cytotoxicity test was performed applying the extracts of the test samples with completed cell culture medium as an extraction vehicle. In the case of each sample, the extraction was carried out in a 48-well-plate in 500 μ l medium at 37°C for 24 hours.

Cells were seeded into 96-well plates at a concentration of 3200 cells/cm² in 100 μ L ($n=5$ for each sample) and maintained at 37°C for 24 h to provide the possibility for attachment to the surface and formation of a semi-confluent monolayer. The culture medium was aspirated from the cells after 24 h incubation. The medium was replaced with 200 μ l of extract (without dilution), while in the case of control, the replacing solution was fresh culture medium. The blank wells did not contain cells.

After 24 h and 72 h treatments, the cells were examined to identify morphological alterations using a phase-contrast microscope (Nikon Eclipse TS100, Nikon, Japan) equipped with a CCD camera (COHU, USA). The WST-1 cell proliferation reagent was used for the colorimetric quantification of cell viability in each well before treatment and after 24 or 72 h treatment. The reagent was diluted with uncompleted MEM solution without phenol red at a ratio of 1:20. After washing away the non-adherent and loosely attached cells with PBS, 200 μ l of the diluted WST-1 solution was added to each well and the plate was incubated at 37°C for 4 hours. The absorbance of the supernatant was measured at 450 nm with a reference wavelength of 655 nm using a microplate reader (Model 3550, Bio-Rad Laboratories, Japan).

For the data analysis, one-way ANOVA analysis (Welch's correction) was performed on the cell viability values using the GraphPad Prism 8.0.1 software (GraphPad Inc., USA).

3.9.4 Multiphoton microscopy

To visualize the MG-63 cells growing on the surface or the 155BR cells infiltrating the ultrasonicated fibrous scaffolds, they were labelled with a fluorescent vital dye (Vybrant DiD) before seeding (according to the manufacturer's suggested protocol). For the MG-63 cells, scaffolds of 6 mm in diameter (compressed PSIDAB and PASPDAB) were placed into Lab-tek 8 chamber slides (Nunc, USA) with tissue culture surface treatment. For 155BR cells, PASPDAB and PASPDAB US scaffolds of 16 mm in diameter ($m = 4.75 \pm 0.86$ mg) were prepared and freeze-dried.

After the sterilization, the samples were immersed in the completed cell culture medium for 2 hours, then placed into 6-well-plates, and 40 000 cells were seeded onto each disk. The same amount of control cells was seeded on a cover glass. After 24 and 72 hours, the samples were fixed by soaking in 4% paraformaldehyde solution (in PBS) for 2 hours at room temperature with subsequent washing with PBS. The samples were stored in PBS at 4°C until investigation under a multiphoton microscope (Femto2D, Femtonics, Hungary) applying a 10x objective and 800 nm wavelength to excite the photoactive dye. The size of the images was 1.6 μ m x 1.6 μ m and they were taken by the MES 4.4v program. The low red channel (600-700 nm) was used to detect the red fluorescence of the cells due to the Vybrant DiD vital staining while the low green channel

(490-560 nm) was used to detect the autofluorescence of the PASPDAB scaffolds [103]. After image capturing, the ImageJ program was used for further modifications.

4 Results

4.1 Poly(amino acid) based fibrous scaffolds with tuneable *in vivo* biodegradation (2D) [RP1] [103]

At first, following the method published by our research group [45], I produced electrospun fibrous hydrogels with different chemical composition, and investigated their interaction with cells.

To create electrospun fibrous scaffolds, PSI (the anhydrous form of PASP) as a base polymer was used. In order to make these samples mechanically durable and shelf-stable, nine layers were compressed together. To prevent them from dissolution under physiological condition, the polymer chains were chemically crosslinked after the electrospinning process by immersing them in 0.5 M DAB (1,4-Diaminobutane) solution (resulting PSIDAB). After hydrolyzation, hydrogel (PASPDAB) was formed, which tend to take up water, and swell, while preserving its fibrous structure (Figure 13).

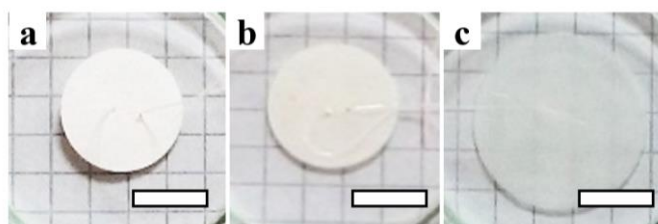


Figure 13 Macroscopic images of dry PSI (a), wet PSIDAB (b), and wet PASPDAB (c) scaffolds. The scale bars indicate 1 cm.

4.1.1 Cell viability on the surface of the compressed scaffolds

First, a cell viability assay was conducted by using MG-63 (adherent) cell line on 96 well low cell binding plates. Low cell binding plates ensured that the cells can only adhere to the scaffolds. The cell viability on the surface of the 2D PSIDAB and PASPDAB scaffolds was followed for 24 and 72 h and determined by a colorimetric assay based on the mitochondrial activity of the living cells (WST-1 reagent).

During the incubation for 24 and 72 hours, PASPDAB could maintain its physical properties. However, PSIDAB underwent hydrolysis and partially turned into PASPDAB, while shifting the pH of MEM (Minimal Essential Media) toward the acidic region indicated by the color of the MEM turning yellow. The results of the viability assays (Figure 14a) show that the viability of MG-63 cells seeded onto PSIDAB and PASPDAB

scaffolds were not significantly different to the control 24 h after the seeding. On the contrary the viability on PSIDAB significantly decreased by 72 h (from $84 \pm 28\%$ to $18 \pm 12\%$). PASPDAB scaffolds showed no signs of cytotoxicity as the MG-63 osteosarcoma cells were able to attach to their surface and proliferate on it (the viability significantly increased from $168 \pm 68\%$ to $520 \pm 190\%$ by 72 h). The viability of the control wells significantly decreased because of the low binding coverage of the wells prevents cell attachment (from $100 \pm 50\%$ to $40 \pm 11\%$ by 72 h).

By applying fluorescent pre-labelling (Vybrant DiD), the cells could be visualized by multiphoton microscopy 24 hours after seeding (Figure 14b). Due to the autofluorescence of the PSI and PASP scaffolds, they were detectable without staining. On the plastic surface of the tissue culture wells, many cells are showing normal, star-like morphology as it can be seen in Figure 14b. However, we could not find any cells on the PSIDAB scaffolds, nevertheless, large number of cells with typical star-like morphology were observed on the surface of the PASPDAB scaffolds. Based on the micrographs, no cellular penetration into the scaffolds was observable.

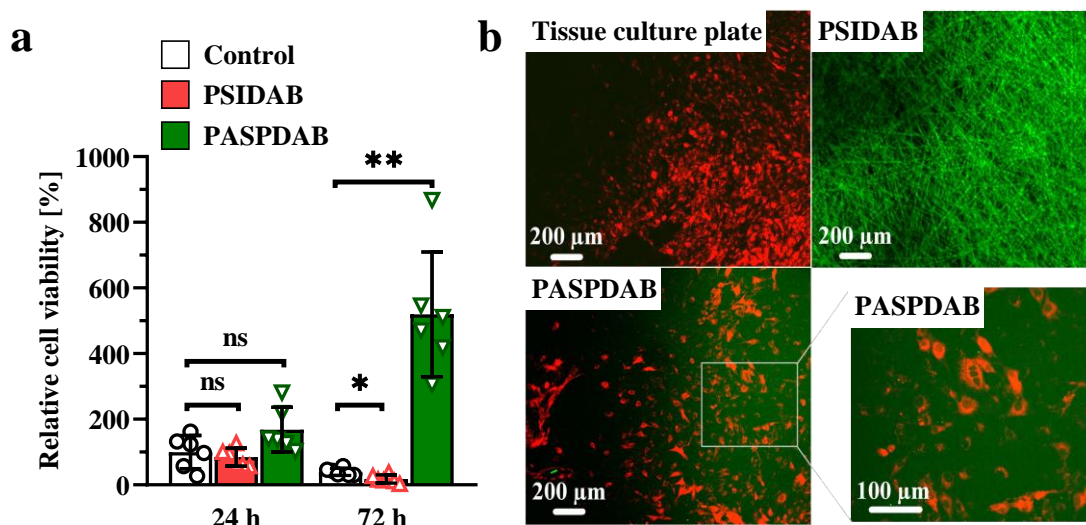


Figure 14 Viability of MG-63 cells after 24 h and 72 h cultivation on the surfaces of low cell binding plastic plates (control) and PSIDAB or PASPDAB scaffolds (a). Multiphoton microscopic images of the Vybrant DiD-labelled MG-63 cells after 24-hour-long cultivation on the surfaces of tissue culture plastic plates, or PSIDAB, or PASPDAB based fibrous scaffolds (b). The cells show red fluorescence due to the Vybrant DiD staining while the green color indicates the autofluorescence of the PSI or PASP based scaffolds. The figure was adapted from [RPI] [103] with minor modifications.

4.2 Ultrasound induced, easy-to-store porous poly(amino acid) based electrospun scaffolds (3D) [RP2] [135]

In the second part, my aim was to enhance the cellular penetration and the overall pore properties of the scaffolds based on the previous results. Another goal was to make progress in the storage conditions of fibrous hydrogels, to improve their shelf life without compression and degradation. In our previous study [RP1] [103], the mechanical durability and shelf stability was provided by the compression of numerous layers of electrospun scaffolds, causing low porosity and poor cellular infiltration. To overcome these limitations, ultrasonication process as a method to enhance scaffold porosity, and freeze-drying as an alternative storage condition was investigated.

4.2.1 Preparation of scaffolds and the effect of ultrasonication

After PSI synthesis and solution preparation, electrospinning was performed. The obtained white fibrous scaffold was cut into adequate forms (without folding and compressing), crosslinked, and hydrolysed as described in details in our previous article [RP1] [103] and previous studies of our research group [45]. After creating crosslinks between the polymer chains (PSIDAB) by wet chemistry, and hydrolysis of the PSI to PASP in a pH 8 buffer, the samples were freeze-dried to get back to the dry format (PASPDAB) (Figure 15). The schematic representation of the preparation and the experimental design can be seen in Figure 12.

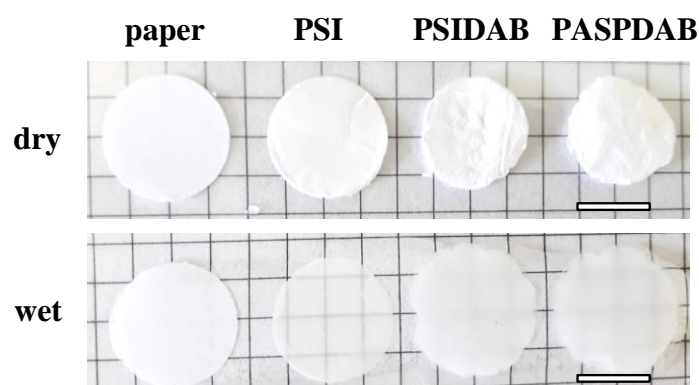


Figure 15 Macroscopic images of dry and wet PSI, PSIDAB, and PASPDAB membranes compared to a piece of paper. The scale bars indicate 1 cm.

The PASPDAB scaffold originally has a flat 2D expansion [RP1] [103], which is not the ideal shape for tissue engineering [155]. To enhance cell migration and expand the meshes in the 3rd dimension and hereby generate multilayer tissues instead of a cell layer, ultrasonication was used. Ultrasonication resulted in the expansion of fibre scaffolds. As shown in Figure 16, the cross-sectional thickness measured on freeze-dried PASPDAB US scaffolds was increasing due to ultrasonication. Already after 5 minutes, a significant expansion is observable ($148 \pm 11\%$). The maximum thickness of the PASPDAB US scaffolds was more than 300% compared to those of a PASPDAB scaffold and this change was saturated after 1 hour ($389 \pm 31\%$). These thicker scaffolds show reduced fiber density. The shape of the disk-formed scaffolds also changed slightly due to ultrasonication. Their diameter decreased moderately, and instead of a cylinder, the scaffolds take the shape of a pillow, staying thinner near the edges, where the hole puncher had cut them. Since the thickness did not increase significantly after 60 minutes of ultrasonication, the scaffolds were chosen to be subjected to this duration of treatment in further experiments.

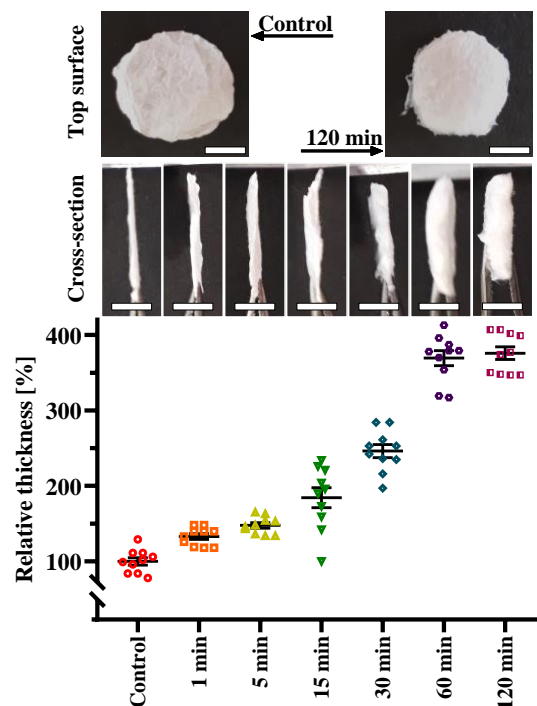


Figure 16 The cross-sectional thickness of freeze-dried PASPDAB scaffolds as a function of ultrasonication time. The scale bars are 5 mm.

4.2.2 Attenuated Total Reflectance Fourier Transform Infrared (ATR-FTIR) Spectroscopy

After the different chemical steps mentioned above and the US treatment of the samples, the chemical structure of the meshes was determined using ATR-FTIR spectrometry (Figure 17).

In the case of synthesized polymer (PSI powder) and the electrospun PSI fibers, the characteristic peaks of PSI can be observed at wavenumbers of 1795 cm^{-1} , and 1709 cm^{-1} (sharp, asymmetric stretching vibration of the imide rings), 1390 cm^{-1} (sharp, bending vibration of the C-O bond), and 1357 cm^{-1} (sharp, stretching vibration of the imide ring) [156]. In the case of PSIDAB, the crosslinking with DAB opened the imide rings of the PSI and it resulted in the appearance of a shoulder at 1662 cm^{-1} . In the case of PASPDA, the hydrolysis of PSIDAB resulted in the disappearance of the peak at 1795 cm^{-1} and a significant decrease of the peak at 1709 cm^{-1} and 1357 cm^{-1} marking further imide ring-opening. Around 3280 cm^{-1} , a new broad peak appeared indicating that new -OH groups are present on the polymer backbone due to the hydrolysis of the carboxyl groups. After the ultrasonication process (PASPDA US) and the UV treatment (PASPDA UV), the spectra did not differ from the original PASPDA form regarding the chemical structure.

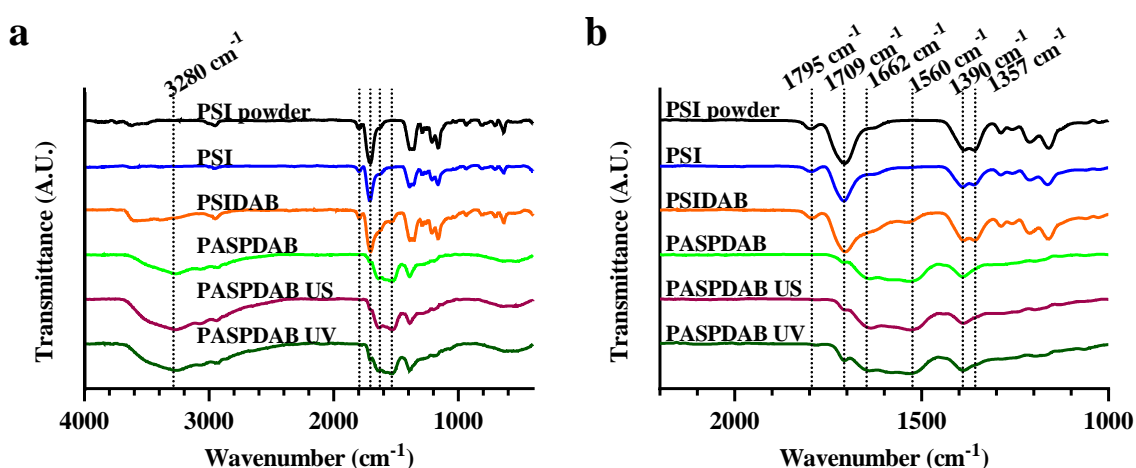


Figure 17 ATR-FTIR spectra of PSI powder, PSI electrospun fiber, and its derivatives. The figure was adapted from [RP2] [135].

4.2.3 Scanning electron microscopy (SEM)

The morphology of the dry electrospun fibers at different modification steps were observed by SEM (Figure 18). The electrospinning of PSI resulted in a non-woven mat with an average fiber diameter of around 590 ± 124 nm. These fibers show a smooth surface and bead-free structure as it was shown previously [131]. Further images show that the scaffolds kept their fibrous structure during either the chemical processing (Figure 18b and c) or the ultrasonication (Figure 18d). Based on the SEM micrographs, after hydrolysis, the fibers tend to run parallel and adhere together in groups.

All my data followed a normal distribution based on the Shapiro-Wilk normality test. Statistical analysis showed that the average fiber diameter (presented as means \pm standard deviation) after crosslinking (resulting PSIDAB) significantly decreased (486 ± 86 nm), and after the hydrolysis (resulting PASPDAB) significantly increased (1106 ± 113 nm) compared to the initial values (PSI, 590 ± 124 nm; $p < 0.05$). The ultrasonication process had no significant effect on the average fiber diameter (PASPDAB US, 1155 ± 151 nm).

Although the porous structure of the PASPDAB samples is already striking before the ultrasonication process on the SEM images (Figure 18e and f), the size and shape of the pores became distorted after ultrasonication, but the sponge-like structure was retained. The PASPDAB samples contain a dense layer of fibers on both sides of the scaffold, which could hinder cell penetration.

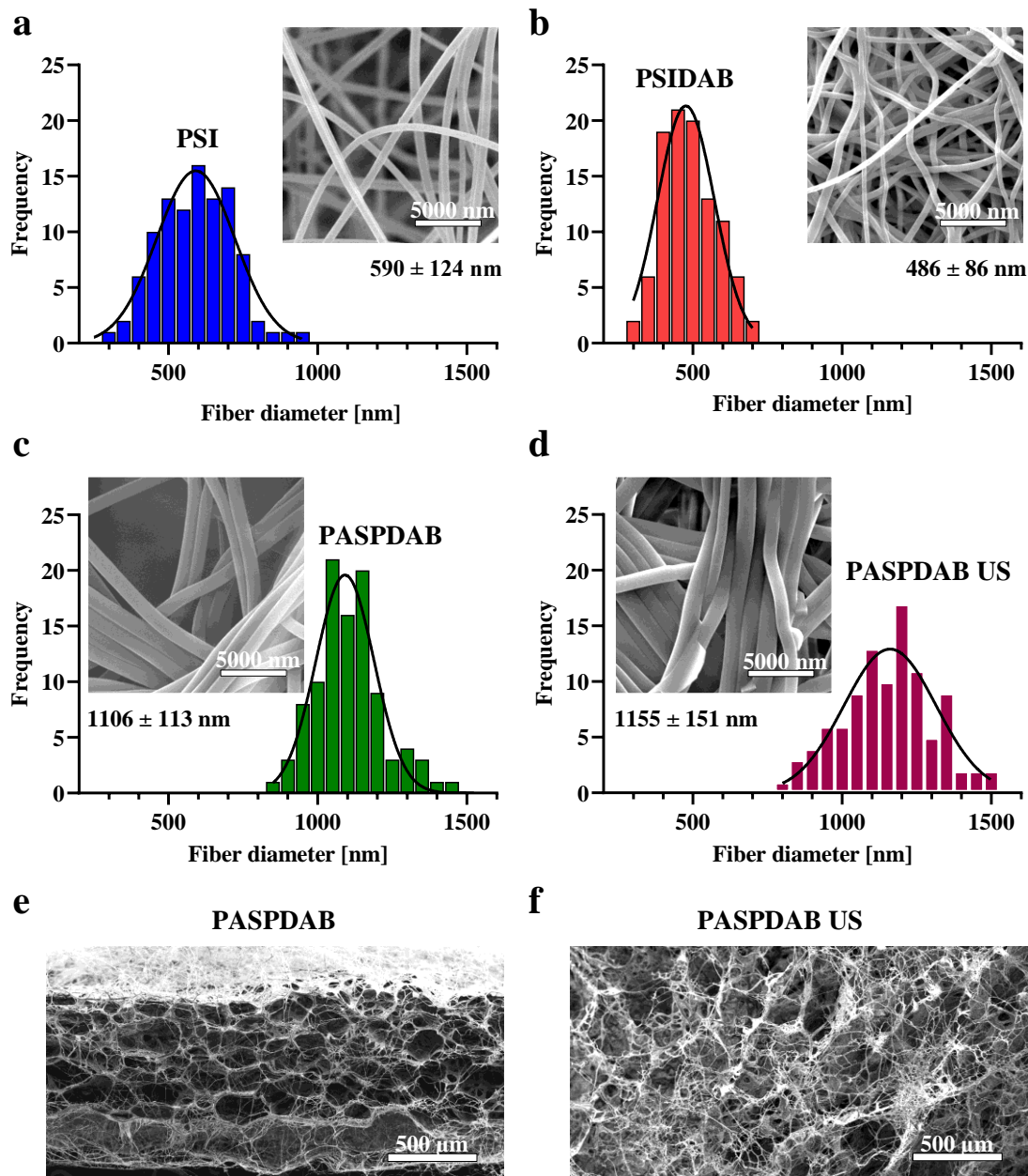


Figure 18 SEM micrographs and fiber size distribution of PSI (a), PSIDAB (b), PASPDAB (c), and ultrasonicated PASPDAB (d). The fiber diameters were presented as the means \pm standard deviations. SEM micrographs showing the cross-section of the PASPDAB (e) and PASPDAB US (f) scaffolds. The figure was adapted from [RP2] [135] with minor modifications.

4.2.4 Mechanical analysis and degradation

The degradational and mechanical properties of scaffolds for tissue engineering are pivotal, as the tissue healing should not be hindered by mechanical failure or degradation of the construct [52].

One of my main goals was to improve the storage conditions of fibrous hydrogels to extend their shelf life. Hydrogel scaffolds underwent significant degradation and had structural damage under the 4-month storage in PBS at room temperature (Figure 19). The residual weight of the PASPDAB and PASPDAB US samples decreased to $88.0 \pm 5.3\%$ and $90.7 \pm 5.5\%$ in the first 3 months, and to $83.2 \pm 7.0\%$ and $81.6 \pm 6.8\%$ by the end of the fourth month. The transparency of the samples slightly increased, and in some cases their integrity got damaged. To prevent the samples from degradation, they were kept in freeze-dried form, which is easy-to-store and transport.

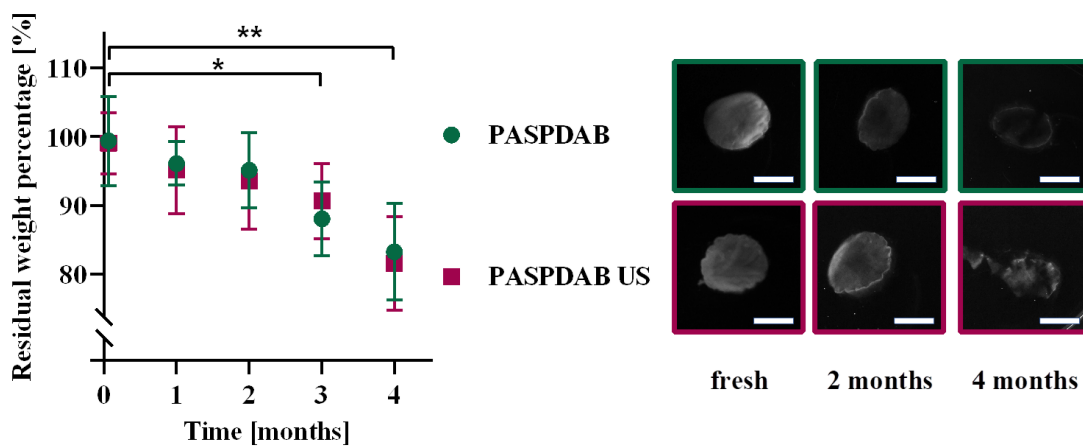


Figure 19 Degradation of PASPDAB and PASPDAB US samples after storing in PBS at RT for 4 months. The presented data show the average of 5 independent measurements. The error bars correspond to the standard deviation of the mean. The “” indicates if statistical significance exists between two groups (one-way ANOVA, $*p < 0.05$; $**p < 0.01$). The scale bars indicate 1 cm. The figure was adapted from [RP2] [131].*

Mechanical strength and ductility of the scaffolds in dry and wet states were measured using a uniaxial mechanical testing machine (Figure 20). In the case of wet state samples (PSIDAB, PASPDAB, PASPDAB US), the scaffolds were investigated immediately after production (fresh, “f”) or freeze-dried and hydrated (rehydrated, “rh”) to examine the effect of freeze-drying on the mechanical properties.

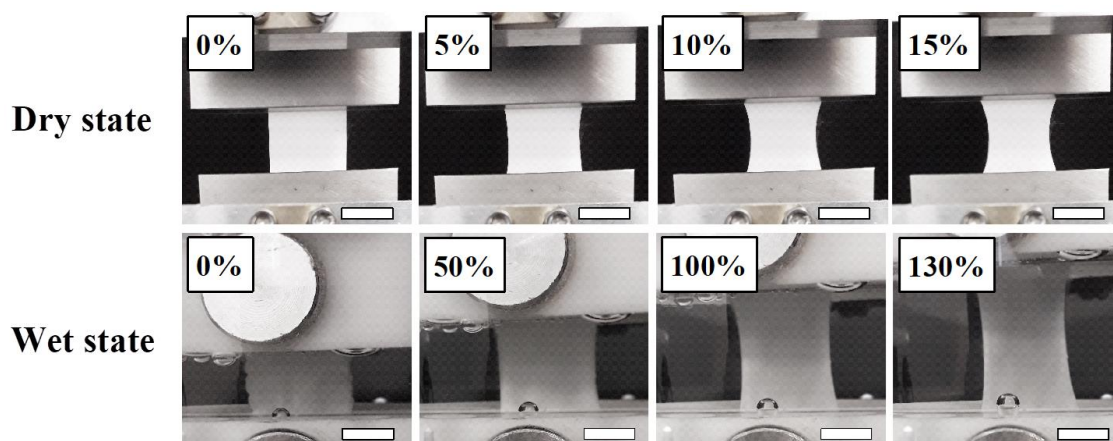


Figure 20 Representative macroscopical images of mechanical tensile test of PSI in a dry state and PASPDAB in a wet state at different elongations. Scale bars indicate 1 cm. The figure was adapted from [RP2] [131].

Regarding the specific load capacity values of the dry state scaffolds (Figure 21a), it is observable that there is a significant difference between the PSI ($0.08 \pm 0.01 \text{ Nm}^2/\text{g}$) and PSIDAB ($0.24 \pm 0.02 \text{ Nm}^2/\text{g}$). Although the hydrolysis has not changed the mechanical strength of the samples (PASPDAB $0.23 \pm 0.03 \text{ Nm}^2/\text{g}$), ultrasonication has decreased it significantly (PASPDAB US $0.11 \pm 0.01 \text{ Nm}^2/\text{g}$).

Concerning the specific load capacity of the wet state scaffolds (Figure 21b - PSIDAB, PASPDAB, PASPDAB US), they were lower by an order of magnitude compared to the dry samples (Figure 21a, PSI, PSIDAB, PASPDAB). The effect of ultrasonication on wet samples was not as obvious as at the dry ones and did not show a clear tendency of decreasing the specific load capacity. The only significant difference was observable in between the rehydrated PASPDAB ($0.021 \pm 0.003 \text{ Nm}^2/\text{g}$) and the rehydrated PASPDAB US ($0.014 \pm 0.004 \text{ Nm}^2/\text{g}$). The effect of freeze-drying and rehydrating on the scaffolds mechanical strength was also investigated, and neither the PASPDAB nor the PASPDAB US showed a significant difference between the freshly prepared and the freeze-dried - rehydrated samples.

Investigating the elongation at breakpoint values of the dry samples (Figure 21), the PSI ($16 \pm 3 \%$), PSIDAB ($7 \pm 3 \%$), and the PASPDAB ($35 \pm 5 \%$) showed similar characters. After ultrasonication, the elongation increased significantly by the time point of rupture (PASPDAB US $146 \pm 8 \%$). It means that the scaffold is ductile, and it can increase its length about to 2,5x without fracture as predicted from the SEM images (Figure 18e and f) where the fibers moved more to the center of the pores, thus becoming more flexible.

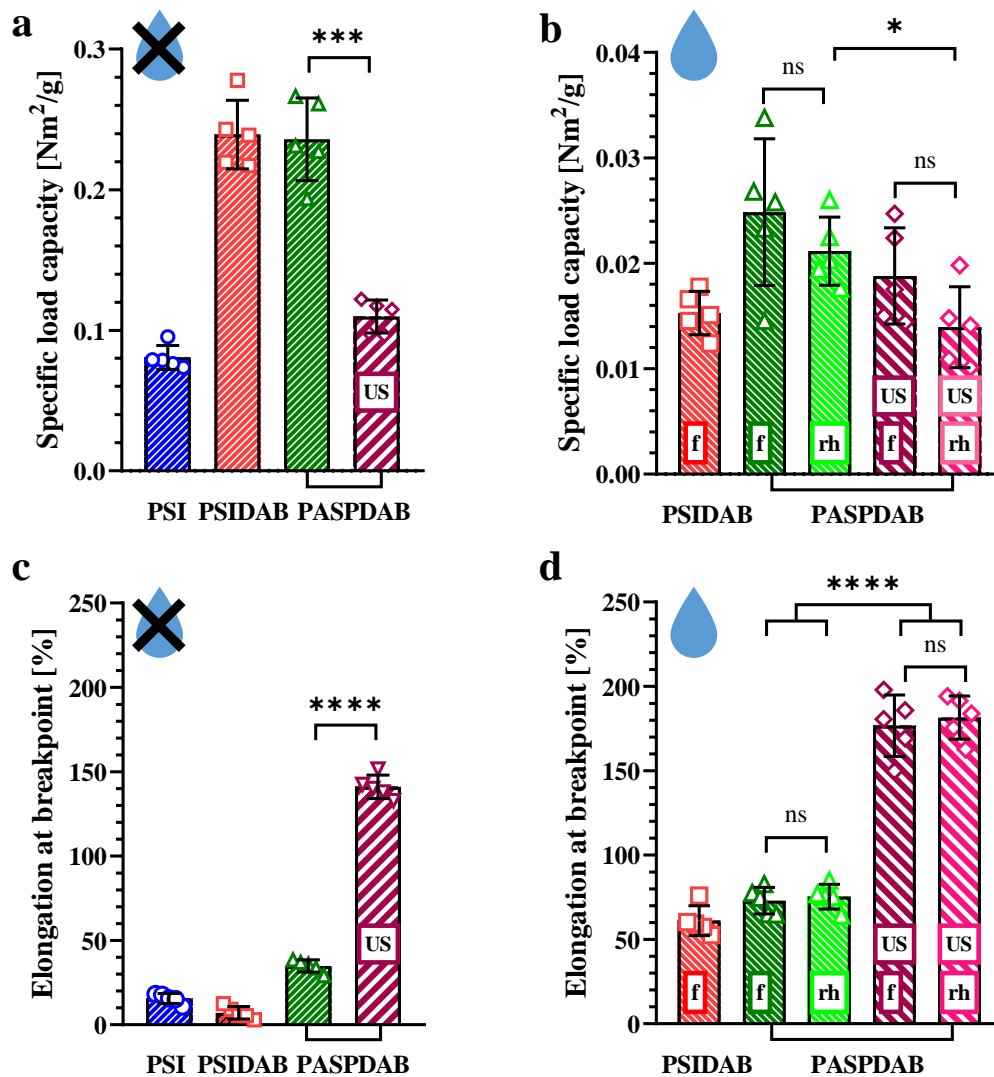


Figure 21 Specific load capacity (a, b) and elongation at breakpoint values (c, d) of dry (a, c) and wet (b, d) samples measured by a tensile test. The presented data show the average of 5 independent measurements. The error bars correspond to the standard deviation of the mean. The "*" indicates statistical significance exists between two groups (one-way ANOVA, * $p < 0.05$; ** $p < 0.01$; **** $p < 0.0001$). The figure was adapted from [RP2] [135] with minor modifications.

Regarding the elongation of the wet scaffolds (Figure 21d), the same phenomenon is observable as by the dry samples. PSIDAB ($61.1 \pm 9\%$), PASPDAB fresh ($73 \pm 8\%$), and PASPDAB rehydrated ($75 \pm 7\%$) showed similar characteristics. After ultrasonication, the fracture happened significantly later, only at $177 \pm 18\%$ (PASPDAB US fresh) and $181 \pm 13\%$ (PASPDAB US rehydrated) compared to the original length. It is also noticeable, that the freeze-drying and rehydrating has no effect on the elongation at breakpoint values.

4.2.5 Cell studies

4.2.5.1 Cytotoxicity

The following cell study experiments were carried out with the PASPDAB and PASPDAB US samples. According to our previous investigations [RP1] [103], the PSI based scaffolds undergo hydrolysis in cell culture media and shift the pH into the acidic range, therefore PSI and PSIDAB are not suitable for supporting cell growth *in vitro*.

In the present work, cytotoxicity studies were conducted on a human skin fibroblast cell line (155BR) to investigate any potential cytotoxic effect, hereby the opportunity of future application of the PASPDAB or the PASPDAB US as scaffolds.

Phase-contrast microscopical images of the fibroblasts after 24 and 72 hours can be seen in Figure 22a. After 24 h, the morphology of the treated cells is similar to the control, and there is no difference observable in the confluency level. After 72 h, the cells formed almost a confluent monolayer in each case indicating that the fibrous meshes did not negatively influence the cell growth. The cells showed their normal fibroblast morphology, no sign of cell death was observed.

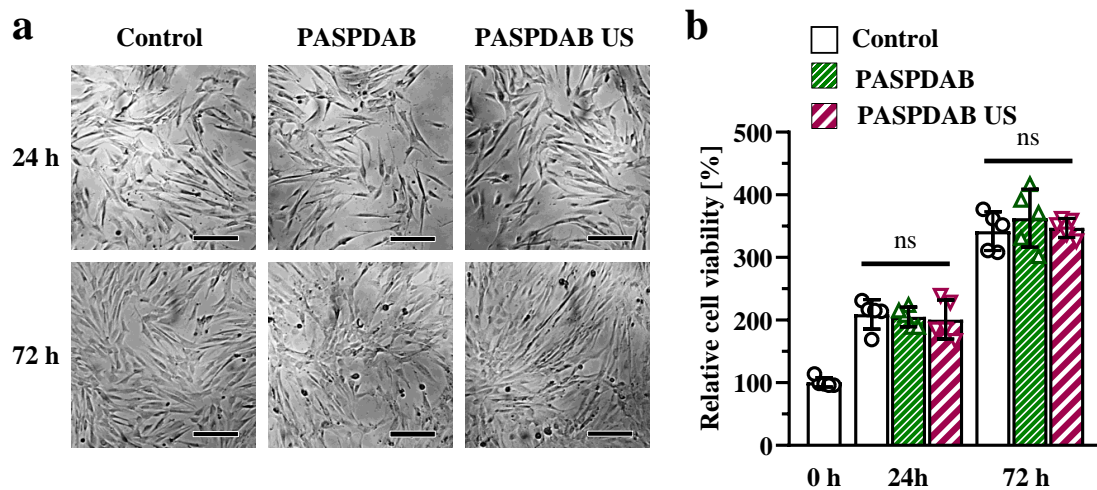


Figure 22 Phase-contrast microscopical images of 155BR cells (a) without treatment (control), treated with PASPDAB or PASPDAB US scaffolds after 24 and 72 hours. The scale bars indicate 100 μm . The cytotoxicity results (b) of PASPDAB and PASPDAB US scaffolds after 24 and 72 hours ($n=5$). The "ns" indicates the lack of statistical significance between the two groups (one-way ANOVA, $p>0.05$).

The figure was adapted from [RP2] [135].

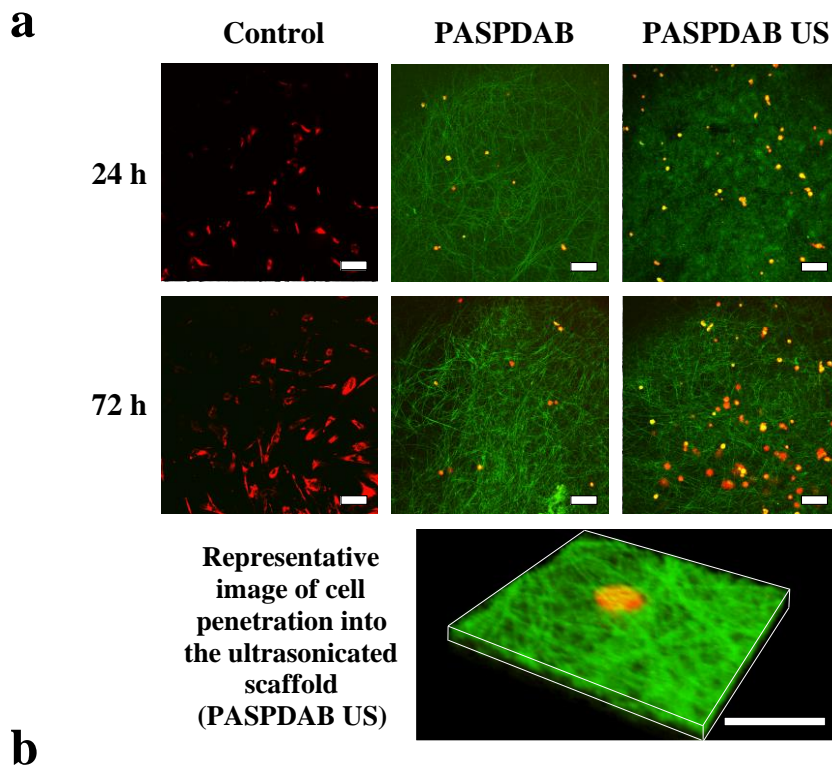
The cell study (Figure 22b) demonstrated that the cell viability in the treated groups (PASPDAB, PASPDAB US) did not show any significant decrease compared to

the control groups. In the first 24 hours, the cell viability doubled in each group (control: 209 ± 24 %; PASPDAB: 205 ± 16 %; PASPDAB US: 201 ± 31 %). After 72 hours, the viability values increased further, reaching 342 ± 31 % in the control group, 362 ± 46 % in the case of PASPDAB, and 347 ± 15 % regarding PASPDAB US.

4.2.5.2 Cell penetration

After staining the cells with a fluorescence dye (Vybrant DiD), the cells were visualized by applying multiphoton microscopy (Figure 23). After 24 hours, the control cells attached to the glass coverslips and showed normal morphology, and their number notably increased by 72 hours. However, on the PASPDAB and PASPDAB US scaffolds, the cells could be found at a significantly lower density, and these cells did not show a widespread morphology.

Fibroblasts seeded on the top of PASPDAB scaffolds showed poor penetration to the center of the scaffold. Cells adhered only to the surface of the scaffold, but they were not able to penetrate into the densely packed electrospun fibers. In contrast, the density of the cells in the case of the PASPDAB US seems to be higher, supposedly due to the penetration, which prevented the cells stuck between the fibers from washing out.



b

PASPDAB US 72 h

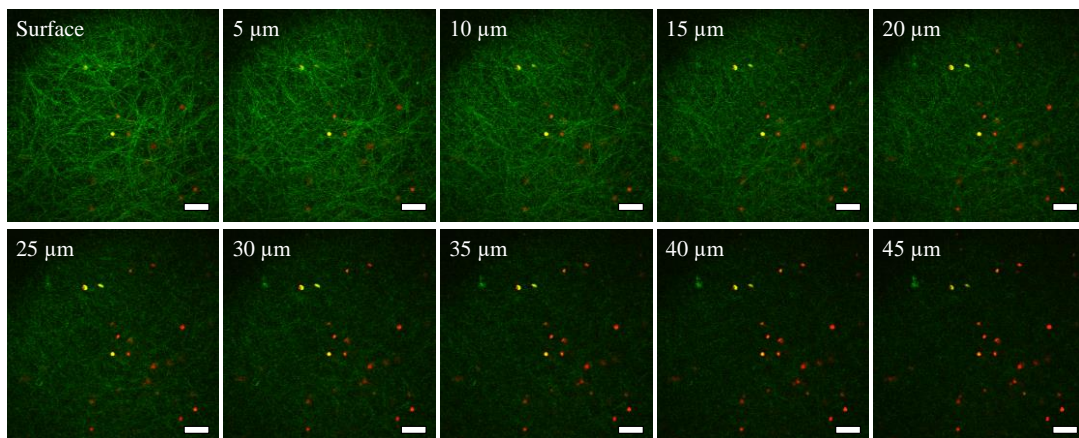


Figure 23 Multiphoton images of Vybrant DiD-labelled 155BR cells seeded on the surface of a glass coverslip (control) or PASPDAB or PASPDAB US fibrous scaffolds after 24 and 72 hours (a). Cell seeded on the surface of PASPDAB US scaffold and captured after 72 h in the marked depth (b). The cells show red fluorescence due to the Vybrant DiD staining, while the green color indicates the autofluorescence of the PASPDAB scaffolds. Scale bars indicate 200 μm . The figure was adapted from [RP2] [135] with modifications.

5 Discussion

5.1 Poly(amino acid) based fibrous scaffolds with tuneable *in vivo* biodegradation [RP1] [103]

5.1.1 Cell viability on the surface of the compressed scaffolds

Due to their biocompatibility and biodegradability, PASP based polymers are promising materials for scaffolds utilized in tissue engineering [157],[158]. In this part of my work, compressed PSIDAB and PASPDAB fibrous scaffolds were studied (Figure 13).

The purpose of the cell study was to investigate the interactions between the cells and the scaffolds. The scaffold is required to enable cell attachment, growth, and proliferation and must fulfil the criteria of biocompatibility, namely that they do not induce any unfavorable physiological response [49].

Regarding the fibrous PASPDAB, our results are in agreement with the previous study of our research group, where biocompatibility of PASPDAB based bulk hydrogels was proven using the same cell line (MG-63) [157]. On the contrary the viability of the cells seeded onto PSIDAB decreased by 72 hours (Figure 14). The hydrolysis of the PSIDAB scaffolds has turned the color of the MEM yellow marking a shift in pH toward the acidic range. MG-63 cells are not viable in acidic MEM which possibly caused cell death, and a documented low cell viability. Therefore, based on this experiment it cannot be decided whether PSIDAB is cytotoxic or not, as cell death was caused most probably by the pH shift. Nevertheless, this phenomenon is amplified in an *in vitro* setting as no fluid exchange is available. To investigate the behavior of PSIDAB scaffolds in *in vivo* conditions, samples were implanted by our research group under the skin of rats. The implants after 3 days were found as soft swollen gels, that means the PSIDAB went under hydrolyzation and turned into PASPDAB *in vivo*. The shift in pH was tolerable for the organism, on the 7th day, there were no macroscopic signs of irritation, infection, or foreign body type reaction. These results supported our theory with the cell experiment, thus the pH shift did not cause any side effect *in vivo*, the surrounding body fluids and vasculature provided a sufficient buffering. The resected scaffolds were investigated by SEM, and a structure with low porosity, and many spheres attached were observable.

These spheres were found with 6 - 8 μm in diameter, suggesting that these were granulocytes, lymphocytes, or red blood cells [RP1] [103]. A mild level of penetration is also observable; however, the small pores were only penetrable for small sized cells.

In my work, while visualizing the cellular attachment to the scaffolds, we could not find any cells on the PSIDAB scaffolds (Figure 14b). Supposedly in this case the cells were only able to loosely attach to the scaffolds and all of them were removed during the fixation process including several washing steps. In addition, PSI based scaffolds shifted the pH value of the cell culture medium into the acidic range (its color turned to yellow) indicating that these scaffolds do not support the survival of the cells under *in vitro* conditions. On the other hand, plenty of spread cells could be seen on PASPDAB fibrous scaffolds, that means the material has desired surface properties to enable cell attachment and growth. Cellular penetration into the scaffold interior was not observable. The dense packing of the scaffolds caused by the compressed layers of electrospun mats can lead to small pores and hereby the inhibition of cellular infiltration.

The MG-63 osteoblast cell line is widely used in the tissue engineering research. Michael P. Francis *et al.* were working with fibrinogen based electrospun scaffolds and investigated the ability of the MG-63 cell to adhere on them [159]. Their results show that the cells were able to attach to the surface of the scaffold, but the histology revealed, that the MG-63 cells seeded on electrospun fibrinogen had completely dissociated from the scaffold by the 7th day, with no sign of penetration. Aidun *et al.* found their PCL/chitosan/collagen electrospun scaffold to be biocompatible using MG-63 cells and observed cellular attachment and proliferation, without infiltration [160]. PASP based bulk hydrogels were also investigated in regard to its interaction with cells. Jinhyeong Jang and Chaenyung Cha synthesized RGD sequence (Arginine-Glycine-Aspartic Acid) linked poly(2-hydroxyethyl-co-hydrazidoadipoyl aspartamide) and Poly(2-hydroxyethyl-co-ethylenediaminoethyl aspartamide) for biomedical application [161]. Their results indicate that the PASP based hydrogels are biocompatible and promotes cell adhesion and proliferation. Creating electrospun fibrous hydrogels is also well known in the literature. Caidan Zhang *et al.* investigated PASP based electrospun hydrogels, and created a colorimetric chemosensor for detection of copper ions [162],[163]. The biocompatibility and cell adhesion to PASP based electrospun scaffolds is firstly investigated by our study [RP1] [103].

My results are in agreement with the literature, regarding that biocompatible electrospun scaffolds could be a possible construct for tissue engineering, as their structural features resemble the ECM. However, based on the relevant literature and our results as well, the cellular infiltration is hindered by the dense packing of the electrospun fibers. This phenomenon also concerns the hydrogel fibrous scaffolds as well, where the small molecules can diffuse efficiently.

Thus, in the other part of my PhD work, I aimed to overcome this limitation regarding the application, namely the low porosity and hindered cellular penetration caused by the conventional electrospinning technique and compressing. The other goal was to improve the storage conditions of fibrous hydrogels and extend their shelf life without compressing and degradation.

5.2 Ultrasound induced, easy-to-store porous poly(amino acid) based electrospun scaffolds [RP2] [135]

5.2.1 Characterization of ultrasonicated samples

To enhance cellular penetration and expand the scaffolds in the 3rd dimension and hereby generate 3D structure from flat scaffolds, ultrasonication was used. Ultrasonication resulted in the expansion of fibre scaffolds. PASPDAB nanofibrous scaffolds needed 1 hour (200 W) of ultrasonication to reach their expansion plateau (Figure 16). The maximum of the relative thickness of the PASPDAB US scaffolds was below 400 %.

Lee *et al.* were the first at physically manipulating PLLA nanofibrous scaffolds by exposing them to ultrasonication [145]. They explored, that varying the time-span and energy of ultrasonication, the pore size, and the porosity could be adjusted. In their further work, chitosan and chitin were used for the same purpose and they found that this process is material-dependent [147],[146]:. In their studies, the maximal thickness was reached by 5 minutes ultrasonication time (150 W) in the case of PLLA fibers, while there was no significant effect observed after 1 minute (225 W) exposition in the case of chitin [147] and chitosan [146]. The average thickness of the samples was increased to a varying extent depending on the type of the used polymer. In the case of PLLA, chitin, and chitosan, the maximal increase in the thickness was 500 %, 2200 %, and 400 % respectively.

Comparing our results to these former studies, it must be pointed out that PASPDAB nanofibrous scaffolds needed more treatment time to reach their expansion plateau and the maximum of the relative thickness of the PASPDAB US scaffolds was below 400 %. A possible explanation of this phenomenon is the existence of crosslinks between the polymer chains that are also able to crosslink the fibers. Moreover, the strong intermolecular hydrogen bonds are also likely to have an important role in creating a densely packed structure.

According to the assumption of Lee *et al.*, the growth of thickness due to ultrasonication is attributed to vibrational energy that allows water to enter inside the scaffolds and mechanically agitate the pores to grow between the fibers [145]. Ma *et al.* explained this phenomenon with ultrasonic cavitation [164]. It means that in aqueous media, ultrasonication induces the formation of gas bubbles inside the scaffold that grow and collapse. A large number of gas bubbles can loosen the dense structure of the scaffold while inducing volume expansion.

The increase in scaffold thickness indicates the decrease of fiber density and a loosened structure with larger pores, that can enable cell migration inside the scaffold. It is possible that ultrasonication has direct or indirect impact on the chemical, morphological or mechanical properties. These crucial properties need to be examined before cell studies will be done.

In the present study, the chemical characterization of the samples was conducted by ATR-FTIR. Firstly, to ensure the success of the synthesis and the fact, that electrospinning process did not affect the chemical structure of PSI, the synthesized polymer (PSI powder) and the electrospun PSI fibers were investigated (Figure 17). These results confirmed that the PSI was successfully synthesized and modified, and the electrospinning process did not affect the chemical structure of PSI. The obtained spectra are in accordance with our previous works [RP1] [103],[45] and with the results of other research groups [165],[166] as well. The effects of further processing like ultrasonication and sterilization by UV light exposition on the chemical structure was also investigated (Figure 17). Importantly, we observed no significant changes following the aforementioned treatments.

The fibrous structure of the scaffolds was confirmed and investigated by utilizing scanning electron microscopy (SEM). The observed changes in fiber diameter are

attributed to the chemical reactions that occurred inside the fibers (Figure 18). It is known that an increase in the crosslinking degree causes a decrease in swelling ratio of gels [167]. In the case of fibrous meshes (PSI – PSIDAB), this effect resulted in a significant decrease of the fiber diameter [RP1] [103],[131] (Figure 18a and b). After hydrolyzation, hydrogels are formed (PASPDAB), which tend to take up water, and swell [168], which is discernible in the increased fiber diameters [RP1] [103] (Figure 18c). Ultrasonication had no significant impact on fiber thickness, which means that the volume of the scaffolds increased due to the increased porosity. The same phenomenon was observed by Jung *et al.* [147] investigating chitin and Lee *et al.* [145] in the case of PLLA. In our previous work, we already observed the fusion of some of the PASPDAB fibers under the same conditions without any optimization [RP1] [103]. In this study, we recognized a cord-like structure consisting of 5 to 15 fibers that run parallel and are adhered together.

5.2.2 Mechanical analysis and degradation

The mechanical properties of scaffolds and their degradation are crucial for tissue engineering, as the tissue healing should not be limited by mechanical failure of the construct [52].

One of my goals was to improve the storage conditions of fibrous hydrogels to extend their shelf life and prevent from degradation. Besides the advantages of hydrogels as scaffolds, they also introduce challenges concerning long-term preservation. Due to their high water content, they are exposed to microbial spoilage [148]. PASP and their derivatives are polypeptides, that means that they can be degraded through cleavage of their peptide bonds under physiological conditions [169],[170]. Lu *et al.* studied, that the chemical modifications on the backbone of the PASP based polymers may influence their degradation [171]. Juriga *et al.* investigated the degradation of PASP based bulk hydrogels in the presence of PBS and found no significant change by the 42nd day [102]. My results are in accordance with those findings, in the first two months, there was no change and for the first time, after 3 month a significant decrease in the residual weight of electrospun PASPDAB and PASPDAB US hydrogels was observable (Figure 19). To prevent the scaffold from degradation, to extend their shelf life, and to decrease the probability of microbiological damage, freeze-drying was chosen as an alternative storage condition.

The mechanical properties of the scaffolds should be consistent with the tissue they are replacing [52]. In my work, mechanical strength and ductility of the scaffolds were investigated in dry, and wet states freshly prepared and rehydrated (Figure 20). The thickness of electrospun PSI scaffolds and their derivatives is hardly measurable, which makes the accepted practice of calculating tensile stress with the cross-sectional area unreliable. To compare the mechanical strength of the scaffolds, maximum load capacity (Eq.1.) was used, that is the quotient of the maximal sustained load [N] and the grammage [g/m^2] [172].

In the case of PSI and PSIDAB, the reinforcing effect of the crosslinking is observable. This effect on the mechanical strength of bulk gels [168] and fibrous materials [82] is already widely investigated in the literature. In our previous work, we observed an inconsistent effect of crosslinking on dry PSI and PSIDAB sutured scaffolds [RP1] [103]. However, in the case of surgical sutures, the increased rigidity (Figure 21c) of the scaffolds is pivotal, and the different electrospinning setup can also modify the properties of the samples.

The ultrasonication treatment significantly decreased the mechanical strength of the dry state samples (by 50%) (Figure 21a), which is in good agreement with the results of other research groups [145],[146],[173]. This loss of mechanical strength could be the consequence of the loosened structure caused by ultrasonication weakening the interactions between the fibers. To the best of our knowledge, wet and ultrasonicated samples were examined only by Gu *et al.*[146] so far, and they found a considerable decrease (to 40%) in tensile strength after ultrasonic treatment. However, in our case, this tendency was not unequivocal, the only significant difference was found between the fresh PASPDAB and the rehydrated PASPDAB UH (Figure 21b).

The ductility of ultrasonicated samples was investigated by Lee *et al.* [145] and Gu *et al.* [146], but they found contrary results. Regarding elongation at break, Lee *et al.* [145] observed an almost 7-fold increase (from 14.1% to 95.8%) after ultrasonication in a dry state using PLLA. In contrast, Gu *et al.*[146] found no significant increase using neutralized chitosan neither in dry nor in the wet state. Since in our case the elongation after ultrasonication (Figure 21c and d PASPDAB – PASPDAB US) become four times larger in the dry state and three times larger in the wet state, our results are in agreement with Lee *et al.* [145].

To the best of our knowledge, there was no other research group investigating the effect of freeze-drying and rehydrating on the mechanical properties of wet electrospun samples up to now (Figure 21b and d). My results indicate that the PASPDAB and PASPDAB US samples can be stored in the freeze-dried state without losing mechanical strength after rehydration. In the dry state, the scaffolds are easy to transport and store, in addition, they have a longer shelf life. Improving the storage conditions of these scaffolds is a huge step towards making these grafts an off-the-shelf product.

5.2.3 Cell studies

My results (Figure 22) are in agreement with previous studies, where cytotoxicity of PASPDAB bulk hydrogels [102] or PASPDAB fibrous hydrogels [RP1] [103] were investigated. My results are in concordance with a previous report where the 155BR fibroblast cells showed a doubling time around 32 h [174]. My data also indicate that, the ultrasonication process does not affect the cytotoxicity of PASPDAB scaffolds.

The investigation of cell penetration showed, that the ultrasonication process was effective in creating a structure with larger porosity. The dense packing of fibers was loosened by this treatment and encouraged the cells to penetrate the PASPDAB US scaffolds. However, considering the PASPDAB scaffolds, no infiltration was observed (Figure 23). These results are in accordance with the previous findings on ultrasonicated electrospun scaffolds [145],[147],[175]. In these studies they also used fibroblast from mouse [145] and human [147],[175].

PASPDAB had fewer observable cells compared to the PASPDAB US. Such decrease in cell density can be explained by the loose attachment of the cells to the scaffolds, hereby they could be washed away by the subsequent washing steps of the fixation [RP1] [103].

The PASPDAB US scaffolds were not cytotoxic, and the fibroblast cells were able to migrate inside therefore the pore sizes are suitable for cellular penetration. With these investigations, two of the most crucial requirements of synthetic scaffolds were proved to be fulfilled: biocompatibility and suitable porosity.

6 Conclusions

New scientific accomplishments are summarized in the following points:

- T1. Electrospinning was used to create two-dimensional polysuccinimide (PSI) fibers and with post-electrospinning methods, poly(aspartic acid)-based fibrous hydrogel scaffolds (PSI crosslinked with DAB (PSIDAB) and its hydrolysed form, PASPDAB) were produced. The cell study on PSIDAB revealed that hydrolyzing PSIDAB in cell culture media caused a pH shift toward the acidic region, resulting in cell death in the MG-63 osteosarcoma cell line. PASPDAB scaffolds showed no signs of cytotoxicity after 24 and 72 hours on the same cell line. While visualizing the cellular attachment of pre-labelled MG-63 cells with multiphoton microscopy 24 hours after seeding, on PSIDAB scaffolds no attached cells were observable, nevertheless on the surface of PASPDAB scaffolds plenty of attached cells could be seen. [RP1]
- T2. Ultrasonication can be used to increase scaffold porosity and the cross-sectional thickness by 400% after 1 hour of treatment (200 W) of the two-dimensional PASPDAB scaffolds. This can enable cellular penetration. The average fiber diameter (PASPDAB: 1106 ± 113 nm; PASPDAB US: 1155 ± 151 nm) and chemical composition of the scaffolds did not change as a result of ultrasonication, as evidenced by SEM micrographs and ATR-FTIR analyses. [RP2]
- T3. Ultrasonication process affected the mechanical properties of the PASPDAB scaffolds. After ultrasonication, the specific load capacity of the dry PASPDAB samples decreased significantly (from 0.23 ± 0.03 Nm²/g to 0.11 ± 0.01 Nm²/g). The specific maximum load of wet state scaffolds was lower by an order of magnitude, and ultrasonication had no discernible effect on mechanical strength. The elongation at breakpoint of dry state (freeze-dried) PASPDAB scaffolds significantly increased after ultrasonication (PASPDAB: $35 \pm 5\%$; PASPDAB US: $146 \pm 8\%$). On wet scaffolds, due to ultrasonication elongation at breakpoint increased from $73 \pm 8\%$ to $177 \pm 18\%$ in freshly prepared samples. [RP2]

- T4. To prevent PASPDAB and PASPDAB US hydrogel scaffolds from degradation, structural damage and microbiological spoilage caused by wet state storage, freeze-drying as an alternative condition was used to increase the shelf-life of the samples. The mechanical properties of fibrous poly(aspartic-based) hydrogels are unaffected by freeze-drying and hydrating. The specific load capacity of freshly prepared PASPDAB wet samples was $0.025 \pm 0.007 \text{ Nm}^2/\text{g}$, while that of freeze-dried and rehydrated samples was $0.021 \pm 0.003 \text{ Nm}^2/\text{g}$. The mechanical strength of PASPDAB US was $0.019 \pm 0.004 \text{ Nm}^2/\text{g}$ in fresh and $0.014 \pm 0.004 \text{ Nm}^2/\text{g}$ in rehydrated form. The elongation at breakpoint was $73 \pm 8\%$ for freshly prepared wet PASPDAB samples and $75 \pm 7\%$ for rehydrated ones. During the investigation of PASPDAB US samples, the elongation of fresh samples was $177 \pm 18\%$, while rehydrated samples had $181 \pm 13\%$. Based on these results, fibrous hydrogel scaffolds in freeze-dried form can be stored, transported, and rehydrated before use without changing mechanical properties. [RP2]
- T5. PASPDAB and PASPDAB US scaffolds were found to be noncytotoxic to 155BR fibroblast cells after 24 and 72 h of an indirect cytotoxicity test. Ultrasonication process created a porous structured PASPDAB US and enabled the penetration of 155BR cells inside the poly(aspartic acid) based scaffolds based on the multiphoton microscopy results, on the other hand, the cells seeded on the PASPDAB scaffolds, were attached on the surface. [RP2]

7 Summary

Electrospinning is commonly used in the biomedical field to create tissue engineering scaffolds. In ideal case, the cells colonize the scaffold, synthesize new extracellular matrix as the scaffold degrades. Finding the appropriate material for each type of tissue with tuneable properties is currently a challenge for scientists. In this work, poly(aspartic acid) (PASP) and its anhydride, polysuccinimide (PSI) was used as a base polymer to create hydrogel scaffolds with electrospinning setup.

First, I produced electrospun fibrous scaffolds of PSI and after crosslinking with 1,4-Diaminobutane (DAB), hydrogels with varying chemical compositions (PSIDAB and PASPDAB) were formed. While investigating their interactions with cells, PSIDAB made the culturing media acidic *in vitro*, decreasing the cell viability. However, PASPDAB was found noncytotoxic for MG-63 cells and the two-photon microscopy confirmed that after 24 hours, cells were able to attach to the surface of the PASPDAB scaffold. Based on these results, PASPDAB is a possible material for scaffolds, but based on the micrographs there was no evidence of cellular penetration into the scaffolds.

The reason for the poor infiltration is the densely deposited structure of randomly arrayed electrospun fibers resulting in low porosity. Thus, I attempted to overcome this limitation by using ultrasonication treatment on PASPDAB, to loosen the structure, and enhance the cellular infiltration. Ultrasonication has increased the cross-sectional thickness of the scaffolds to 400%. The ultrasonication affected the mechanical properties of the scaffold. The specific load capacity of the dry samples has halved; however, the elongation at breakpoint has significantly increased by both dry (4-fold) and wet state (2,5-fold) scaffolds. As an alternative for wet state storage, freeze-drying was used. Based on my findings, drying and rehydrating of the fibrous poly(aspartic based) hydrogels do not affect their mechanical properties, thus the freeze-dried form of scaffolds can be stored, transported, and be prevented from degradation. While investigating their interactions with cells, ultrasonicated PASPDAB scaffolds were found to be noncytotoxic for 155BR fibroblast cells, and ultrasonication process created a porous structure and enabled the cellular penetration inside the poly(aspartic acid) based scaffolds.

Due to the increased cellular infiltration of the PASPDAB scaffolds and their alternative dry state storage, this kind of scaffold could be a huge step towards an off-the-shelf and effective product for tissue regeneration.

8 References

- [1] J.P. Vacanti, R. Langer, Tissue Engineering, *Science* (80-.). 260 (1993) 920. <https://doi.org/10.1080/00131725009342110>.
- [2] E. Polykandriotis, L.M. Popescu, R.E. Horch, Regenerative medicine: Then and now - an update of recent history into future possibilities, *J. Cell. Mol. Med.* 14 (2010) 2350–2358. <https://doi.org/10.1111/j.1582-4934.2010.01169.x>.
- [3] B.D. Ratner, A History of Biomaterials, *Biomater. Sci. An Introd. to Mater.* Third Ed. (2013) xli–liiii. <https://doi.org/10.1016/B978-0-08-087780-8.00154-6>.
- [4] M. Yang, L. Liu, MHC II gene knockout in tissue engineering may prevent immune rejection of transplants, *Med. Hypotheses.* 70 (2008) 798–801. <https://doi.org/10.1016/j.mehy.2007.08.009>.
- [5] T.H. Kim, J.J. Yan, J.Y. Jang, G.M. Lee, S.K. Lee, B.S. Kim, J.J. Chung, S.H. Kim, Y. Jung, J. Yang, Tissue-engineered vascular microphysiological platform to study immune modulation of xenograft rejection, *Sci. Adv.* 7 (2021) 1–14. <https://doi.org/10.1126/sciadv.abg2237>.
- [6] L. Tan, Y. Guo, C. Feng, Y. Hou, X. Xie, Y. Zhao, The Dual Regulatory Roles of Macrophages in Acute Allogeneic Organ Graft Rejection, *Engineering.* 10 (2022) 21–29. <https://doi.org/10.1016/j.eng.2021.10.015>.
- [7] R. Papini, ABC of burns: Management of burn injuries of various depths, *Br. Med. J.* (2004).
- [8] F. Berthiaume, T.J. Maguire, M.L. Yarmush, Tissue engineering and regenerative medicine: History, progress, and challenges, *Annu. Rev. Chem. Biomol. Eng.* 2 (2011) 403–430. <https://doi.org/10.1146/annurev-chembioeng-061010-114257>.
- [9] S. Reardon, First pig-to-human heart transplant: what can scientists learn?, *Nature.* 601 (2022) 305–306. <https://doi.org/10.1038/d41586-022-00111-9>.
- [10] C.M. Otto, R.A. Nishimura, R.O. Bonow, B.A. Carabello, J.P. Erwin, F. Gentile, H. Jneid, E. V. Krieger, M. Mack, C. McLeod, P.T. O’Gara, V.H. Rigolin, T.M. Sundt, A. Thompson, C. Toly, 2020 ACC/AHA Guideline for the Management of Patients With Valvular Heart Disease: A Report of the American College of Cardiology/American Heart Association Joint Committee on Clinical Practice Guidelines, *J. Am. Coll. Cardiol.* 77 (2021) e25–e197. <https://doi.org/10.1016/j.jacc.2020.11.018>.

- [11] J. Kluin, H. Talacua, A.I.P.M. Smits, M.Y. Emmert, M.C.P. Brugmans, E.S. Fioretta, P.E. Dijkman, S.H.M. Söntjens, R. Duijvelshoff, S. Dekker, M.W.J.T. Janssen-van den Broek, V. Lintas, A. Vink, S.P. Hoerstrup, H.M. Janssen, P.Y.W. Dankers, F.P.T. Baaijens, C.V.C. Bouten, In situ heart valve tissue engineering using a bioresorbable elastomeric implant – From material design to 12 months follow-up in sheep, *Biomaterials*. 125 (2017) 101–117. <https://doi.org/10.1016/j.biomaterials.2017.02.007>.
- [12] J.G. Rheinwald, H. Green, Serial cultivation of strains of human epidermal keratinocytes: the formation of keratinizing colonies from single cells, *Cell*. (1975).
- [13] E. Bell, H.P. Ehrlich, D. Buttle, T. Nakatsuji, Bell E, Ehrlich HP, Buttle DJ, Nakatsuji T Living tissue formed in vitro and accepted as skin-equivalent tissue of full thickness. *Science* 211:1052-1054, 1981. <https://doi.org/10.1126/science.7008197>.
- [14] I. V. Yannas, J.F. Burke, D.P. Orgill, E.M. Skrabut, Wound tissue can utilize a polymeric template to synthesize a functional extension of skin, *Science* (80-.). (1982). <https://doi.org/10.1126/science.7031899>.
- [15] J.P. Vacanti, Beyond Transplantation: Third Annual Samuel Jason Mixter Lecture, *Arch. Surg.* (1988). <https://doi.org/10.1001/archsurg.1988.01400290027003>.
- [16] P. Kemp, History of regenerative medicine: looking backwards to move forwards., *Regen. Med.* 1 (2006) 653–669. <https://doi.org/10.2217/17460751.1.5.653>.
- [17] S. Roberts, Howard Green, Who Found a Way to Grow Skin and Saved Lives, Dies at 90, (2015).
- [18] J.G. Rheinwald, H. Green, Serial cultivation of strains of human epidermal keratinocytes: the formation of keratinizing colonies from single cells, *Cell*. (1975). [https://doi.org/10.1016/S0092-8674\(75\)80001-8](https://doi.org/10.1016/S0092-8674(75)80001-8).
- [19] H. Green, O. Kehinde, J. Thomas, Growth of cultured human epidermal cells into multiple epithelia suitable for grafting, *Proc. Natl. Acad. Sci. U. S. A.* (1979). <https://doi.org/10.1073/pnas.76.11.5665>.
- [20] N.E. O’Connor, J.B. Mulliken, S. Banks-Schlegel, O. Kehinde, H. Green, GRAFTING OF BURNS WITH CULTURED EPITHELIUM PREPARED FROM AUTOLOGOUS EPIDERMAL CELLS, *Lancet*. (1981).

- [https://doi.org/10.1016/S0140-6736\(81\)90006-4](https://doi.org/10.1016/S0140-6736(81)90006-4).
- [21] Y. Cao, J.P. Vacanti, K.T. Paige, J. Upton, C.A. Vacanti, Transplantation of chondrocytes utilizing a polymer-cell construct to produce tissue-engineered cartilage in the shape of a human ear, *Plast. Reconstr. Surg.* 100 (1997) 297–304. <https://doi.org/10.1097/00006534-199708000-00001>.
- [22] M. Casarin, A. Morlacco, F. Dal Moro, Bladder substitution: The role of tissue engineering and biomaterials, *Processes.* 9 (2021) 1–16. <https://doi.org/10.3390/pr9091643>.
- [23] A. Atala, S.B. Bauer, S. Soker, J.J. Yoo, A.B. Retik, Tissue-engineered autologous bladders for patients needing cystoplasty, *Lancet.* 367 (2006) 1241–1246. [https://doi.org/10.1016/S0140-6736\(06\)68438-9](https://doi.org/10.1016/S0140-6736(06)68438-9).
- [24] Epicel - Surgical Guidelines, (2018). <https://www.epicel.com/pdfs/EpicelSurgicalGuide2018DIGITAL.pdf>.
- [25] A. Tapalaga, The Ear-Mouse That Changed Our World, (n.d.). <https://historyofyesterday.com/the-ear-mouse-that-changed-our-world-e40f0e98756d>.
- [26] H. Pearson, Scientists grow bladder replacement in lab, (n.d.). <https://www.nature.com/news/2006/060403/full/news060403-3.html>.
- [27] J. Wang, D. Huang, H. Yu, Y. Cheng, H. Ren, Y. Zhao, Developing tissue engineering strategies for liver regeneration, *Eng. Regen.* 3 (2022) 80–91. <https://doi.org/10.1016/j.engreg.2022.02.003>.
- [28] G. Mazza, W. Al-Akkad, K. Rombouts, M. Pinzani, Liver tissue engineering: From implantable tissue to whole organ engineering, *Hepatol. Commun.* 2 (2018) 131–141. <https://doi.org/10.1002/hep4.1136>.
- [29] J. Rawe, What Will Be the 10 Hottest Jobs?, *Time Mag.* (2000). <http://content.time.com/time/magazine/article/0,9171,997028,00.html>.
- [30] G. Kratz, F. Huss, Tissue engineering - Body parts from the petri dish, *Scand. J. Surg.* (2003). <https://doi.org/10.1177/145749690309200402>.
- [31] A.S. Mao, D.J. Mooney, Regenerative medicine: Current therapies and future directions, *Proc. Natl. Acad. Sci. U. S. A.* (2015). <https://doi.org/10.1073/pnas.1508520112>.
- [32] B.T. O'Donnell, C.J. Ives, O.A. Mohiuddin, B.A. Bunnell, Beyond the Present

- Constraints That Prevent a Wide Spread of Tissue Engineering and Regenerative Medicine Approaches, *Front. Bioeng. Biotechnol.* 7 (2019) 1–12. <https://doi.org/10.3389/fbioe.2019.00095>.
- [33] R. Goedkoop, R. Juliet, P.H.K. You, J. Daroczy, K.P. De Roos, R. Lijnen, E. Rolland, T. Hunziker, Wound stimulation by growth-arrested human keratinocytes and fibroblasts: HP802-247, a new-generation allogeneic tissue engineering product, *Dermatology.* 220 (2010) 114–120. <https://doi.org/10.1159/000277380>.
- [34] P. Pleguezuelos-Beltrán, P. Gálvez-Martín, D. Nieto-García, J.A. Marchal, E. López-Ruiz, Advances in spray products for skin regeneration, *Bioact. Mater.* 16 (2022) 187–203. <https://doi.org/10.1016/j.bioactmat.2022.02.023>.
- [35] R. Esteban-Vives, A. Corcos, M.S. Choi, M.T. Young, P. Over, J. Ziembicki, J.C. Gerlach, Cell-spray auto-grafting technology for deep partial-thickness burns: Problems and solutions during clinical implementation, *Burns.* 44 (2018) 549–559. <https://doi.org/10.1016/j.burns.2017.10.008>.
- [36] A. Mogedas-Vegara, E. Agut-Busquet, M. Yébenes Marsal, J. Luelmo Aguilar, Ò. Escuder de la Torre, Integra as Firstline Treatment for Scalp Reconstruction in Elderly Patients, *J. Oral Maxillofac. Surg.* 79 (2021) 2593–2602. <https://doi.org/10.1016/j.joms.2021.07.009>.
- [37] M.J. Stein, A. Arnaout, J.B. Lichtenstein, S.G. Frank, E. Cordeiro, A. Roberts, B. Ghaedi, J. Zhang, A comparison of patient-reported outcomes between Alloderm and Dermacell in immediate alloplastic breast reconstruction: A randomized control trial, *J. Plast. Reconstr. Aesthetic Surg.* 74 (2021) 41–47. <https://doi.org/10.1016/j.bjps.2020.08.018>.
- [38] H. Park, A.M. Collignon, W.C. Lepry, J.L. Ramirez-GarciaLuna, D.H. Rosenzweig, C. Chaussain, S.N. Nazhat, Acellular dense collagen-S53P4 bioactive glass hybrid gel scaffolds form more bone than stem cell delivered constructs, *Mater. Sci. Eng. C.* 120 (2021) 111743. <https://doi.org/10.1016/j.msec.2020.111743>.
- [39] C.P. Barnes, S.A. Sell, E.D. Boland, D.G. Simpson, G.L. Bowlin, Nanofiber technology: Designing the next generation of tissue engineering scaffolds, *Adv. Drug Deliv. Rev.* 59 (2007) 1413–1433. <https://doi.org/10.1016/j.addr.2007.04.022>.

- [40] S. Pompili, G. Latella, E. Gaudio, R. Sferra, A. Vetuschi, The Charming World of the Extracellular Matrix: A Dynamic and Protective Network of the Intestinal Wall, *Front. Med.* 8 (2021) 1–19. <https://doi.org/10.3389/fmed.2021.610189>.
- [41] M. Scarritt, M. Murdock, S.F. Badylak, *Biologic Scaffolds Composed of Extracellular Matrix for Regenerative Medicine*, Elsevier Inc., 2019. <https://doi.org/10.1016/B978-0-12-809880-6.00035-7>.
- [42] S.N. Popova, E. Lundgren-Åkerlund, H. Wiig, D. Gullberg, Physiology and pathology of collagen receptors, *Acta Physiol.* 190 (2007) 179–187. <https://doi.org/10.1111/j.1748-1716.2007.01718.x>.
- [43] S.A. Sell, P.S. Wolfe, K. Garg, J.M. McCool, I.A. Rodriguez, G.L. Bowlin, The use of natural polymers in tissue engineering: A focus on electrospun extracellular matrix analogues, *Polymers (Basel)*. 2 (2010) 522–553. <https://doi.org/10.3390/polym2040522>.
- [44] A. Kumar, K.C. Nune, R.D.K. Misra, Biological functionality of extracellular matrix-ornamented three-dimensional printed hydroxyapatite scaffolds, *J. Biomed. Mater. Res. - Part A*. 104 (2016) 1343–1351. <https://doi.org/10.1002/jbm.a.35664>.
- [45] K. Molnar, D. Juriga, P.M. Nagy, K. Sinko, A. Jedlovszky-Hajdu, M. Zrinyi, Electrospun poly(aspartic acid) gel scaffolds for artificial extracellular matrix, *Polym. Int.* 63 (2014) 1608–1615. <https://doi.org/10.1002/pi.4720>.
- [46] E.H. Lim, J.P. Sardinha, S. Myers, Nanotechnology biomimetic cartilage regenerative scaffolds, *Arch. Plast. Surg.* 41 (2014) 231–240. <https://doi.org/10.5999/aps.2014.41.3.231>.
- [47] J.A. Matthews, G.E. Wnek, D.G. Simpson, G.L. Bowlin, Electrospinning of collagen nanofibers, *Biomacromolecules*. 3 (2002) 232–238. <https://doi.org/10.1021/bm015533u>.
- [48] F.J. O'Brien, Biomaterials & scaffolds for tissue engineering, *Mater. Today*. 14 (2011) 88–95. [https://doi.org/10.1016/S1369-7021\(11\)70058-X](https://doi.org/10.1016/S1369-7021(11)70058-X).
- [49] S. Naahidi, M. Jafari, M. Logan, Y. Wang, Y. Yuan, H. Bae, B. Dixon, P. Chen, Biocompatibility of hydrogel-based scaffolds for tissue engineering applications, *Biotechnol. Adv.* 35 (2017) 530–544. <https://doi.org/10.1016/j.biotechadv.2017.05.006>.
- [50] B. V. Slaughter, S.S. Khurshid, O.Z. Fisher, A. Khademhosseini, N.A. Peppas,

- Hydrogels in regenerative medicine, *Adv. Mater.* 21 (2009) 3307–3329. <https://doi.org/10.1002/adma.200802106>.
- [51] J.M. Anderson, A. Rodriguez, D.T. Chang, Foreign body reaction to biomaterials, *Semin. Immunol.* 20 (2008) 86–100. <https://doi.org/10.1016/j.smim.2007.11.004>.
- [52] D.W. Hutmacher, Scaffolds in tissue engineering bone and cartilage, *Biomater. Silver Jubil. Compd.* 21 (2000) 175–189. <https://doi.org/10.1016/B978-008045154-1.50021-6>.
- [53] B. Saad, U.W. Suter, Biodegradable Polymeric Materials, *Encycl. Mater. Sci. Technol.* (2001) 551–555. <https://doi.org/10.1016/b0-08-043152-6/00105-4>.
- [54] A.C. Panayi, D.P. Orgill, Current use of biological scaffolds in plastic surgery, *Plast. Reconstr. Surg.* 143 (2019) 209E–220E. <https://doi.org/10.1097/PRS.00000000000005102>.
- [55] N.H.A. Ngadiman, M.Y. Noordin, D. Kurniawan, A. Idris, A.S.A. Shakir, Influence of Polyvinyl Alcohol Molecular Weight on the Electrospun Nanofiber Mechanical Properties, *Procedia Manuf.* 2 (2015) 568–572. <https://doi.org/10.1016/j.promfg.2015.07.098>.
- [56] V.M. Torres, J.A. LaNasa, B.D. Vogt, R.J. Hickey, Controlling nanostructure and mechanical properties in triblock copolymer/monomer blends via reaction-induced phase transitions, *Soft Matter.* 17 (2021) 1505–1512. <https://doi.org/10.1039/d0sm01661f>.
- [57] S. Yang, K.F. Leong, Z. Du, C.K. Chua, The design of scaffolds for use in tissue engineering. Part I. Traditional factors, *Tissue Eng.* 7 (2001) 679–689. <https://doi.org/10.1089/107632701753337645>.
- [58] B.J. Lawrence, S. V. Madhally, Cell colonization in degradable 3D porous matrices., *Cell Adh. Migr.* 2 (2008) 9–16. <https://doi.org/10.4161/cam.2.1.5884>.
- [59] F.J. O'Brien, B.A. Harley, I. V. Yannas, L.J. Gibson, The effect of pore size on cell adhesion in collagen-GAG scaffolds, *Biomaterials.* 26 (2005) 433–441. <https://doi.org/10.1016/j.biomaterials.2004.02.052>.
- [60] K.P. Feltz, E.A.G. Kalaf, C. Chen, R.S. Martin, S.A. Sell, A review of electrospinning manipulation techniques to direct fiber deposition and maximize pore size, *Electrospinning.* 1 (2017) 46–61. <https://doi.org/10.1515/esp-2017-0002>.

- [61] M. Vanpeene, R. Rajesh, Y.D. Ravichandran, Y.C. Kuo, G. Gure, Biomimetic Graphene Oxide-Xanthan Gum-Hydroxyapatite Composite Scaffold for Bone Tissue Engineering, *Chem. Africa*. (2022). <https://doi.org/10.1007/s42250-022-00368-7>.
- [62] C. Voniatis, L. Balsevicius, D. Barczikai, D. Juriga, A. Takács, L. Kóhidai, K. Nagy, A. Jedlovszky-Hajdu, Co-electrospun polysuccinimide/poly(vinyl alcohol) composite meshes for tissue engineering, *J. Mol. Liq.* 306 (2020) 0–8. <https://doi.org/10.1016/j.molliq.2020.112895>.
- [63] L.A. de Sousa Iwamoto, M.T. Duailibi, G.Y. Iwamoto, D.C. de Oliveira, S.E. Duailibi, Evaluation of ethylene oxide, gamma radiation, dry heat and autoclave sterilization processes on extracellular matrix of biomaterial dental scaffolds, *Sci. Rep.* 12 (2022) 1–10. <https://doi.org/10.1038/s41598-022-08258-1>.
- [64] X.L. Deng, M.M. Xu, D. Li, G. Sui, X.Y. Hu, X.P. Yang, Electrospun PLLA/MWNTs/HA Hybrid Nanofiber Scaffolds and Their Potential in Dental Tissue Engineering, *Key Eng. Mater.* 330–332 (2007) 393–396. <https://doi.org/10.4028/www.scientific.net/kem.330-332.393>.
- [65] M. Farno, C. Lamarche, C. Tenailleau, S. Cavalié, B. Duployer, D. Cussac, A. Parini, B. Sallerin, S. Girod Fullana, Low-energy electron beam sterilization of solid alginate and chitosan, and their polyelectrolyte complexes, *Carbohydr. Polym.* 261 (2021). <https://doi.org/10.1016/j.carbpol.2020.117578>.
- [66] V. Santos-Rosales, B. Magariños, C. Alvarez-Lorenzo, C.A. García-González, Combined sterilization and fabrication of drug-loaded scaffolds using supercritical CO₂ technology, *Int. J. Pharm.* 612 (2022). <https://doi.org/10.1016/j.ijpharm.2021.121362>.
- [67] C.E. Holy, C. Cheng, J.E. Davies, M.S. Shoichet, Optimizing the sterilization of PLGA scaffolds for use in tissue engineering, *Biomaterials*. 22 (2000) 25–31. [https://doi.org/10.1016/S0142-9612\(00\)00136-8](https://doi.org/10.1016/S0142-9612(00)00136-8).
- [68] K. Haberstroh, K. Ritter, J. Kuschnierz, K.H. Bormann, C. Kaps, C. Carvalho, R. Mülhaupt, M. Sittinger, N.C. Gellrich, Bone repair by cell-seeded 3D-bioplotting composite scaffolds made of collagen treated tricalciumphosphate or tricalciumphosphate-chitosan-collagen hydrogel or PLGA in ovine critical-sized calvarial defects, *J. Biomed. Mater. Res. - Part B Appl. Biomater.* 93 (2010) 520–

530. <https://doi.org/10.1002/jbm.b.31611>.
- [69] X. Liu, P.X. Ma, Polymeric scaffolds for bone tissue engineering, *Ann. Biomed. Eng.* 32 (2004) 477–486. <https://doi.org/10.1023/B:ABME.0000017544.36001.8e>.
- [70] T.S. Karande, C.M. Agrawal, Functions and requirements of synthetic scaffolds in tissue engineering, *Nanotechnol. Tissue Eng. Scaffold.* (2008) 53–86. <https://doi.org/10.1201/9781420051834.ch3>.
- [71] J.O. Baur, A. Rahmanian-Schwarz, M. Held, J. Schiefer, A. Daigeler, W. Eisler, Evaluation of a cross-linked versus non-cross-linked collagen matrix in full-thickness skin defects, *Burns.* 47 (2021) 150–156. <https://doi.org/10.1016/j.burns.2020.03.018>.
- [72] S. Liu, C. Fan, Y. Xie, L. Wang, Y. Cui, B. Wang, Collagen scaffold loaded allogeneic neural stem cells promoted locomotion recovery of spinal cord injury mainly through secreting neurotrophic factors, *Mater. Des.* 219 (2022) 110804. <https://doi.org/10.1016/j.matdes.2022.110804>.
- [73] J. Indrakumar, P. Balan, P. Murali, A. Solaimuthu, A.N. Vijayan, P.S. Korrapati, Applications of molybdenum oxide nanoparticles impregnated collagen scaffolds in wound therapeutics, *J. Trace Elem. Med. Biol.* 72 (2022) 126983. <https://doi.org/10.1016/j.jtemb.2022.126983>.
- [74] A.R. Matheson, E.J. Sheehy, G.D. Jay, W.M. Scott, F.J. O'Brien, T.A. Schmidt, The role of synovial fluid constituents in the lubrication of collagen-glycosaminoglycan scaffolds for cartilage repair, *J. Mech. Behav. Biomed. Mater.* 118 (2021) 104445. <https://doi.org/10.1016/j.jmbbm.2021.104445>.
- [75] S. Minardi, M. Guo, X. Zhang, X. Luo, An elastin-based vasculogenic scaffold promotes marginal islet mass engraftment and function at an extrahepatic site, *J. Immunol. Regen. Med.* 3 (2019) 1–12. <https://doi.org/10.1016/j.regen.2018.12.001>.
- [76] T. Liu, C. Qiu, H. Lu, H. Li, S. Zhu, L. Ma, A novel recombinant human collagen hydrogel as minced split-thickness skin graft overlay to promote full-thickness skin defect reconstruction, *Burns.* (2022) 1–15. <https://doi.org/10.1016/j.burns.2022.02.015>.
- [77] N. Pallua, C. V. Suschek, Tissue engineering: From lab to clinic, *Tissue Eng. From Lab to Clin.* 9783642028 (2011) 1–634. <https://doi.org/10.1007/978-3-642-02824->

3.

- [78] D. Xu, Z. XU, L. Cheng, X. Gao, J. Sun, L. Chen, Improvement of the Mechanical Properties and Osteogenic Activity of 3D Printed Polylactic Acid Porous Scaffolds by the Nano Hydroxyapatite and Nano Magnesium Oxide, *SSRN Electron. J.* 8 (2022) e09748. <https://doi.org/10.2139/ssrn.4065412>.
- [79] C.C. Lin, J.Y. Chiu, Glycerol-modified γ -PGA and gellan composite hydrogel materials with tunable physicochemical and thermal properties for soft tissue engineering application, *Polymer (Guildf)*. 230 (2021) 124049. <https://doi.org/10.1016/j.polymer.2021.124049>.
- [80] J. Wei, Y. Yan, J. Gao, Y. Li, R. Wang, J. Wang, Q. Zou, Y. Zuo, M. Zhu, J. Li, 3D-printed hydroxyapatite microspheres reinforced PLGA scaffolds for bone regeneration, *Mater. Sci. Eng. C*. 133 (2022) 112618. <https://doi.org/10.1016/j.msec.2021.112618>.
- [81] P. Gentile, V. Chiono, I. Carmagnola, P. V. Hatton, An overview of poly(lactic-co-glycolic) Acid (PLGA)-based biomaterials for bone tissue engineering, *Int. J. Mol. Sci.* 15 (2014) 3640–3659. <https://doi.org/10.3390/ijms15033640>.
- [82] D. Nataraj, R. Reddy, N. Reddy, Crosslinking electrospun poly (vinyl) alcohol fibers with citric acid to impart aqueous stability for medical applications, *Eur. Polym. J.* 124 (2020) 109484. <https://doi.org/10.1016/j.eurpolymj.2020.109484>.
- [83] J. Chen, T. Zhang, W. Hua, P. Li, X. Wang, 3D Porous poly(lactic acid)/regenerated cellulose composite scaffolds based on electrospun nanofibers for biomineralization, *Colloids Surfaces A Physicochem. Eng. Asp.* 585 (2020) 124048. <https://doi.org/10.1016/j.colsurfa.2019.124048>.
- [84] C. Voniatis, D. Barczikai, G. Gyulai, A. Jedlovszky-Hajdu, Fabrication and characterisation of electrospun Polycaprolactone/Polysuccinimide composite meshes, *J. Mol. Liq.* 323 (2021). <https://doi.org/10.1016/j.molliq.2020.115094>.
- [85] Y. Xu, C.S. Kim, D.M. Saylor, D. Koo, Polymer degradation and drug delivery in PLGA-based drug–polymer applications: A review of experiments and theories, *J. Biomed. Mater. Res. - Part B Appl. Biomater.* 105 (2017) 1692–1716. <https://doi.org/10.1002/jbm.b.33648>.
- [86] R.A. Miller, J.M. Brady, D.E. Cutright, Degradation rates of oral resorbable implants (polylactates and polyglycolates): Rate modification with changes in

- PLA/PGA copolymer ratios, *J. Biomed. Mater. Res.* 11 (1977) 711–719. <https://doi.org/10.1002/jbm.820110507>.
- [87] H. Liu, E.B. Slamovich, T.J. Webster, Less harmful acidic degradation of poly(lactic-co-glycolic acid) bone tissue engineering scaffolds through titania nanoparticle addition, *Int. J. Nanomedicine.* 1 (2006) 541–545. <https://doi.org/10.2147/nano.2006.1.4.541>.
- [88] J.H. An, N.T. Huynh, Y. Sil Jeon, J.H. Kim, Surface modification using bio-inspired adhesive polymers based on polyaspartamide derivatives, *Polym. Int.* 60 (2011) 1581–1586. <https://doi.org/10.1002/pi.3116>.
- [89] H. Adelnia, H.D.N. Tran, P.J. Little, I. Blakey, H.T. Ta, Poly(aspartic acid) in Biomedical Applications: From Polymerization, Modification, Properties, Degradation, and Biocompatibility to Applications, *ACS Biomater. Sci. Eng.* 7 (2021) 2083–2105. <https://doi.org/10.1021/acsbiomaterials.1c00150>.
- [90] E.G.R. Fernandes, V. Zucolotto, A.A.A. De Queiroz, Electrospinning of hyperbranched poly-L-lysine/polyaniline nanofibers for application in cardiac tissue engineering, *J. Macromol. Sci. Part A Pure Appl. Chem.* 47 (2010) 1203–1207. <https://doi.org/10.1080/10601325.2010.518847>.
- [91] T. Xu, R. Yang, X. Ma, W. Chen, S. Liu, X. Liu, X. Cai, H. Xu, B. Chi, Bionic Poly(γ -Glutamic Acid) Electrospun Fibrous Scaffolds for Preventing Hypertrophic Scars, *Adv. Healthc. Mater.* 8 (2019) 1–12. <https://doi.org/10.1002/adhm.201900123>.
- [92] T. Tajima, S. Ueno, N. Yabu, S. Sukigara, F. Ko, Fabrication and Characterization of Poly-c-glutamic Acid Nanofiber, *J. Appl. Polym. Sci.* 122 (2011) 150–158. <https://doi.org/10.1002/app>.
- [93] B. Gyarmati, E.Z. Mészár, L. Kiss, M.A. Deli, K. László, A. Szilágyi, Supermacroporous chemically cross-linked poly(aspartic acid) hydrogels, *Acta Biomater.* 22 (2015) 32–38. <https://doi.org/10.1016/j.actbio.2015.04.033>.
- [94] E. Çatıker, E. Konuk, T. Gültan, M. Gümüşderelioğlu, Enhancement of scaffolding properties for poly(3-hydroxybutyrate): blending with poly- β -alanine and wet electrospinning, *Int. J. Polym. Mater. Polym. Biomater.* 68 (2019) 338–349. <https://doi.org/10.1080/00914037.2018.1552862>.
- [95] D. Juriga, E. Sipos, O. Hegedus, G. Varga, M. Zrínyi, K.S. Nagy, A. Jedlovsky-

- Hajdú, Fully amino acid-based hydrogel as potential scaffold for cell culturing and drug delivery, *Beilstein J. Nanotechnol.* 10 (2019) 2579–2593. <https://doi.org/10.3762/bjnano.10.249>.
- [96] C. Németh, D. Szabó, B. Gyarmati, A. Gerasimov, M. Varfolomeev, T. Abdullin, K. László, A. Szilágyi, Effect of side groups on the properties of cationic polyaspartamides, *Eur. Polym. J.* 93 (2017) 805–814. <https://doi.org/10.1016/j.eurpolymj.2017.02.024>.
- [97] D. Juriga, I. Laszlo, K. Ludanyi, I. Klebovich, C.H. Chae, M. Zrinyi, Kinetics of dopamine release from poly(aspartamide)-based prodrugs, *Acta Biomater.* 76 (2018) 225–238. <https://doi.org/10.1016/j.actbio.2018.06.030>.
- [98] G. Horvát, B. Gyarmati, S. Berkó, P. Szabó-Révész, B.Á. Szilágyi, A. Szilágyi, J. Soós, G. Sandri, M.C. Bonferoni, S. Rossi, F. Ferrari, C. Caramella, E. Csányi, M. Budai-Szucs, Thiolated poly(aspartic acid) as potential in situ gelling, ocular mucoadhesive drug delivery system, *Eur. J. Pharm. Sci.* 67 (2015) 1–11. <https://doi.org/10.1016/j.ejps.2014.10.013>.
- [99] M. Xu, Y. Zhao, M. Feng, Polyaspartamide derivative nanoparticles with tunable surface charge achieve highly efficient cellular uptake and low cytotoxicity, *Langmuir.* 28 (2012) 11310–11318. <https://doi.org/10.1021/la3025028>.
- [100] K. Molnar, R. Varga, B. Jozsa, D. Barczikai, E. Krisch, K.S. Nagy, G. Varga, A. Jedlovszky-Hajdu, J.E. Puskas, Investigation of the cytotoxicity of electrospun polysuccinimide-based fiber mats, *Polymers (Basel).* 12 (2020) 1–11. <https://doi.org/10.3390/polym12102324>.
- [101] K.T. Nguyen, J.L. West, Photopolymerizable hydrogels for tissue engineering applications, *Biomaterials.* 23 (2002) 4307–4314.
- [102] D. Juriga, K.S. Nagy, A. Jedlovszky-Hajdu, K. Perczel-Kovach, Y.M. Chen, G. Varga, M. Zrinyi, Biodegradation and osteosarcoma cell cultivation on poly(aspartic acid) based hydrogels, *ACS Appl. Mater. Interfaces.* 8 (2016) 23463–23476. <https://doi.org/10.1021/acsami.6b06489>.
- [103] K. Molnar, C. Voniatis, D. Feher, G. Szabo, R. Varga, L. Reiniger, D. Juriga, Z. Kiss, E. Krisch, G. Weber, A. Ferencz, G. Varga, M. Zrinyi, K.S. Nagy, A. Jedlovszky-Hajdu, Poly(amino acid) based fibrous membranes with tuneable in vivo biodegradation, *PLoS One.* 16 (2021) e0254843.

- <https://doi.org/10.1371/journal.pone.0254843>.
- [104] D. Poly, D. Juriga, E.E. Kalman, K. Toth, D. Barczikai, D. Szöll, A. Földes, K.S. Nagy, Analysis of Three-Dimensional Cell Migration in Dopamine-Modified Poly(aspartic acid)-Based Hydrogels, (2022).
- [105] A. Sola, J. Bertacchini, D. D’Avella, L. Anselmi, T. Maraldi, S. Marmioli, M. Messori, Development of solvent-casting particulate leaching (SCPL) polymer scaffolds as improved three-dimensional supports to mimic the bone marrow niche, *Mater. Sci. Eng. C.* 96 (2019) 153–165. <https://doi.org/10.1016/j.msec.2018.10.086>.
- [106] I.K. Januariyasa, Y. Yusuf, Porous carbonated hydroxyapatite-based scaffold using simple gas foaming method, *J. Asian Ceram. Soc.* 8 (2020) 634–641. <https://doi.org/10.1080/21870764.2020.1770938>.
- [107] J. Wang, Y. Zhang, N.H. Aghda, A.R. Pillai, R. Thakkar, A. Nokhodchi, M. Maniruzzaman, Emerging 3D printing technologies for drug delivery devices: Current status and future perspective, *Adv. Drug Deliv. Rev.* 174 (2021) 294–316. <https://doi.org/10.1016/j.addr.2021.04.019>.
- [108] M. Sharafeldin, A. Jones, J.F. Rusling, 3D-printed biosensor arrays for medical diagnostics, *Micromachines.* 9 (2018) 1–22. <https://doi.org/10.3390/mi9080394>.
- [109] Z. Wang, Y. Wang, J. Yan, K. Zhang, F. Lin, L. Xiang, L. Deng, Z. Guan, W. Cui, H. Zhang, Pharmaceutical electrospinning and 3D printing scaffold design for bone regeneration, *Adv. Drug Deliv. Rev.* 174 (2021) 504–534. <https://doi.org/10.1016/j.addr.2021.05.007>.
- [110] J. Babilotte, B. Martin, V. Guduric, R. Bareille, R. Agniel, S. Roques, V. Héroguez, M. Dussauze, M. Gaudon, D. Le Nihouannen, S. Catros, Development and characterization of a PLGA-HA composite material to fabricate 3D-printed scaffolds for bone tissue engineering, *Mater. Sci. Eng. C.* 118 (2021) 111334. <https://doi.org/10.1016/j.msec.2020.111334>.
- [111] J.W. D. Annis, A. Bornat, R.O. Edwards, A. Higham, B. Loveday, An elastomeric vascular prosthesis, *Trans. Am. Soc. Artif. Intern. Organs.* 24 (1978) 209–214.
- [112] G.E. Martin, I.D. Cockshott, F.J.T. Fildes, FIBRILLAR LINING FOR PROSTHETIC DEVICE, 1977.
- [113] A. Kazsoki, B. Palcsó, A. Alpár, R. Snoeck, G. Andrei, R. Zelkó, Formulation of

- acyclovir (core)-dexpanthenol (sheath) nanofibrous patches for the treatment of herpes labialis, *Int. J. Pharm.* 611 (2022). <https://doi.org/10.1016/j.ijpharm.2021.121354>.
- [114] K. Kiss, K. Hegedüs, P. Vass, D. Vári-Mező, A. Farkas, Z.K. Nagy, L. Molnár, J. Tóvári, G. Mező, G. Marosi, Development of fast-dissolving dosage forms of curcuminoids by electrospinning for potential tumor therapy application, *Int. J. Pharm.* 611 (2022). <https://doi.org/10.1016/j.ijpharm.2021.121327>.
- [115] J. Chen, G. Zhang, Y. Zhao, M. Zhou, A. Zhong, J. Sun, Promotion of skin regeneration through co-axial electrospun fibers loaded with basic fibroblast growth factor, *Adv. Compos. Hybrid Mater.* (2022). <https://doi.org/10.1007/s42114-022-00439-w>.
- [116] V. Perez-Puyana, P. Wieringa, Y. Yuste, F. de la Portilla, A. Guerro, A. Romero, L. Moroni, Fabrication of hybrid scaffolds obtained from combinations of PCL with gelatin or collagen via electrospinning for skeletal muscle tissue engineering, *J. Biomed. Mater. Res. - Part A.* 109 (2021) 1600–1612. <https://doi.org/10.1002/jbm.a.37156>.
- [117] Y. Chen, W. Xu, M. Shafiq, J. Tang, J. Hao, X. Xie, Z. Yuan, X. Xiao, Y. Liu, X. Mo, Three-dimensional porous gas-foamed electrospun nanofiber scaffold for cartilage regeneration, *J. Colloid Interface Sci.* 603 (2021) 94–109. <https://doi.org/10.1016/j.jcis.2021.06.067>.
- [118] E. Saatcioglu, S. Ulag, A. Sahin, B.K. Yilmaz, N. Ekren, A.T. Inan, Y. Palaci, C.B. Ustundag, O. Gunduz, Design and fabrication of electrospun polycaprolactone/chitosan scaffolds for ligament regeneration, *Eur. Polym. J.* 148 (2021). <https://doi.org/10.1016/j.eurpolymj.2021.110357>.
- [119] M.A. Asl, S. Karbasi, S. Beigi-Boroujeni, S. Zamanlui Benisi, M. Saeed, Evaluation of the effects of starch on polyhydroxybutyrate electrospun scaffolds for bone tissue engineering applications, *Int. J. Biol. Macromol.* 191 (2021) 500–513. <https://doi.org/10.1016/j.ijbiomac.2021.09.078>.
- [120] X. Chen, X. Ge, Y. Qian, H. Tang, J. Song, X. Qu, B. Yue, W.E. Yuan, Electrospinning Multilayered Scaffolds Loaded with Melatonin and Fe₃O₄ Magnetic Nanoparticles for Peripheral Nerve Regeneration, *Adv. Funct. Mater.* 30 (2020) 1–12. <https://doi.org/10.1002/adfm.202004537>.

- [121] Z.K. Nagy, A. Balogh, G. Drávavölgyi, J. Ferguson, H. Pataki, B. Vajna, G. Marosi, Solvent-free melt electrospinning for preparation of fast dissolving drug delivery system and comparison with solvent-based electrospun and melt extruded systems, *J. Pharm. Sci.* 102 (2013) 508–517. <https://doi.org/10.1002/jps.23374>.
- [122] G.R. William, B.T. Raimi-Abraham, C.J. Luo, *Nanofibres in Drug Delivery*, 2018.
- [123] D.W. Schubert, Revealing Novel Power Laws and Quantization in Electrospinning Considering Jet Splitting—Toward Predicting Fiber Diameter and Its Distribution, *Macromol. Theory Simulations*. 28 (2019) 1–9. <https://doi.org/10.1002/mats.201900006>.
- [124] Q. Zhou, L. Lin, G. Chen, Z. Du, Prediction and optimization of electrospun polyacrylonitrile fiber diameter based on grey system theory, *Materials (Basel)*. 12 (2019). <https://doi.org/10.3390/ma12142237>.
- [125] K.H. Sizeland, K.A. Hofman, I.C. Hallett, D.E. Martin, J. Potgieter, N.M. Kirby, A. Hawley, S.T. Mudie, T.M. Ryan, R.G. Haverkamp, M.H. Cumming, Nanostructure of electrospun collagen: Do electrospun collagen fibers form native structures?, *Materialia*. 3 (2018) 90–96. <https://doi.org/10.1016/j.mtla.2018.10.001>.
- [126] S. Asadpour, S. Kargozar, L. Moradi, A. Ai, H. Nosrati, J. Ai, Natural biomacromolecule based composite scaffolds from silk fibroin, gelatin and chitosan toward tissue engineering applications, *Int. J. Biol. Macromol.* 154 (2020) 1285–1294. <https://doi.org/10.1016/j.ijbiomac.2019.11.003>.
- [127] P. Ginestra, E. Ceretti, A. Fiorentino, Electrospinning of Poly-caprolactone for Scaffold Manufacturing: Experimental Investigation on the Process Parameters Influence, *Procedia CIRP*. 49 (2016) 8–13. <https://doi.org/10.1016/j.procir.2015.07.020>.
- [128] Utkarsh, H. Hegab, M. Tariq, N.A. Syed, G. Rizvi, R. Pop-Iliev, Towards Analysis and Optimization of Electrospun PVP (Polyvinylpyrrolidone) Nanofibers, *Adv. Polym. Technol.* 2020 (2020) 1–9. <https://doi.org/10.1155/2020/4090747>.
- [129] M. Alessandri, G. Lizzo, C. Gualandi, C. Mangano, A. Giuliani, M.L. Focarete, L. Calzà, Influence of biological matrix and artificial electrospun scaffolds on proliferation, differentiation and trophic factor synthesis of rat embryonic stem cells, *Matrix Biol.* 33 (2014) 68–76. <https://doi.org/10.1016/j.matbio.2013.08.001>.

- [130] C. Németh, B. Gyarmati, J. Gacs, D. V. Salakhieva, K. Molnár, T. Abdullin, K. László, A. Szilágyi, Fast dissolving nanofibrous matrices prepared by electrospinning of polyaspartamides, *Eur. Polym. J.* 130 (2020) 109624. <https://doi.org/10.1016/j.eurpolymj.2020.109624>.
- [131] K. Molnar, A. Jedlovszky-Hajdu, M. Zrinyi, S. Jiang, S. Agarwal, Poly(amino acid)-Based Gel Fibers with pH Responsivity by Coaxial Reactive Electrospinning, *Macromol. Rapid Commun.* 38 (2017) 1700147. <https://doi.org/10.1002/marc.201700147>.
- [132] Z. Tan, H. Wang, X. Gao, T. Liu, Y. Tan, Composite vascular grafts with high cell infiltration by co-electrospinning, *Mater. Sci. Eng. C.* 67 (2016) 369–377. <https://doi.org/10.1016/j.msec.2016.05.067>.
- [133] G.M. Kim, K.H.T. Le, S.M. Giannitelli, Y.J. Lee, A. Rainer, M. Trombetta, Electrospinning of PCL/PVP blends for tissue engineering scaffolds, *J. Mater. Sci. Mater. Med.* 24 (2013) 1425–1442. <https://doi.org/10.1007/s10856-013-4893-6>.
- [134] Z. Arabpour, A. Baradaran-Rafii, N.L. Bakhshaiesh, J. Ai, S. Ebrahimi-Barough, H. Esmaeili Malekabadi, N. Nazeri, A. Vaez, M. Salehi, F. Sefat, S.N. Ostad, Design and characterization of biodegradable multi layered electrospun nanofibers for corneal tissue engineering applications, *J. Biomed. Mater. Res. - Part A.* 107 (2019) 2340–2349. <https://doi.org/10.1002/jbm.a.36742>.
- [135] R. Pázmány, K.S. Nagy, Á. Zsembery, A. Jedlovszky, Ultrasound induced , easy-to-store porous poly (amino acid) based electrospun scaffolds, *J. Mol. Liq.* 359 (2022). <https://doi.org/10.1016/j.molliq.2022.119243>.
- [136] P. Vass, E. Hirsch, R. Kóczyán, B. Démuth, A. Farkas, C. Fehér, E. Szabó, Á. Németh, S.K. Andersen, T. Vigh, G. Verreck, I. Csontos, G. Marosi, Z.K. Nagy, Scaled-Up production and tableting of grindable electrospun fibers containing a protein-type drug, *Pharmaceutics.* 11 (2019) 1–12. <https://doi.org/10.3390/pharmaceutics11070329>.
- [137] S. Omer, L. Forgách, R. Zelkó, I. Sebe, Scale-up of electrospinning: Market overview of products and devices for pharmaceutical and biomedical purposes, *Pharmaceutics.* 13 (2021) 1–21. <https://doi.org/10.3390/pharmaceutics13020286>.
- [138] Z.K. Nagy, A. Balogh, B. Démuth, H. Pataki, T. Vigh, B. Szabó, K. Molnár, B.T. Schmidt, P. Horák, G. Marosi, G. Verreck, I. Van Assche, M.E. Brewster, High

- speed electrospinning for scaled-up production of amorphous solid dispersion of itraconazole, *Int. J. Pharm.* 480 (2015) 137–142. <https://doi.org/10.1016/j.ijpharm.2015.01.025>.
- [139] S. Khorshidi, A. Solouk, H. Mirzadeh, S. Mazinani, J.M. Lagaron, S. Sharifi, S. Ramakrishna, A review of key challenges of electrospun scaffolds for tissue-engineering applications, *J. Tissue Eng. Regen. Med.* 10 (2016) 715–738. <https://doi.org/10.1002/term>.
- [140] N. Maurmann, D.P. Pereira, D. Burguez, F.D.A.D.S. Pereira, P.I. Neto, R.A. Rezende, D. Gamba, J.V.L. Da Silva, P. Pranke, Mesenchymal stem cells cultivated on scaffolds formed by 3D printed PCL matrices, coated with PLGA electrospun nanofibers for use in tissue engineering, *Biomed. Phys. Eng. Express.* 3 (2017). <https://doi.org/10.1088/2057-1976/aa6308>.
- [141] C. Vaquette, J.J. Cooper-White, Increasing electrospun scaffold pore size with tailored collectors for improved cell penetration, *Acta Biomater.* 7 (2011) 2544–2557. <https://doi.org/10.1016/j.actbio.2011.02.036>.
- [142] B.M. Baker, A.O. Gee, R.B. Metter, A.S. Nathan, R.A. Marklein, J.A. Burdick, R.L. Mauck, The potential to improve cell infiltration in composite fiber-aligned electrospun scaffolds by the selective removal of sacrificial fibers, *Biomaterials.* 29 (2008) 2348–2358. <https://doi.org/10.1016/j.biomaterials.2008.01.032>.
- [143] P. Pal, P.K. Srivas, P. Dadhich, B. Das, D. Maulik, S. Dhara, Nano-/Microfibrous Cotton-Wool-Like 3D Scaffold with Core-Shell Architecture by Emulsion Electrospinning for Skin Tissue Regeneration, *ACS Biomater. Sci. Eng.* 3 (2017) 3563–3575. <https://doi.org/10.1021/acsbiomaterials.7b00681>.
- [144] J. Jiang, M.A. Carlson, M.J. Teusink, H. Wang, M.R. MacEwan, J. Xie, Expanding Two-Dimensional Electrospun Nanofiber Membranes in the Third Dimension by a Modified Gas-Foaming Technique, *ACS Biomater. Sci. Eng.* 1 (2015) 991–1001. <https://doi.org/10.1021/acsbiomaterials.5b00238>.
- [145] J.B. Lee, S.I. Jeong, M.S. Bae, D.H. Yang, D.N. Heo, C.H. Kim, E. Alsberg, I.K. Kwon, Highly porous electrospun nanofibers enhanced by ultrasonication for improved cellular infiltration, *Tissue Eng. - Part A.* 17 (2011) 2695–2702. <https://doi.org/10.1089/ten.tea.2010.0709>.
- [146] B.K. Gu, S.J. Park, M.S. Kim, C.M. Kang, J. Il Kim, C.H. Kim, Fabrication of

- sonicated chitosan nanofiber mat with enlarged porosity for use as hemostatic materials, *Carbohydr. Polym.* 97 (2013) 65–73. <https://doi.org/10.1016/j.carbpol.2013.04.060>.
- [147] S. Jung, B.K. Gu, Y.J. Gin, S.J. Park, I.K. Kwon, C. Kim, Thickness and Pore Size Control of Chitin Nanofibers by Ultra-sonication and Its Biological Effect in vitro, *Biomater. Res.* 16 (2012) 11–18.
- [148] F. Smaniotto, V. Prosapio, I. Zafeiri, F. Spyropoulos, Freeze drying and rehydration of alginate fluid gels, *Food Hydrocoll.* 99 (2020) 105352. <https://doi.org/10.1016/j.foodhyd.2019.105352>.
- [149] S. Watson, M. Toner, Cryopreservation of harvested skin and cultured skin or cornea equivalents by slow freezing, 1999.
- [150] D. Applegate, J. Kim, Cryopreservation process scaleup for a tissue-engineered, metabolically active, human dermal replacement, dermagraft., *Cryobiology.* 37 (1998) 409–10.
- [151] A. Merivaara, J. Zini, E. Koivunotko, S. Valkonen, O. Korhonen, F.M. Fernandes, M. Yliperttula, Preservation of biomaterials and cells by freeze-drying: Change of paradigm, *J. Control. Release.* 336 (2021) 480–498. <https://doi.org/10.1016/j.jconrel.2021.06.042>.
- [152] Z. Varga, K. Molnár, V. Torma, M. Zrínyi, Kinetics of volume change of poly(succinimide) gels during hydrolysis and swelling., *Phys. Chem. Chem. Phys.* 12 (2010) 12670–5. <https://doi.org/10.1039/c0cp00527d>.
- [153] A. Ghasemi, S. Zahediasl, Normality tests for statistical analysis: A guide for non-statisticians, *Int. J. Endocrinol. Metab.* 10 (2012) 486–489. <https://doi.org/10.5812/ijem.3505>.
- [154] C. Ao, Y. Niu, X. Zhang, X. He, W. Zhang, C. Lu, Fabrication and characterization of electrospun cellulose/nano-hydroxyapatite nanofibers for bone tissue engineering, *Int. J. Biol. Macromol.* 97 (2017) 568–573. <https://doi.org/10.1016/j.ijbiomac.2016.12.091>.
- [155] M. Mabrouk, H.H. Beherei, D.B. Das, Recent progress in the fabrication techniques of 3D scaffolds for tissue engineering, *Mater. Sci. Eng. C.* 110 (2020) 110716. <https://doi.org/10.1016/j.msec.2020.110716>.
- [156] A.G. Juhasz, K. Molnar, A. Idrissi, A. Jedlovszky-Hajdu, Salt induced fluffy

- structured electrospun fibrous matrix, *J. Mol. Liq.* 312 (2020) 113478. <https://doi.org/10.1016/j.molliq.2020.113478>.
- [157] D. Juriga, K. Nagy, A. Jedlovszky-Hajdú, K. Perczel-Kovács, Y.M. Chen, G. Varga, M. Zrínyi, Biodegradation and Osteosarcoma Cell Cultivation on Poly(aspartic acid) Based Hydrogels, *ACS Appl. Mater. Interfaces.* 8 (2016) 23463–23476. <https://doi.org/10.1021/acsami.6b06489>.
- [158] H.J. Kim, U.J. Kim, H.S. Kim, C. Li, M. Wada, G.G. Leisk, D.L. Kaplan, Bone tissue engineering with premineralized silk scaffolds, *Bone.* 42 (2008) 1226–1234. <https://doi.org/10.1016/j.bone.2008.02.007>.
- [159] M.P. Francis, Y.M. Moghaddam-White, P.C. Sachs, M.J. Beckman, S.M. Chen, G.L. Bowlin, L.W. Elmore, S.E. Holt, Modeling early stage bone regeneration with biomimetic electrospun fibrinogen nanofibers and adipose-derived mesenchymal stem cells, *Electrospinning.* 1 (2016) 10–19. <https://doi.org/10.1515/esp-2016-0002>.
- [160] A. Aidun, A. Safaei Firoozabady, M. Moharrami, A. Ahmadi, N. Haghhighipour, S. Bonakdar, S. Faghihi, Graphene oxide incorporated polycaprolactone/chitosan/collagen electrospun scaffold: Enhanced osteogenic properties for bone tissue engineering, *Artif. Organs.* 43 (2019) E264–E281. <https://doi.org/10.1111/aor.13474>.
- [161] J. Jang, C. Cha, Multivalent Polyaspartamide Cross-Linker for Engineering Cell-Responsive Hydrogels with Degradation Behavior and Tunable Physical Properties, *Biomacromolecules.* 19 (2018) 691–700. <https://doi.org/10.1021/acs.biomac.8b00068>.
- [162] C. Zhang, L.Y. Wan, S. Wu, D. Wu, X. Qin, F. Ko, A reversible colorimetric chemosensor for naked-eye detection of copper ions using poly (aspartic acid) nanofibrous hydrogel, *Dye. Pigment.* 123 (2015) 380–385. <https://doi.org/10.1016/j.dyepig.2015.07.028>.
- [163] C. Zhang, S. Wu, J. Wu, D. Wu, X. Qin, Preparation and characterization of microporous sodium poly(aspartic acid) nanofibrous hydrogel, *J. Porous Mater.* 24 (2017) 75–84. <https://doi.org/10.1007/s10934-016-0239-3>.
- [164] F. fang Ma, D. Zhang, T. Huang, N. Zhang, Y. Wang, Ultrasonication-assisted deposition of graphene oxide on electrospun poly(vinylidene fluoride) membrane

- and the adsorption behavior, *Chem. Eng. J.* 358 (2019) 1065–1073. <https://doi.org/10.1016/j.cej.2018.10.121>.
- [165] S.L. Lim, W.N.H. Tang, C.W. Ooi, E.S. Chan, B.T. Tey, Rapid swelling and deswelling of semi-interpenetrating network poly(acrylic acid)/poly(aspartic acid) hydrogels prepared by freezing polymerization, *J. Appl. Polym. Sci.* 133 (2016). <https://doi.org/10.1002/app.43515>.
- [166] C. Zhang, S. Wu, X. Qin, Facile fabrication of novel pH-sensitive poly(aspartic acid) hydrogel by crosslinking nanofibers, *Mater. Lett.* 132 (2014) 393–396. <https://doi.org/10.1016/j.matlet.2014.06.031>.
- [167] S. Khan, N.M. Ranjha, Effect of degree of cross-linking on swelling and on drug release of low viscous chitosan/poly(vinyl alcohol) hydrogels, *Polym. Bull.* 71 (2014) 2133–2158. <https://doi.org/10.1007/s00289-014-1178-2>.
- [168] E. Krisch, B. Gyarmati, A. Szilágyi, Preparation of pH-responsive poly(Aspartic acid) nanogels in inverse emulsion, *Period. Polytech. Chem. Eng.* 61 (2017) 19–26. <https://doi.org/10.3311/PPch.9788>.
- [169] D.D. Alford, A.P. Wheeler, C.A. Pettigrew, Biodegradation of thermally synthesized polyaspartate, *J. Environ. Polym. Degrad.* 2 (1994) 225–236. <https://doi.org/10.1007/BF02071970>.
- [170] T. Nakato, M. Yoshitake, K. Matsubara, M. Tomida, T. Kakuchi, Relationships between structure and properties of poly(aspartic acid)s, *Macromolecules.* 31 (1998) 2107–2113. <https://doi.org/10.1021/ma971629y>.
- [171] Y. Lu, M. Chau, A.J. Boyle, P. Liu, A. Niehoff, D. Weinrich, R.M. Reilly, M.A. Winnik, Effect of pendant group structure on the hydrolytic stability of polyaspartamide polymers under physiological conditions, *Biomacromolecules.* 13 (2012) 1296–1306. <https://doi.org/10.1021/bm2018239>.
- [172] C. Voniatis, R. Gottscháll, D. Barcikai, G. Szabó, A. Jedlovszky-Hajdú, Enhancing critical features of poly (amino acid) based meshes, *J. Appl. Polym. Sci.* (2021). <https://doi.org/10.1002/app.51933>.
- [173] M. Aghajanpoor, S. Hashemi-Najafabadi, M. Baghaban- Eslaminejad, F. Bagheri, S. Mohammad Mousavi, F. Azam Sayyahpour, The effect of increasing the pore size of nanofibrous scaffolds on the osteogenic cell culture using a combination of sacrificial agent electrospinning and ultrasonication, *J. Biomed. Mater. Res. - Part*

- A. 105 (2017) 1887–1899. <https://doi.org/10.1002/jbm.a.36052>.
- [174] L. Grossman, S.I. Moriwaki, S. Ray, R.E. Tarone, Q. Wei, K.H. Kraemer, Age-associated changes in DNA repair and mutation rates, *Adv. Cell Aging Gerontol.* 4 (2001) 17–30. [https://doi.org/10.1016/S1566-3124\(01\)04025-1](https://doi.org/10.1016/S1566-3124(01)04025-1).
- [175] S.I. Jeong, N.A. Burns, C.A. Bonino, I.K. Kwon, S.A. Khan, E. Alsberg, Improved cell infiltration of highly porous 3D nanofibrous scaffolds formed by combined fiber-fiber charge repulsions and ultra-sonication, *J. Mater. Chem. B.* 2 (2014) 8116–8122. <https://doi.org/10.1039/c4tb01487a>.

9 Bibliography of the candidate's publications – related to the thesis

- [RP1] Molnar, K., Voniatis, C., Feher, D., Szabo, G., Varga, R., Reiniger, L., Juriga, D., Kiss, Z., Krisch, E., Weber, G., Ferencz, A., Varga, G., Zrinyi, M., Nagy, K. S., Jedlovszky-Hajdu, A. (2021). Poly(amino acid) based fibrous membranes with tuneable in vivo biodegradation. *Plos One*, 16(8), e0254843. (2021). <https://doi.org/10.1371/journal.pone.0254843>
- [RP2] R. Pázmány, K.S. Nagy, Á. Zsembery, A. Jedlovszky, Ultrasound induced, easy-to-store porous poly (amino acid) based electrospun scaffolds, *J. Mol. Liq.* 359 (2022). <https://doi.org/10.1016/j.molliq.2022.119243>.

10 Bibliography of the candidate's publications – not related to the thesis

K. Molnar, R. Varga, B. Jozsa, D. Barczikai, E. Krisch, K.S. Nagy, G. Varga, A. Jedlovszky-Hajdu, J.E. Puskas, Investigation of the cytotoxicity of electrospun polysuccinimide-based fiber mats, *Polymers (Basel)*. 12 (2020) 1–11. <https://doi.org/10.3390/polym12102324>.

11 Acknowledgements

I'm incredibly grateful for the guidance and instructions of my supervisor and scientific mother, Dr. Angéla Jedlovszky-Hajdú. Words can neither qualify nor quantify how helpful your encouragement and advice have been. Your supervision helped me to become a better researcher. I am forever grateful for your support!

I'm grateful to Prof. Miklós Kellermayer, and Prof. Miklós Zrínyi for their confidence in me and for letting me be a part of their team for many years. I'm thankful to Kristóf Molnár for persuading me to join this lab after a choir rehearsal. Thank you for teaching me almost everything I know about electrospinning and spectroscopy. Your advice and encouragement are the best!

My appreciation goes to all members of the Laboratory of Nanochemistry, who made the lab a lovely place. I'm grateful to Dávid Juriga for sharing insights regarding microscopy and many other things, to Krisztina Nagy for the advice and constructive feedback I received during my work, and for support and feedback on drafts of this paper. I was blessed with one of the most supporting teams a doctoral student could ask for. Special thanks to Evelin Forró, Krisztina Tóth, Ákos Juhász, Constantinos Voniatis, Dóra Barczikai and Bálint Budavári, I'm grateful for your kindness. Thank you, Elza Simon, for making the lab a warm place, not just in an abstract sense of the word.

I'm grateful to Prof. Gábor Varga and Prof. Ákos Zsembery for providing me space in their cell culture labs, and to Anna Földes for her advice and help with cell studies. I'm also grateful to Prof. László Smeller for letting me use his freeze-drying device and to Judit Gál-Somkuti for teaching me how to use it. Special thanks to Erzsébet Besze for her kindness, and patience and for her assistance in navigating a lot of administrative issues.


I was so fortunate to work with Dimitris Missirlis and Prof. Joachim Spatz in the Max Planck Institute for Medical Research in Heidelberg, during my PhD. I'm grateful for their faith in me, and to Julia Ivanova and Lara Heckmann for their support and hospitality. I genuinely appreciate it from the bottom of my heart.

I'm also grateful to my parents for raising and supporting me. Lastly, I wish to acknowledge the support of my husband, József Pázmány, I can't imagine how I could complete this thesis without such a man by my side.

12 Statement of Originality

I, Rita Pázmány (Neptun code: K04FEE) hereby confirm that the content of this thesis is my own work. This thesis has not been submitted for any degree or other purposes. I certify that the intellectual content of this thesis is the product of my own work and that all the assistance received in preparing this thesis and sources have been acknowledged.

Budapest, December 19, 2022


.....
Rita Pázmány

RESEARCH ARTICLE

Poly(amino acid) based fibrous membranes with tuneable *in vivo* biodegradation

Kristof Molnar^{1,2}, Constantinos Voniatis^{1,3}, Daniella Feher³, Gyorgyi Szabo³, Rita Varga¹, Lilla Reiniger⁴, David Juriga¹, Zoltan Kiss^{5,6}, Eniko Krisch², Gyorgy Weber³, Andrea Ferencz³, Gabor Varga⁷, Miklos Zrinyi¹, Krisztina S. Nagy^{1,7}, Angela Jedlovszky-Hajdu^{1*}

1 Laboratory of Nanochemistry, Department of Biophysics and Radiation Biology, Semmelweis University, Budapest, Hungary, **2** Department of Food, Agricultural and Biological Engineering, College of Food, Agricultural, and Environmental Sciences, The Ohio State University, Wooster, OH, United States of America, **3** Department of Surgical Research and Techniques, Semmelweis University, Budapest, Hungary, **4** 1st Department of Pathology and Experimental Cancer Research, Semmelweis University, Budapest, Hungary, **5** Department of Polymer Engineering, Faculty of Mechanical Engineering, Budapest University of Technology and Economics, Budapest, Hungary, **6** Biomechanical Research Center, Faculty of Mechanical Engineering, Budapest University of Technology and Economics, Budapest, Hungary, **7** Department of Oral Biology, Semmelweis University, Budapest, Hungary

* hajdu.angela@med.semmelweis-univ.hu



OPEN ACCESS

Citation: Molnar K, Voniatis C, Feher D, Szabo G, Varga R, Reiniger L, et al. (2021) Poly(amino acid) based fibrous membranes with tuneable *in vivo* biodegradation. PLoS ONE 16(8): e0254843. <https://doi.org/10.1371/journal.pone.0254843>

Editor: Wenguo Cui, Shanghai Jiao Tong University Medical School Affiliated Ruijin Hospital, CHINA

Received: May 7, 2021

Accepted: July 4, 2021

Published: August 13, 2021

Copyright: © 2021 Molnar et al. This is an open access article distributed under the terms of the [Creative Commons Attribution License](https://creativecommons.org/licenses/by/4.0/), which permits unrestricted use, distribution, and reproduction in any medium, provided the original author and source are credited.

Data Availability Statement: All relevant data are within the manuscript and its [S1 File](#) and [S1 Graphical abstract files](#).

Funding: This work was supported by the National Research, Development and Innovation Office (NKFIH FK 124147), the János Bolyai Research Scholarship of the Hungarian Academy of Sciences (JHA) and by the new national excellence program of the Ministry for Innovation and Technology (ÚNKP-20-5-SE-9). The research was further financed by the Higher Education Institutional Excellence Programme of the Ministry for

Abstract

In this work two types of biodegradable polysuccinimide-based, electrospun fibrous membranes are presented. One contains disulfide bonds exhibiting a shorter (3 days) *in vivo* biodegradation time, while the other one has alkyl crosslinks and a longer biodegradation time (more than 7 days). According to the mechanical measurements, the tensile strength of the membranes is comparable to those of soft the connective tissues and visceral tissues. Furthermore, the suture retention test suggests, that the membranes would withstand surgical handling and *in vivo* fixation. The *in vivo* biocompatibility study demonstrates how membranes undergo *in vivo* hydrolysis and by the 3rd day they become poly(aspartic acid) fibrous membranes, which can be then enzymatically degraded. After one week, the disulfide cross-linked membranes almost completely degrade, while the alkyl-chain crosslinked ones mildly lose their integrity as the surrounding tissue invades them. Histopathology revealed mild acute inflammation, which diminished to a minimal level after seven days.

1. Introduction

Polymer hydrogels are three-dimensional polymer networks that contain a large amount of aqueous solution. Hydrogels possess the properties of both solid and liquid materials: they can maintain their shape as solids do, yet small molecules for example drugs, can migrate through them by diffusion (as they would do in fluids). Furthermore, due to their high water content, they resemble the mammalian soft tissues, therefore, hydrogels are commonly used in clinical practice and experimental medicine in a wide range of applications including diagnostics, drug delivery, regenerative medicine [1–5]. However, hydrogels are typically fragile, brittle

Innovation and Technology in Hungary, within the framework of the Therapeutic Development thematic programme of the Semmelweis University and by EFOP-3.6.3-VEKOP-16-2017-00009.

Competing interests: The authors have declared that no competing interests exist.

resulting in breaking upon bending, suturing or other basic handling maneuvers during surgeries, severely limiting their applicability as implants [6, 7].

Fibrous hydrogel membranes are soft materials composed of sub-micron diameter hydrogel fibers bundled together that create a loose and flexible sheet. While still being considered as hydrogels, fibrous hydrogel membranes have additional advantages. Not only these membranes possess the favorable features of hydrogels, but their structure is similar to the extracellular matrix found ubiquitously around almost every human cell. Therefore, these membranes are exceptional candidates for cell cultivation or tissue regeneration applications. Furthermore, being composed of fibers, the material should be more flexible, but also more resistant to the damage caused by the sutures due to the free movement and bending of their fibers.

Fibrous membranes have been extensively researched for a wide variety of fields [8] including biomaterials [9, 10]. One method for polymer fiber preparation is electrospinning, where polymer fibers are created under the effect of a strong electrical field [11]. By introducing a crosslinking reaction to electrospinning, the aforementioned gel fibers can be obtained, which, without chemical or enzymatic degradation, will not dissolve after being immersed in a solution but only absorb the surrounding fluid [12]. It is important to note here that in gel fibers crosslinks are between polymer chains inside the fibers and not between fibers. Typically, one of the two following implementation methods is utilized for the synthesis of crosslinked fibrous membranes (gel fibers). In post-electrospinning methods, the fibrous membrane (having the crosslinking agent already in the polymer solution) is electrospun first and the crosslinks are formed subsequently in a chemical reaction [13–15]. By utilizing this method, however, the number of crosslinks cannot be properly regulated. On the other hand, in reactive electrospinning, the chemical crosslinking reaction takes place during the fiber formation. Typically, a UV active reagent is added to the polymer that under the effect of UV light will auto-crosslink the polymer chains inside the fibers. Although by utilizing this method the number of crosslinks can be regulated, most of these UV active reagents are toxic [16, 17].

Poly(aspartic acid) (PASP) is a synthetic biocompatible polymer composed of aspartic acid molecules interconnected by peptide bonds and thus exhibits a peptide-like chemical structure, which ensures its biodegradability [18–24]. PASP based hydrogels are promising materials for tissue engineering and cell cultivation. Juriga *et al.* displayed how MG-63 cells could not just attach and proliferate on PASP based hydrogels, but were also able to grow inside the gels and establish 3D colonies [25]. Nevertheless, PASP based hydrogels are simply too fragile for conventional implantation. In addition, although the fabrication these membranes was proven feasible, [26, 27] as promising as these materials are, no information is available regarding any implantation attempts, *in vivo* biocompatibility or a biodegradability profile.

PASP can be prepared from its anhydride, polysuccinimide (PSI) via hydrolysis under mild alkaline conditions (Fig 1) [28]. Unlike PASP, PSI is a reactive polymer, therefore, it can be easily modified at room temperature by nucleophilic reagents such as primary amines, giving PSI a major advantage compared to other synthetic biocompatible and biodegradable polymers. This enables us to synthesize a large variety of PSI derivatives with adjustable properties for different applications (Fig 1), which can be later on hydrolyzed to the corresponding PASP derivatives either *in vitro* or *in vivo* [19–24, 29–31]. By utilizing multifunctional amines for crosslinking, advanced functional PSI gels or with their hydrolysis PASP hydrogels can be created [28].

In this work we present the fabrication and characterization two PSI based crosslinked fibrous membranes (referred to as fibrous membranes from now on) which can be implanted by conventional surgical techniques while also retaining their hydrolytic and enzymatic degradability. The two types of membranes were fabricated having different chemical compositions: a disulfide crosslinked one intended for fast biodegradation and an alkyl-chain

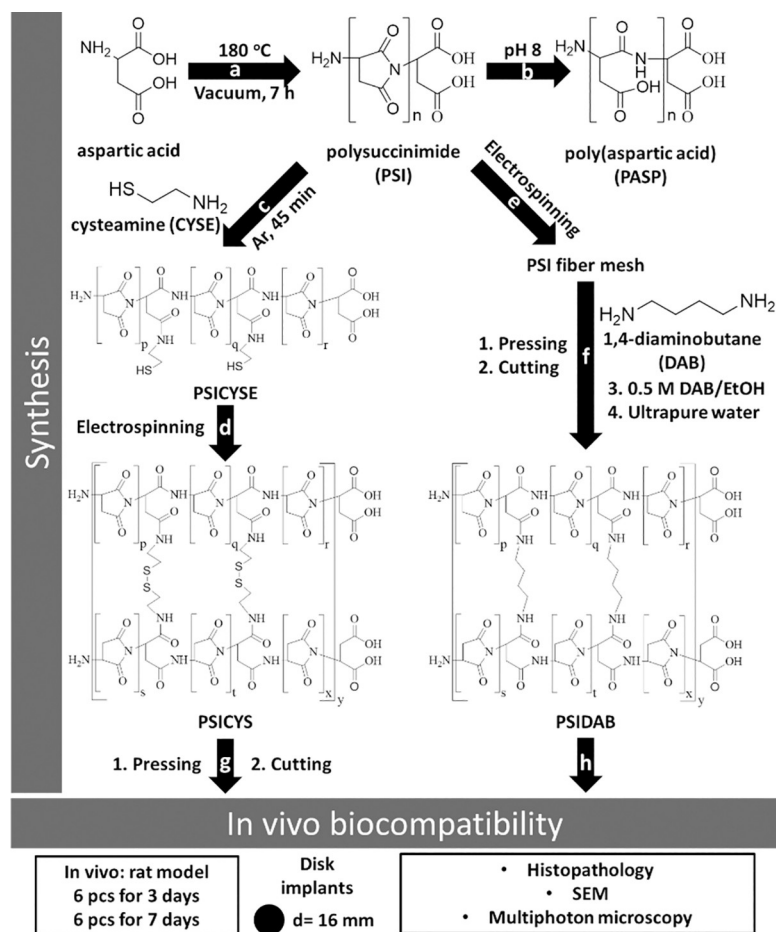


Fig 1. Schematic of the synthesis and investigation of materials subjected in this paper: synthesis of PSI (a); hydrolysis of PSI (b); modification of PSI with cysteamine (c); reactive electrospinning of cysteamine modified PSI (d); electrospinning of PSI (e); pressing, cutting and heterogenous crosslinking of polysuccinimide fibers with 1,4-diaminobutane (f); pressing and cutting of PSICYS samples and implantation in a rat animal model (g); implantation of PSIDAB disks in a rat animal model (h).

<https://doi.org/10.1371/journal.pone.0254843.g001>

crosslinked one with possibly longer biodegradation time, both intended for tissue engineering. These samples were implanted under the skin in PSI form to see if they can hydrolyze and form PASP based samples, how fast the hydrolysis occurs, how the surrounding tissue reacts to these changes and to see the short-term biodegradability of the membranes. The biocompatibility/biodegradability was comprehensively investigated.

2. Experimental

2.1. Materials

L-aspartic acid (Sigma-Aldrich, UK), cysteamine (CYSE) (Sigma-Aldrich, UK), dimethylformamide (DMF) (VWR International, USA), dimethylsulfoxide (DMSO) (Sigma-Aldrich), o-phosphoric acid (VWR), 1,4-diaminobutane (DAB) (99%, Aldrich), imidazole (ACS reagent, $\geq 99\%$, Sigma-Aldrich), citric-acid*H₂O (ACS reagent, $\geq 99.9\%$, VWR), sodium chloride (99–100.5%, Sigma-Aldrich), phosphate buffer saline (PBS) (Tablet, Sigma), sodium hydroxide (VWR International, USA) were of analytical grade and were used as received. For the aqueous solutions, ultrapure water (Human Corporation ZeneerPower I Water Purification System)

was used. For 1 L of imidazole buffer imidazole (pH 8: 12.988 g), citrate (pH 8: 1.728 g), sodium chloride (pH 8: 11.466 g) and ultrapure water were used. In all cases the exact pH was adjusted by the addition of hydrochloric acid and followed by digital pH meter (Thermo Scientific™ Orion™ 4-Star Plus pH/ISE Benchtop Multiparameter Meter).

For the *in vitro* experiments MG-63 human osteosarcoma cell line (Sigma-Aldrich, USA), Minimum Essential Medium (Gibco, USA), fetal bovine serum (Gibco, USA), non-essential amino acids (Gibco, USA), L-glutamine (Gibco, USA), penicillin and streptomycin (Gibco, USA), commercially available cell proliferation reagent (WST-1, Roche, Switzerland), Vybrant DiD vital dye (Molecular Probes, USA) were used.

2.2. Preparation of polysuccinimide and cysteamine modified polysuccinimide

PSI was prepared by thermal polycondensation of L-aspartic acid in the presence of o-phosphoric acid catalyst, under vacuum at 180 °C as described in our previous paper (Fig 1A) [18]. For the modification of PSI with cysteamine (CYSE), first 0.04 g of CYSE was dissolved in a mixture of 0.7 g DMF and 0.4 g DMSO in a glass reactor, then 2 g of PSI dissolved in DMF (25 w/w%) was added and mixed vigorously under Argon atmosphere at room temperature for 45 minutes (Fig 1C). After the synthesis, the final polymer concentration was 15 w/w% and theoretically, every 10th repeating unit was modified with cysteamine (PSICYSE). Details of the synthesis and chemical characterization can be found in our previous paper.²⁹

2.3. Preparation of electrospun cystamin crosslinked polysuccinimide fibers

Cystamine crosslinked PSI fibers were prepared by a homemade apparatus consisting of a Genvolt 73030P high voltage power supply, a KD Scientific KDS100 syringe pump, a Fortuna Optima 7.140 33 glass syringe with Luer-lock, a blunt G18 needle made by Hamilton and a grounded plate collector covered with aluminum foil. The electrospinning parameters were set at 0.8 ml/h flow rate, 15 cm target distance (distance between the tip of the needle and collector) and 12 kV potential. Samples were prepared from 1 ml of 15 w/w% PSICYSE solution. During the electrospinning process, as fibers were expelled from the needle, the thiol side chains of the PSICYSE formed disulfide bonds between the polymer chains upon oxidation by the atmospheric oxygen before reaching the collector (Fig 1D). The crosslinked polymer is denoted as PSICYS. Due to practical reasons and restrictions of our current setup the amount of electrospun material we can synthesize during a single electrospinning session is limited. A simple solution to this issue is removing a sample from the aluminum collector, folding it then compressing it resulting in smaller yet thicker membranes. In our case 3 x 4 cm rectangles were prepared (Fig 1G). To reinforce them, they were then compressed by 5 t weight along their whole surface for 5 min using an Atlas Manual 15T Hydraulic Press (GS15011). Finally, disks of 16 mm diameter (Fig 1G) were cut out and subsequently sterilized by dry heat thermal sterilization in a Memmert SLP 500 at 120 °C for 2 hours [32]. According to thermal gravimetry and differential thermal analysis, there is no physical or chemical change in the samples after applying this sterilization method: further details can be found in our previous paper [26].

2.4. Preparation of 1,4-diaminobutane crosslinked PSI fibers (PSIDAB)

25 w/w% PSI/DMF solution was electrospun at 15 cm collector distance and 1 ml/h feeding rate (Fig 1E). 1 x 1 cm square samples were then cut and immersed in a 0.5 M DAB/EtOH

solution (crosslinker solution) for different time intervals (1 min, 5 min, 10 min, 20 min, 30 min, 60 min, 120 min, 180 min, 1 day). After the reaction, samples were thoroughly immersed in DMF as a simple dissolution test. The reaction between PSI and DAB can be seen on Fig 1F. For the *in vivo* experiments, the PSIDAB samples of the 1-hour crosslinking time were chosen. Before the crosslinking, (similarly to the PSICYS samples) the PSI membrane was folded and compressed, then disks of 16 mm diameter were cut before immersing them in the crosslinker solution. Finally, samples were thoroughly washed with ultrapure water. Samples were securely sealed and stored in ultrapure water containing a small amount of ClO₂ for sterilization (Fig 1F) [33].

2.5. Characterization

2.5.1. Scanning Electron Microscopy (SEM). For SEM studies, the samples were treated in different ways according to their type: PSI-based membranes: a small part of the membrane was cut out and placed on conductive tape for coating and microscopy; PASP-based membranes: samples were first thoroughly washed with ultrapure water and freeze-dried, then a small portion was placed on conductive tape for coating and microscopy; samples from *in vivo* experiments: a small portion of membranes was resected from the *in vivo* samples and was washed in an excessive amount of 100 mM Na-cacodylate (pH 7.2) solution, then stored in a 1 V/V% glutaraldehyde solution in 100 mM Na-cacodylate (pH 7.2). To dehydrate the membranes, the samples were first placed for 5 min in a series of ethanol solutions: 20, 50, 70, 85, 96 V/V% (diluted with water) then in a 1:1 ethanol (96 V/V%) and acetone mixture and finally in a porous container with pure acetone. In a slow process, acetone was replaced with supercritical CO₂ and slowly heated until complete evaporation. The dry samples were then placed on conductive tape for coating and microscopy. Micrographs were taken using a ZEISS EVO 40 XVP scanning electron microscope equipped with an Oxford INCA X-ray spectrometer (EDS). An accelerating voltage of 20 kV was applied. For the measurements, samples were sputter-coated with gold in 20–30 nm thickness with a 2SPI Sputter Coating System. Fiber diameters were measured with ImageJ software. In every case where membranes had clear fiber morphology, 50 individual fibers were measured and averages were calculated.

2.5.2. Multiphoton microscopy. Multiphoton microscopy enables the in-depth investigation of samples that either have auto-fluorescent properties or have been labelled with fluorescent dyes prior to the investigation. For the examination of PSI and PASP based membranes, a two-photon microscope (Femto2d, Femtonics, Hungary) with a Spectra Physics Deep See laser was used at an 800 nm wavelength to induce the auto-fluorescence of PSI and PASP [25]. The emitted photons were detected in the green channel. Images were taken with 10x objective by the MES4.4v program. The brightness and contrast of the pictures were enhanced for better visualization.

2.5.3. Attenuated Total Reflectance Fourier Transform Infrared Spectroscopy (ATR-FTIR). Chemical structures and the success of synthesis were investigated with a Jasco FT/IR-4700 (Able-Jasco, Japan) with DTGS detector. All spectra were collected over the range 400–4000 cm⁻¹ at a resolution of 2 cm⁻¹. The background spectra were measured on a clean and dry diamond crystal. The number of scans accumulated was 128.

2.5.4. Synthesis of PASP-based membranes by the hydrolysis of the PSI membranes. The hydrolytic stability of PSI and PASP based samples were investigated *in vitro*. PASP samples were prepared by mild alkaline hydrolysis of the electrospun PSI membranes (PSICYS or PSIDAB) in an imidazole-based buffer solution of pH 8 (I = 250mM). The chemical reaction of PSI turning into PASP is depicted in Fig 1B. A consequence of the hydrolysis is the swelling of the membranes [28]. 100% conversion is achieved when the membranes reach their equilibrium size. Based on our previous study, PSIDAB spheres with a diameter of 5.5 mm obtain

their equilibrium size in 5 hours [28]. Furthermore, the smaller the spheres were, the faster they obtained their equilibrium size during hydrolysis. Although the fiber in the membranes are much smaller, to ensure complete hydrolysis samples were kept in the buffer for 24 hours. The swelling investigation was performed as it is crucial regarding technical surgical aspects but also to compare any *in vitro* and *in vivo* differences. The diameter of 3 PSI disks was measured before and after hydrolysis with a caliper. Changes in thickness were considered negligible therefore the degree of swelling was calculated as diameter PASPDAB/PSIDAB*100. The average fiber diameter was calculated with standard error (confidence of 95%) using standard procedure.

After the hydrolysis, samples were washed with ultrapure water to get rid of the salts and were subsequently freeze-dried for SEM and ATR-FTIR. PASP membranes are denoted by changing the PSI part in the original sample name to PASP (PASPCYS, PASPDAB).

2.5.5. Mechanical analysis. Mechanical analysis of the PSICYS and PSIDAB membranes was performed to assess their loading capacity but also investigate whether they can be reliably used during a standard surgical procedure (suturability). Therefore, the methods we followed aimed to assess both the properties of the materials themselves, as well as the membrane-suture interactions. All samples were immersed in saline to replicate the *in vivo* environment where the samples would inevitably swell. For the measurements, a ZWICK Z005 tensile testing machine (Ulm, Germany) was used with standard clamps holding the samples, while registering the force and displacement of the crosshead at a constant pulling rate of 10 mm/min. The initial sample size was always 2 cm long and 1 cm wide. Sample thickness was measured with a caliper. From the recorded data, the maximum bearing load was obtained. The ultimate tensile strength was calculated by dividing the maximum bearing load by the initial cross-section area. From each sample type at least 4 parallel samples were measured. In the case of suture-sample interaction investigation (Suture Retention Test), on one side of the previously mentioned samples, a simple interrupted suture was placed in the center 0.5 cm from the top and 0.5 cm from each side. The suture was pulled out from the fixed sample at a constant speed of 10 mm/min. This is in line with the recommendation of Pensalfini *et al.* for the measurement of suture retention strength and is in line with AAMI/ISO/ANSI 7198 Standard (2016) [34]. In their work they found that sample width of 1 cm and suture placed 0.5 cm from the edge of the sample are necessary to exclude any effect of sample geometry on the suture retention.

2.6. *In vitro* tests

2.6.1. Cell culture. A human osteosarcoma cell line, MG-63 was cultured as a subconfluent monolayer under standard conditions (100% humidity, 37°C and 5% CO₂) in a humidified incubator (Nuair, USA). These osteoblast-like cells were cultured in Minimum Essential Medium, supplemented with 10% fetal bovine serum, 1% non-essential amino acids, 2 mM L-glutamine, 100 units/ml penicillin and 100 mg/ml streptomycin.

2.6.2. Cell viability assay. Disks of an average diameter of 6 mm were cut from the electrospun membranes. To minimize the probability of a bacterial or fungal infection, the samples were stored in sterile-filtered PBS containing sodium azide. Before introducing the disks to the cells, the membrane samples were sterilized in a 300 ppm chlorine-dioxide solution (in PBS) for 10 min and they were incubated in the completed medium for 1 hour. First, the gel disks were placed into the wells of *low cell binding* 96 well microplates (flat bottom, Nunc, Denmark). After that, the MG-63 cells were seeded onto the gel disks at a concentration of 20 000 cells/well in 200 µl medium/well and incubated for 24 or 72 hours at 37°C.

Cell viability was evaluated by a colorimetric assay using a commercially available cell proliferation reagent (WST-1). The WST-1 reagent was diluted with uncompleted MEM solution

(lacking phenol red) in a ratio of 1:20. After washing the wells with PBS to remove the non-attached and slightly attached cells, 200 μ l of WST-1 solution was added to each well and the cells were incubated at 37°C for 4 h. The absorbance of the supernatant was measured at 450 nm with a reference wavelength of 655 nm using a microplate reader (Model 3550, Bio-Rad Laboratories, Japan).

2.6.3. Multiphoton microscopy of the cells. To visualize the MG-63 cells growing on the surface of the fibrous membranes, they were labelled with the fluorescent vital dye Vybrant DiD before seeding (according to the manufacturer's suggested protocol). Membrane disks of 6 mm in diameter were placed into Lab-tek 8 chamber slides (Nunc, USA) with tissue culture surface treatment, and 40 000 cells were seeded onto each disk. After 24 hours, the samples were fixed in 4% paraformaldehyde (in PBS) at RT and they were stored in PBS at 4°C until investigation under a multiphoton microscope. The red fluorescence shows the cells due to the Vybrant DiD vital staining while the green color indicates the autofluorescence of the PSI or PASP based membranes [25].

2.7. Animal model

Biocompatibility and biodegradability of electrospun PSICYS and PSIDAB samples were investigated on 24 male Wistar rats (250 g) as 12 parallel measurements were carried out for each sample type. Before implantation, the PSICYS and PSIDAB samples were immersed in sterile physiological saline (0.9%) for 10 minutes to reach their equilibrium size. Sedation of animals was performed with a mixture of ketamine and xylazine (~0.8 ml/animal). Samples were implanted at the nape under the skin. After a 1–2 cm long incision along the dorsal midline, samples were placed and fixed on the paramedian line via a single simple interrupted suture using an Atramat 2-0 polyglycolic acid absorbable suture material. Skin closure was performed with 3–4 simple interrupted stitches using the same suture material. Post-operatively for both PSICYS and PSIDAB, animals were randomly divided into two groups of 6 animals each. Animals were kept in individual cages and observed daily for evidence of wound complications, such as skin dehiscence seroma, hematoma, or infection. The experimental protocol adhered to rules laid down by the Directive of the European Parliament and of the Council on the protection of animals used for scientific purposes and was approved by the Semmelweis University's Institutional Animal Care and Use Committee. The accreditation number of the laboratory is 22.1/1244/3/2015. We have not used control animals in the experiments for two reasons: firstly, according to 2010/63/EU guideline of the European Union, in animal studies the number of animals used should be reduced as low as reasonably possible; if applicable animals should be replaced with animals of lower hierarchy or other types of studies (*in vitro*); additionally, the *in vivo* study should be refined to provide animal care of the highest possible standards. Secondly, for the control animal, the surgical procedure would just involve a simple incision on the skin of the animal then sutured with the same technique and material. This would result in a standard wound healing process that is comprehensively documented in basic pathology books, like Robbins Pathology [35]. Termination and sample retrieval were performed after 3 days (Group A) and 7 days (Group B). Samples were preserved in formaldehyde and then sent for histological evaluation, whereas in the case of PSI-DAB, SEM micrographs were also taken from retrieved and then freeze-dried samples.

2.7.1. Histology. PSIDAB and PSICYS samples were collected on the 3rd and 7th days after implantation as follows: the skin tissue was separated, and the samples were dissected around the suture including the muscle tissue then placed in 4 V/V% formaldehyde solution. After fixation, water was eliminated according to a standardized protocol in a Leica ASP300 enclosed tissue processor, samples were then embedded in paraffin and slices of 4 μ m

Table 1. Scoring system used to evaluate the histopathology samples [35].

Point Value	0	1	2	3	4
Average Score	0–0.49	0.50–1.49	1.50–2.49	2.50–3.50	> 3.50
Inflammation Grade	None	Mild	Moderate	Severe	
Macrophage infiltration	None	Mild	Moderate	Severe	
Lymphocyte Infiltration	None	Mild	Moderate	Severe	
Foreign Body Giant Cell Formation	None	Mild	Moderate	Severe	
Granulation Tissue and Fibrosis thickness	None	Narrow Band	Moderate Band	Wide Band	Extensive Band

<https://doi.org/10.1371/journal.pone.0254843.t001>

thickness were cut (Leica microtome). After removing the paraffin, slices were stained by standard haematoxylin-eosin staining protocol. All slides were digitalized with a Panoramic 250 Flash Scanner (3DHISTECH Ltd.). Although no standardized protocol for specifically evaluating foreign body inflammatory reactions exists, some indicators are widely accepted as criteria of grading the inflammatory response and used in other areas of medicine. For quantifying the immune response and inflammatory grade to the implanted samples, a scoring system based on the work of Planck *et al.* was used as shown in Table 1 [36]. A small piece from the 7th day PSIDAB was collected with a tweezer and investigated by a multiphoton microscope without any staining, and after freeze-drying by SEM to try and visualize leukocytes (macrophages, lymphocytes).

2.8. Statistical analysis

When applicable, the data written in the text is represented by an average followed by the standard error calculated at $p = 0.05$ confidence level. The same confidence level was used for all calculations. The number of elements in each sample is given in brackets at the corresponding averages and errors. The error bars on figures represent the standard errors. For the hypothesis tests in Section 3.5 double-sided, two-sample Student t-tests were conducted using the averages and standard deviations of the samples. In the *in vitro* analysis Kruskal-Wallis ANOVA and median test were used for statistical evaluation of the data, applying the STATISTICA 10 software (Statsoft, USA). In case of $p < 0.05$ was considered a difference as statistically significant.

3. Results and discussion

3.1. Preparation of PSI, PSICYs and PSIDAB membranes

Regarding the synthesis, electrospinning and physicochemical properties of PSI and cysteine modified polysuccinimide (PSICYSE) can be found in detail in our previous article.²⁹ After electrospinning of both PSI and PSICYs a white sheet of fibrous material was obtained, that was easy to remove from the collector. Small parts of the white fibrous sheets were dipped in N,N-dimethylformamide (DMF) to check dissolution. The PSI sheet dissolved immediately contrary to the PSICYs sheet that only swelled indicating the presence of crosslinks. The reactive electrospinning had no significant effects on the fiber formation as the average diameter of PSICYs fibers (900 ± 70 nm ($n = 50$), Fig 2B) does not differ significantly from that of the PSI fibers (910 ± 80 nm ($n = 50$), Fig 2A). According to the SEM images, both the PSI and the PSICYs fibers had a smooth surface without any defects.

The idea for the implementation of post electrospinning crosslinking for the synthesis of PSIDAB was to immerse the fibrous membrane in the solution of a crosslinker to elicit crosslinks between the polymer chains inside the fibers. To check whether this hypothesis was right, previously prepared PSI fiber membranes were immersed in a 0.5 M DAB/EtOH solution for

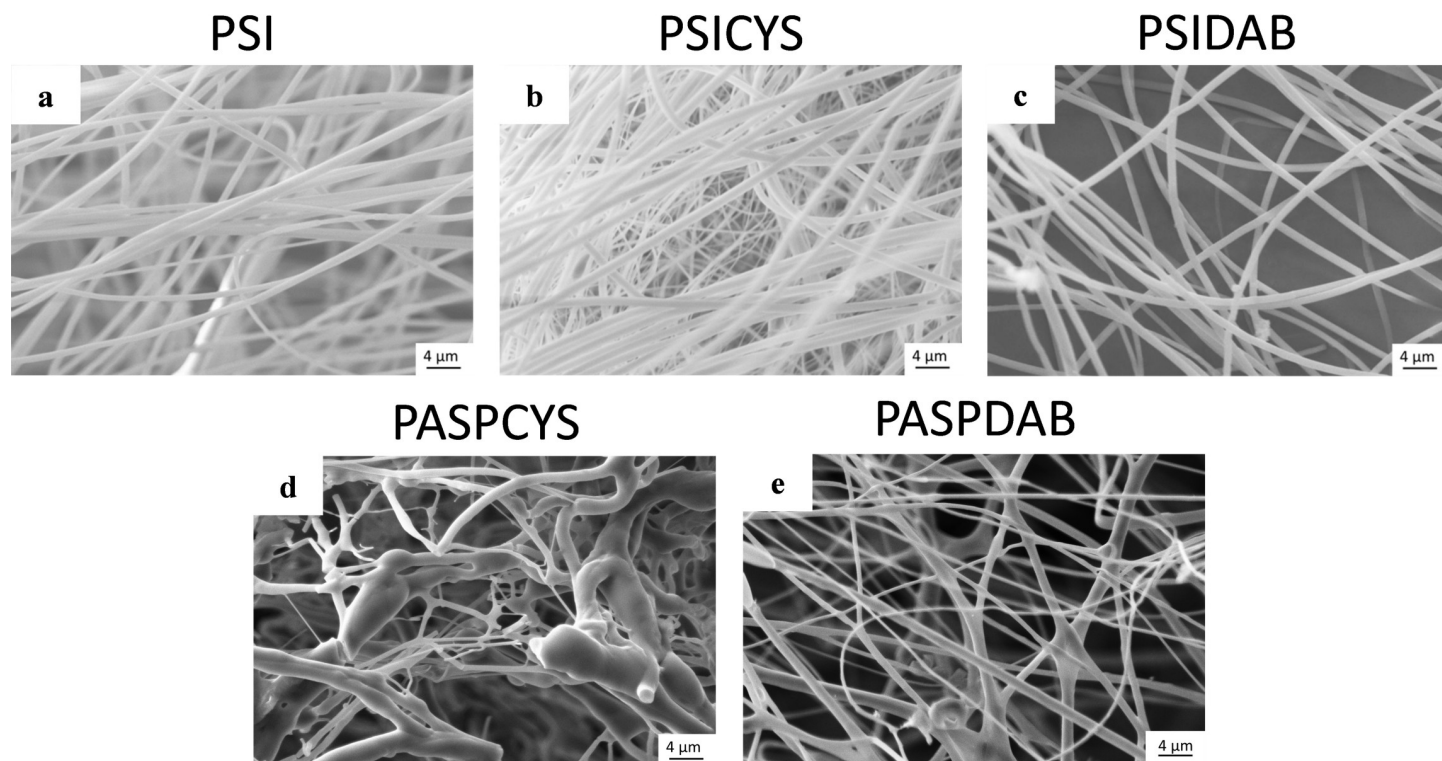


Fig 2. SEM micrographs of electrospun PSI fibers (a), PSICYS fibers (b), PASPCYS fibers (c), PSIDAB fibers without compression (d), SEM (e) and multiphoton micrographs (f) of freeze-dried PASPDAB fibers.

<https://doi.org/10.1371/journal.pone.0254843.g002>

different periods and then washed with DMF to confirm dissolution. DAB is a feasible cross-linker for PSI as proven in some published works [18, 37]. PSI is soluble in N,N-dimethylformamide, dimethyl sulfoxide and partly in N-methylpyrrolidone. To prevent PSI from dissolving, we chose ethanol as the reaction solvent in which the crosslinking process is a heterogeneous reaction. After a 1- and 5-minute long immersion time in DAB/EtOH, samples dissolved in DMF. Only after a 10-minute immersion time did samples remain intact when immersed in DMF. In other words, the minimal reaction time for crosslinking of this system is 10 minutes. However, to ensure full crosslinking and reproducibility, 1 hour of crosslinking time was chosen at the preparation of PSIDAB for the *in vivo* experiments as no significant difference was found in either shape or morphology between the 10 minute and 1 hour samples (S1 Fig in S1 File). The average fiber diameter of PSIDAB was slightly smaller (800 ± 30 nm, $n = 50$) (Fig 2C), compared to the PSI fibers used in this series (average fiber diameter was 911 ± 41 nm, $n = 50$), since the more crosslinks there are in a hydrogel, the more it shrinks.

3.2. Preparation of PASPCYS and PASPDAB membranes

Our objective was to synthesize fibrous samples that can be easily degraded *in vivo* (fast biodegradation) and samples whose degradation takes a longer time (slow biodegradation). PSICYS and PSIDAB differ from each other in both synthesis and chemical structure, which leads to different reactions *in vivo*. Disulfide bridges, such as the ones in PSICYS, are often in the focus of drug delivery research since those are cleavable in redox environments found *in vivo* [18, 37]. On the contrary, PSIDAB contains crosslinks that are not sensitive to such conditions and thus theoretically cannot be cleaved that easily, resulting in longer *in vivo*

biodegradation times. Juriga *et al.* demonstrated that PASPCYS bulk hydrogels degrade in a *collagenase type I* solution but also in minimal essential media used for cell cultivation, which supports the original idea of the fast dissolution of PSICYS membranes and slow degradation of PSIDAB samples [25]. The membranes in the present project were implanted in the animals in PSI forms. However, for biodegradability, the membranes must first undergo hydrolysis after implantation, in other words turn into their respective PASP forms (S2 and S3 Figs in [S1 File](#)). Without hydrolysis the biodegradation would be compromised. Typically, pH in the connective tissue is approximately 7.4 while in the skin ranges between 4–6. However, in the case of acute inflammation due to surgery or damage to the skin tissue, it can rise to pH 7.4 or in the case of chronic inflammation even pH 8 [38]. Since PSI hydrolyzes to PASP at $\text{pH} \geq 7.4$, it is strongly suggested that hydrolysis occurs *in vivo* for both PSICYS and PSIDAB samples implanted under the skin.

As samples were implanted in PSI based form, it was essential to investigate morphological changes caused by hydrolysis. To imitate these, PSICYS and PSIDAB samples were hydrolyzed *in vitro* as well. During this process, the PSI based membranes turn into the PASP-based membranes and swell in aqueous medium. Considerable change was observed in the fibrous structure of PSICYS after hydrolysis. During hydrolysis, the PASPCYS fibers fuse creating bundles and bulk parts along the fibers, therefore the fibrous structure was only partially maintained ([Fig 2D](#)). This is often observable in gel fiber systems in different degrees. In the case of PSIDAB fibers, although crosslinking by itself did not change the fiber morphology, hydrolysis did. As evidenced by SEM images on washed and freeze-dried PASPDAB samples (with 1 hour crosslinking time), the fusion of fibers occurred in two ways: a. in some cases where fibers happened to be parallel and touched each other they fused into flat sheets ([Fig 2E](#)) b. in other instances where fibers touched each other in any degree an interconnected fibrous structure was created at the connection points. The fusion of fibers is not an unprecedented phenomenon and it has been observed in crosslinked networks [39, 40]. Zhang *et al.* reported a similar method for the post electrospinning crosslinking of PSI fibers with 1,2-diaminoethane in methanol solution, where the fibrous structure was severely damaged due to hydrolysis [41]. Our work demonstrates that PSI fibers crosslinked with DAB proved to be a better option for retaining the fibrous structure of PASPDAB. It caused minimal change in the fiber morphology, which alterations should not have any effect on either the mechanical or *in vivo* performance of the membranes. An example for the macroscopic changes of a PSIDAB–PASPDAB transition can be seen in [Fig 3](#). In this case, the fibrous membranes grew from 16 ± 0 mm to 21 ± 1 mm, which corresponds to $31 \pm 7\%$ ($n = 3$, $p = 0.05$). Similar behavior was demonstrated for PSI based bulk hydrogels [42] but also other PASP based fibrous membranes with different crosslinkers as well [27]. Further details on the swelling behavior of different size PSIDAB membranes during hydrolysis and PASPDAB membranes in different pH solutions can be found in the supporting document. The detailed chemical analysis of PSI, PSICYS, PASPCYS, PSIDAB and PASPDAB can be found in the supplementary information and in [S4 Fig](#) in [S1 File](#).

3.3. Mechanical analysis

Assessment of the mechanical properties of an implant is crucial before commencing *in vivo* experiments. While different methods are available to measure the stiffness, we chose uniaxial stress-strain measurements so we could obtain real-world practical results about the membranes that could be compared with *in vivo* tissues or market available implants and biomaterials [43]. Measurements were performed on wet PSI, PSICYS and PSIDAB membranes (all of the membranes were immersed in saline solution to mimic the environment of the *in vivo*

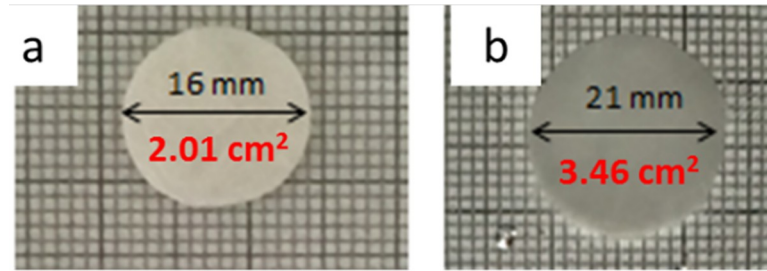


Fig 3. PSIDAB fibrous membrane before (a) and after hydrolysis (b), where red numbers are the area of samples.

<https://doi.org/10.1371/journal.pone.0254843.g003>

experiments). In this regard, tensile strength is generally documented in one of two units: a. In Force/area (N/m^2) for tissue or materials with well-defined dimensions or b. In Force/length (N/cm) for more complex materials with hard to define dimensions e.g., surgical meshes and specialized dressings. We present results as applicable.

In the first set of experiments, the maximum load-bearing capacity and the ultimate tensile strength of the raw membranes were investigated (Fig 4A and S5 Fig in S1 File). All samples exhibited similar initial behavior as their stress-strain curves are very steep, representing the high rigidity of the materials. The ultimate tensile strength of the membranes PSI was 6230 ± 1450 kPa or 12.32 ± 0.94 N/cm ($n = 8, p = 0.05$) of PSICYs it was 3947 ± 1001 kPa or 3.8 ± 0.9 N/cm ($n = 5, p = 0.05$) and of PSIDAB it was 2749 ± 390 kPa or 6.0 ± 1.0 N/cm ($n = 6, p = 0.05$) (Fig 4C and 4D). Since the standard errors in the measurements were quite high, we used two-sample t-test to see if there was a significant difference between the membrane types. According to the analysis, there was no significant difference between the maximum bearing loads of PSICYs and PSIDAB, however, they were both significantly different

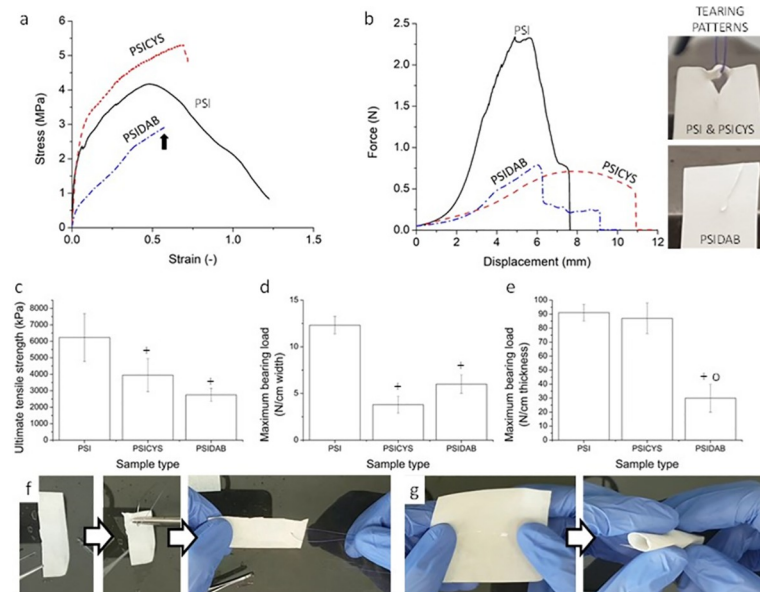


Fig 4. Examples for stress-strain curves of PSI, PSICYs and PSIDAB samples (black arrow indicates the tearing point of PSIDAB) (a), examples for force-displacement curves obtained in single interrupted suture model tests (b); ultimate tensile strengths (c), maximum bearing loads (d, e) of the samples; sutured PSIDAB sample (f), rolled up PSIDAB sample for e.g., laparoscopy (g). “+” means significant ($p = 0.05$) from PSI and “o” means significant difference from PSICYs.

<https://doi.org/10.1371/journal.pone.0254843.g004>

from the PSI membranes. In terms of performance the membranes are not suitable as bone, cartilage, or tendon implants or surgical meshes for hernia repair as their tensile strength is simply not high enough. Nevertheless, they are suitable as soft tissue implants. The tensile strength of the membranes is comparable to the tensile strengths of soft connective tissues and visceral tissues [43–45].

In the second set of experiments, a simple interrupted suture was placed on the samples (Fig 4F), which was then torn out by the mechanical tester while the force and displacement of the crosshead were registered (Suture Retention Test). Similarly, the assessed properties were the ultimate tensile strength and the maximum load-bearing capacity. Typical force-displacement curves of PSI, PSICYS and PSIDAB can be seen in Fig 4B whereas all the measured curves can be found in S6 Fig in S1 File.

In every case, the maximum bearing load of the suture retention test was considerably smaller than compared to the raw sample measurements. Ultimate tensile strength would be in theory calculated by dividing the maximum sustained load with the thickness of the suture material. However, the results would be highly overestimating the strength of the membranes. A relative tensile strength was calculated by dividing the maximum bearing loads by the thicknesses of the samples. For PSI membranes it was 91 ± 6 N/cm ($n = 4$, $p = 0.05$), for PSICYS membranes it was 87 ± 11 N/cm ($n = 6$, $p = 0.05$) while for PSIDAB membranes it was 30 ± 10 N/cm ($n = 6$, $p = 0.05$) (Fig 4E). According to two-sample t-tests, the PSIDAB once again was significantly different from the PSI and PSICYS samples that exhibited the same behavior. The load-bearing capacity of the sample may seem exceedingly small, but it is worth mentioning that no standardized criteria regarding suture retention tests are available. The measurement was rather performed to assess whether the membranes would withstand the surgical handling and *in vivo* suture fixation. Apart from instrument-based evaluations, during a manual surgical maneuver and suture fixation evaluation it was apparent (Fig 4G) that the membranes will indeed resist the intervention and fixation in the animals. Additionally, it is noteworthy that increasing the thickness of the fabricated membranes, will consequently result in an increase of their tensile strength as well. On the contrary, bulk hydrogels will still tear under the effect of sutures as their susceptibility to suturing is not in correlation with their thickness but with their texture.

3.4. *In vitro* experiments

Initially, both PASPCYS, PSIDAB and PASPDAB membranes were planned to be investigated. Although PASPCYS was stable in PBS for several days, it slowly degraded and lost its integrity completely during 8 days in the MEM solution (S7 Fig in S1 File). In contrast to this, PASPDAB could maintain its physical properties. This is in line with the expected biodegradability of the two materials. PSIDAB underwent hydrolysis and turned into PASPDAB, while shifting the pH of MEM toward the acidic region indicated by the MEM turning yellow.

By applying fluorescent pre-labelling, the cells could be visualized by multiphoton microscopy (Fig 5). On the plastic surface of tissue culture wells (Fig 5A), many healthy cells showing normal, star-like morphology can be seen. However, we could not find any cells on the PSIDAB membranes (Fig 5B), supposedly in this case the cells were only able to loosely attach to the membranes and all of them were removed during the fixation process including several washing steps. In addition, PSI based membranes shifted the pH value of the cell culture medium into the acidic range (its color always turned to yellow) indicating that these membranes do not support the survival of the cells under *in vitro* conditions. Nevertheless, large number of cells with healthy star-like morphology were observed on the PASPDAB membranes (Fig 5C and 5D). Fig 5E shows the control PASPDAB sample to demonstrate how the fibrous structure would look like without the cells.

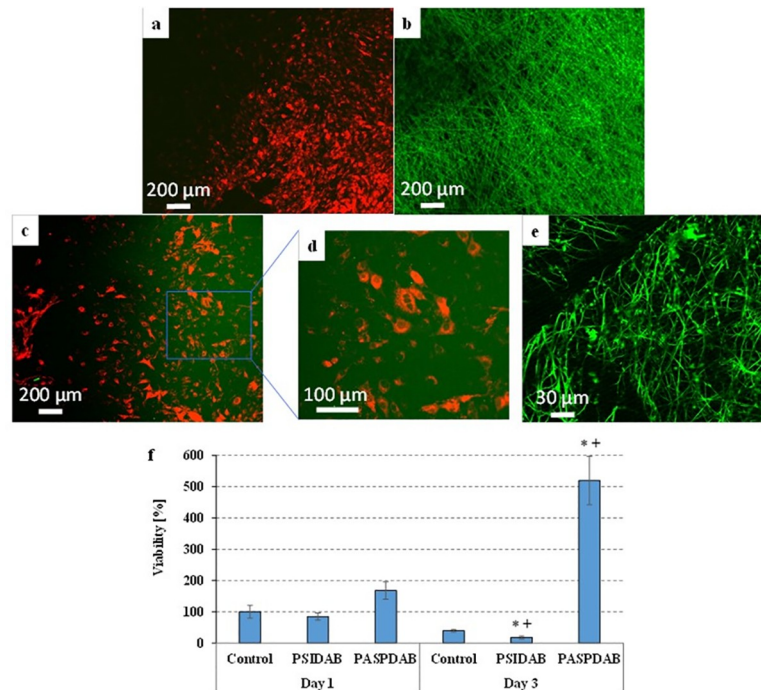


Fig 5. Multiphoton microscopic images of the Vybrant DiD-labelled MG-63 cells after 24-hour-long cultivation on the surfaces of "tissue culture" plastic plates (a) or PSIDAB (b) or PASPDAB based (c and d) fibrous membranes and PASPDAB membrane without cells as a control (e). The cells show red fluorescence due to the Vybrant DiD staining while the green color indicates the autofluorescence of the PSI or PASP membranes. Red and green channels are both shown on all pictures except the (e) where only the green was active. Viability of MG-63 cells after 1- or 3-day-long cultivation on the surfaces of "low cell binding" plastic plates (control) and PSIDAB or PASPDAB membranes (f). * $p < 0.05$ compared to the control. + $p < 0.05$ compared to day 1.

<https://doi.org/10.1371/journal.pone.0254843.g005>

The results of the viability assays (Fig 5F) show that the viability of MG-63 cells seeded onto PSIDAB and PASPDAB were similar to the control 1 day after the seeding. PASPDAB membranes showed no signs of cytotoxicity as the MG-63 osteosarcoma cells were able to attach to their surface and proliferate. These results are in agreement with our previous study, where biocompatibility of PASPDAB based bulk hydrogels was proven using the same cell line [25]. On the contrary the viability on PSIDAB decreased by day 3 (Fig 5F). As it was mentioned earlier, the MEM turned yellow due to the hydrolysis of PSIDAB marking a shift in pH toward the acidic range. MG-63 cells are not viable in acidic MEM which possibly caused the cell death, and a documented low viability. Therefore, based on this experiment it cannot be decided whether PSIDAB is cytotoxic as cell death most probably was caused by the pH shift. Nevertheless, this phenomenon is amplified in an *in vitro* setting as no fluid exchange is available. In contrast, in an *in vivo* environment, the body can readily compensate the lower pH. In this regard the results of the *in vivo* investigation should give further insight whether the shift is pH tolerable and whether meshes are biocompatible.

3.5. *In vivo* experiment

The purpose of the animal experiments was to investigate the surgical applicability of PSICYS and PSIDAB based membranes as suturable implants as well as to evaluate biocompatibility and biodegradability. The most important results of the *in vivo* studies are summarized in Table 2. The intra-operative surgical handling was easy for both materials and implantation took place without any difficulties. Samples were very flexible, and they could be rolled up or

Table 2. Collection of results of *in vivo* experiments, where at the biocompatibility rows the determined scores can be seen inside the brackets.

		PSICYS	PSIDAB
IMPLANTATION	Handling and surgery	Easy handling, good suturability, no difficulties	
	Macroscopic results	Hydrolysis and swelling by approximately 40% in size	
AFTER 3 DAY	Biocompatibility	Moderate acute inflammation (1.83)	Moderate acute inflammation (2.17)
	Biodegradation	Narrow band of granulation tissue (1.33)	Narrow band of granulation tissue (1.00)
AFTER 7 DAY	Tissue invasion	No observable degradation	
	Macroscopic results	No tissue invasion according to histopathology	No tissue invasion according to histopathology Attachment of cells to the surface of the samples
	Biocompatibility	Samples either not found or completely covered and incorporated by new tissue	Samples lost their integrity and strength Easy truncation by tweezers
	Tissue invasion	Mild acute inflammation (1.17)	Mild acute inflammation (1.33)
	Biodegradation	Moderate band of granulation tissue (1.50)	Narrow band of granulation tissue (1.33)
	Biocompatibility	Although degradation was observable macroscopically, histopathology showed the remnants of fibrous samples at implantation area	Degradation was not observable, however the loss of mechanical strength and integrity indicates it
	Tissue invasion	Not according to histopathology	Cells invaded the samples for several millimeters Incorporation of samples into the granulation tissue

<https://doi.org/10.1371/journal.pone.0254843.t002>

twisted in various degrees therefore their application is not limited to open surgical procedures but could be easily used for laparoscopic interventions as well (Fig 4D). Fixation with sutures was successful without any considerable damage to the implant. During the fixation suturability of the membranes was excellent and neither the sutures were torn out, nor the membranes were damaged. During the 3-day (Group A) and 7-day (Group B) observation no visible irritations, animal misbehavior or other macroscopically observable complications were detected. The animals behaved just as they did before surgery: normal food intake and bowel movement, mobility, and behavior with the caretakers were observed.

3.5.1. 3-day results. Three days after implantation (Group A) animals were terminated, implantation area was investigated, and the samples were resected. Both PSICYS (Fig 6A and S8 Fig in S1 File) and PSIDAB (Fig 7A) samples were found in their respective animals with

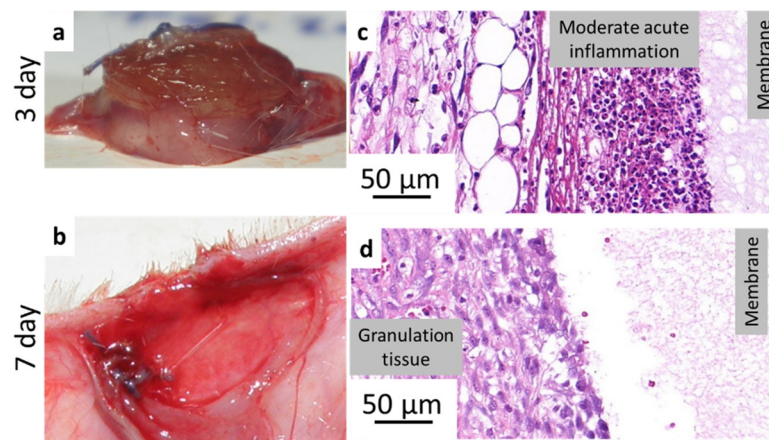


Fig 6. PASPCYS sample resected 3 days after implantation (a) and a representative image from histopathology (c); implantation area without sample after 7 days after implantation (b), a representative image from histopathology (d).

<https://doi.org/10.1371/journal.pone.0254843.g006>

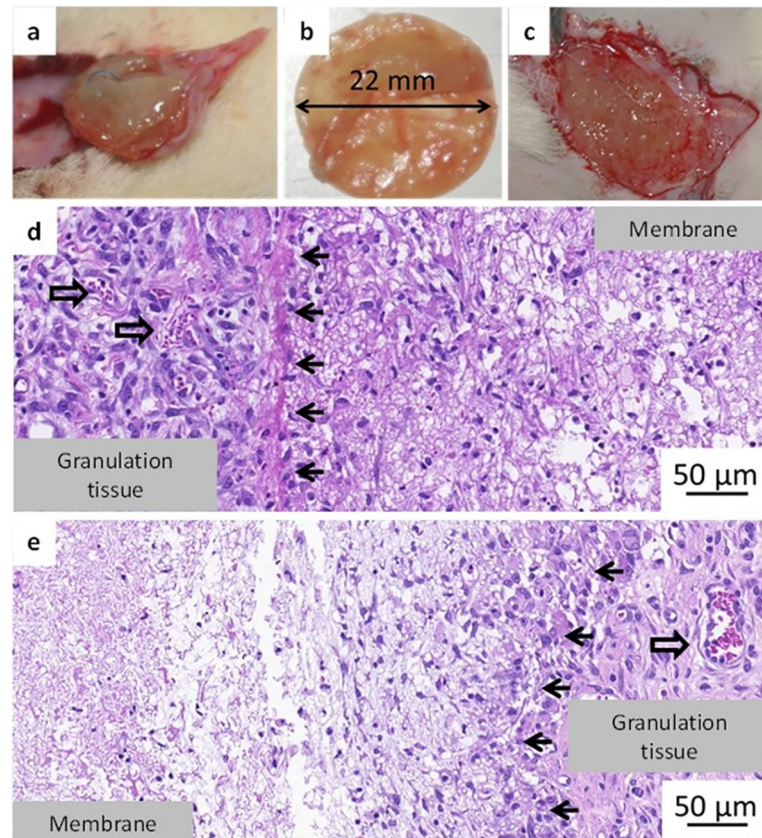


Fig 7. PASPDAB sample 3 days after implantation (a), resected sample grew in size and changed consistency (b), 7 days after implantation (c); representation of histopathology of a sample at day 3 (d) and day 7 (e); Black arrows indicate the boundary between the sample and the tissue and empty black arrows indicate blood vessels.

<https://doi.org/10.1371/journal.pone.0254843.g007>

physiological wound healing without any observable complications. There were no visible differences between the samples in different groups. However, both sample types grew by approximately 40% in diameter (from 16 mm to ~ 22 mm) and turned from the implanted white paper-like membranes to soft swollen gels (Figs 6A, 7A and 7B). Similar size change (16 mm to ~21 mm) due to hydrolysis was observed *in vitro* for both samples (Fig 3A and 3B, PSICYs not shown). This strongly suggests that hydrolysis of PSI based systems occurs *in vivo*, which is the first step in the biodegradation of PSI based materials. PSICYs and PSIDAB did not cause any irritation in the animals macroscopically nor created excessive skin tissue.

When a foreign object is implanted into a body, a natural response, the so-called foreign body type reaction is elicited [46]. Usually, it is a mild inflammation with granulocytes and histiocytes trying to restore the damaged area to its natural state for example by attacking or segregating the foreign object in a capsule (fibrosis) [47]. Although there is always some degree of foreign body type reaction and mild inflammation after any operation it is highly desirable to keep it minimal. Histopathological investigation as expected, revealed an acute inflammation in the tissue surrounding both types of samples further proving a physiological response of the animals to the implants. However, in neither case was this inflammation considered as a strong reaction. According to the scoring of *Planck et al.* [36] this inflammatory response is considered mild or moderate in the case of the PSIDAB samples (Table 2). PASPCYS samples were easily found on the slides surrounded by a rim of inflammatory cells predominantly comprising neutrophil granulocytes (Fig 6C and S9 Fig in S1 File), yet the cells did not invade the

membrane. In the case of the PSIDAB samples the inflammatory reaction of the body was stronger, with a mixture of neutrophil granulocytes, lymphocytes and histiocytes surrounding and invading the outer part of the membrane, making it difficult to distinguish the tissue and the implant (Fig 7D and S10 Fig in S1 File, where the black arrows indicate the supposed boundary between the sample and the tissue). Around both membranes a narrow (Table 2). fibroblastic reaction and granulation tissue are visible (Figs 6 and 7), which will become new connective tissue. It is worth emphasizing, that no giant foreign body cells were observed in any of the samples for either membrane.

3.5.2. 7-day results. Although similar results to the 3-day group were expected after 7 days group as well, significant differences were found between PSICYS and PSIDAB samples. In the case of PSICYS membranes (or in this state PASPCYS, because it was evidenced by the 3-day experiment that hydrolysis takes place) the samples were either not found in the animals (2 cases) or a soft new tissue was found in their place (4 cases) (Fig 6B). The soft granulation tissue grew around the suture, but it was easily deformed and removed. Upon cutting it half, there was no evidence for the presence of any PASPCYS remnants observable with the naked eye leading to the conclusion that these samples degraded and dissolved in 7 days. Furthermore, no signs of irritation, infection, or foreign body reaction neither on nor around the PASPCYS samples was found. Although macroscopically PASPCYS samples were impossible to find in the implantation area after 7 days, microscopically a fibrous substance (supposedly the PASPCYS matrix) was found with a moderate band of granulation tissue surrounding it (Fig 6D and S11 Fig in S1 File). In this state, the previously moderate inflammation declined to mild inflammation, while neovascularization (Table 2) was found in the granulation tissue. The new vessels formation (neovascularization) combined with the fact that no giant foreign body cells were found, highly indicates a healthy granulation tissue progressing to the proliferative phase of physiological wound healing.

In comparison, PASPDAB samples were found in a swollen, softer and more fragile state than their 3-day counterparts (Fig 7C). Therefore, hydrolysis has indeed occurred turning PSIDAB into PASPDAB. These samples were easily torn and dissected into separate layers or truncated by tweezers suggesting a high reduction in physical strength and consistency (S12 Fig in S1 File). Due to the deformation of the samples and incorporation of the surrounding tissue, it was hard to distinguish the samples from the granulation tissue macroscopically. Just as in the case of PSICYS, there were no macroscopic signs of irritation, infection, or foreign body type reaction neither on nor around the PASPDAB samples. Histopathology revealed the resolution of the acute inflammation observed on the 3rd day post-implantation to a mild level (Table 2). Furthermore, the incorporation of the granulation tissue into the sample evolved into a stage where the boundary between the sample and granulation tissue was almost impossible to mark exactly (Fig 7E and S13 Fig in S1 File). The living tissue being able to invade the membrane is an exceptional result as it suggests a proper tissue integration. When examining biomaterials, a very frequent phenomenon is the encapsulation and segregation of the implant via a fibrous capsule which is not considered as true tissue integration [48]. Additionally, giant foreign body cells were not found in the granulation tissue surrounding these samples either, further supporting the results. We found that the granulation tissue band was still narrow even when not considering the part which grew into the samples. However, the thickness of granulation tissue surrounding the samples may have been just inaccurately determined. To determine the exact composition of the PSIDAB matrix after 7 days, a small sample was gathered with a tweezer and investigated by multiphoton- and scanning electron microscope without any treatment (Fig 8). Both the fibrous sample and the cells surrounding it were visible under the microscope glowing in green with similar intensities, and thus it was not possible to properly distinguish the two by digital subtraction. Nonetheless, the retained fibrous structure of

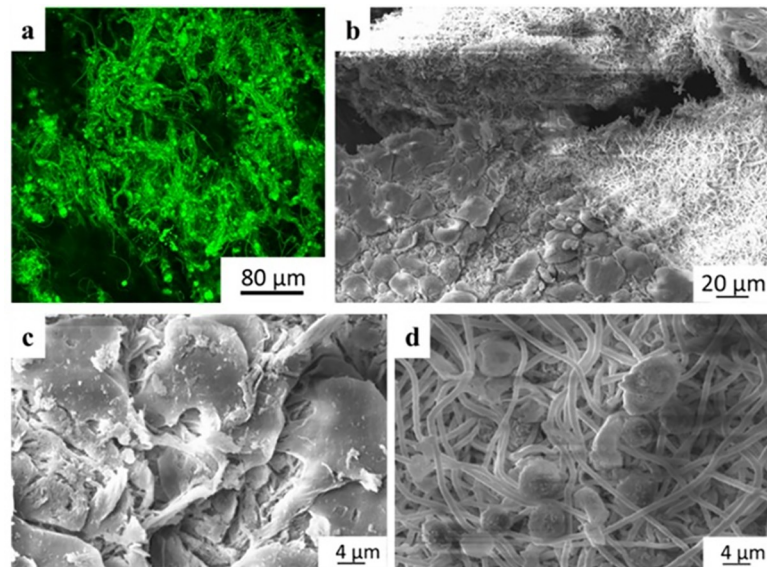


Fig 8. Multiphoton (a) and SEM (b, c, d) micrographs of PSIDAB sample from day 7.

<https://doi.org/10.1371/journal.pone.0254843.g008>

the DAB crosslinked sample was still observable. As a reference, the PASPDAB fibrous microstructure can be found as prepared *in vitro* (without the cells) under the multiphoton microscope in Fig 5F.

This phenomenon was also observed on the scanning electron microscopy investigations of the PASPDAB samples resected 7 days post-implantation (Fig 8B and 8C). The depicted cells are impossible to recognize and classified as they were possibly flattened due to the preparation process [46]. It is also observable in the figure that under the cellular shell the fibrous structure was intact without any observable degradation or morphological change. This was also similar to the fibrous structure of the PASPDAB membranes prepared *in vitro* (Fig 5F). Furthermore, many spheres were found with 6–8 μm in diameter suggesting the presence of either granulocytes, lymphocytes or red blood cells inside the matrix close to the surface, which is understandable given that histopathology showed vascularization around these samples. Therefore, these are the most probable corpuscular elements (based on the literature) with comparable size with the ones found on the SEM images (Fig 8D) [49, 50].

When comparing the two membranes we can clearly see a difference in *in vivo* behavior. The shorter and longer biodegradation times of PSICYs and PSIDAB accordingly are evident. This verifies our hypothesis that both PSIDAB and PSICYs systems hydrolyze and swell *in vivo* turning into the corresponding PASP based systems. The exact degradation mechanism of PSICYs has yet to be clarified, while PSIDAB maintains its physical form after 7 days implanted under the skin showing reduction in physical strength and consistency, thus showing signs of degradation.

4. Conclusion

Poly(aspartic acid) (PASP) hydrogel systems possess advantageous properties such as biodegradability, biocompatibility and easy functionalization. In this work we have presented the fabrication and characterization of electrospun crosslinked fibrous polysuccinimide (PSI) membranes. These membranes can readily hydrolyze into PASP fibrous hydrogels. These provide a reliable system during the implantation and a template even closer to the body's innate ECM. Two types of PSI fibrous membranes were prepared: one based on disulfide crosslinks

exhibiting fast biodegradation and another based on alkyl-chain crosslinks showing longer biodegradation time. According to mechanical assessments, both membranes showed adequate mechanical properties for suturing and surgery. *In vitro* tests showed that the disulfide crosslinked membrane dissolves in cell culture conditions in 8 days whereas the alkyl-chain crosslinked one was still stable. Furthermore, the membranes exhibited no cytotoxic side effects as MG-63 osteosarcoma cells could attach to their surface and freely proliferate. Implantability was tested *in vivo* on small animals. Membranes were implanted in Wistar rats, under the skin at the backside of the neck. The membranes changed into PASP based membranes in 3 days and after 7 days most of the disulfide crosslinked membranes disappeared, proving biodegradation. Histopathologic examinations in both cases showed only a mild to moderate acute inflammation, which diminished after 7 days. Moreover, excessive tissue invasion was also observed proving the biocompatibility and tissue integration capabilities of these systems. These results coupled with the easily modifiable chemical structure of the poly(amino acid) based system makes them ideal for advanced functionalized materials and platforms for biomedical research.

Supporting information

S1 File. Supporting text and figures. Pictures of macroscopic fibrous gel-membranes; additional SEM images, all measured curves of mechanical investigation which was not included in the text, additional macroscopic pictures, and histopathological slides from the *in vivo* experiment. (DOCX)

S1 Graphical abstract.
(TIF)

Author Contributions

Conceptualization: Kristof Molnar, Angela Jedlovszky-Hajdu.

Data curation: Rita Varga.

Formal analysis: Kristof Molnar, Constantinos Voniatis, Zoltan Kiss, Eniko Krisch, Krisztina S. Nagy.

Funding acquisition: Angela Jedlovszky-Hajdu.

Investigation: Constantinos Voniatis, Angela Jedlovszky-Hajdu.

Methodology: Constantinos Voniatis, Daniella Feher, David Juriga, Gyorgy Weber, Krisztina S. Nagy.

Supervision: Gyorgy Weber, Andrea Ferencz, Gabor Varga, Miklos Zrinyi, Krisztina S. Nagy, Angela Jedlovszky-Hajdu.

Validation: Daniella Feher, Gyorgyi Szabo, Lilla Reiniger, David Juriga, Zoltan Kiss.

Visualization: Kristof Molnar, Constantinos Voniatis, Angela Jedlovszky-Hajdu.

Writing – original draft: Kristof Molnar, Constantinos Voniatis, Eniko Krisch, Krisztina S. Nagy, Angela Jedlovszky-Hajdu.

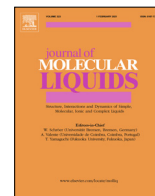
References

1. Caló E, Khutoryanskiy V V. Biomedical applications of hydrogels: A review of patents and commercial products. *Eur Polym J.* 2015; 65: 252–267. <https://doi.org/10.1016/j.eurpolymj.2014.11.024>

2. Yeo CK, Vikhe YS, Li P, Guo Z, Greenberg P, Duan H, et al. Hydrogel Effects Rapid Biofilm Debridement with ex situ Contact-Kill to Eliminate Multidrug Resistant Bacteria in vivo. *ACS Appl Mater Interfaces*. 2018; 10: 20356–20367. <https://doi.org/10.1021/acsami.8b06262> PMID: 29806938
3. Zhu H, Yang X, Genin GM, Lu TJ, Xu F, Lin M. The relationship between thiol-acrylate photopolymerization kinetics and hydrogel mechanics: An improved model incorporating photobleaching and thiol-Michael addition. *J Mech Behav Biomed Mater*. 2018; 88: 160–169. <https://doi.org/10.1016/j.jmbbm.2018.08.013> PMID: 30173068
4. Dong Y, Jin G, Hong Y, Zhu H, Lu TJ, Xu F, et al. Engineering the Cell Microenvironment Using Novel Photoresponsive Hydrogels. *ACS Appl Mater Interfaces*. 2018; 10: 12374–12389. <https://doi.org/10.1021/acsami.7b17751> PMID: 29537822
5. Yao M, Gao F, Xu R, Zhang J, Chen Y, Guan F. A dual-enzymatically cross-linked injectable gelatin hydrogel loaded with BMSC improves neurological function recovery of traumatic brain injury in rats. *Biomater Sci*. 2019. <https://doi.org/10.1039/c9bm00749k> PMID: 31355388
6. Feksa LR, Troian EA, Muller CD, Viegas F, Machado AB, Rech VC. Hydrogels for biomedical applications. *Nanostructures Eng Cells, Tissues Organs From Des to Appl*. 2018; 64: 403–438. <https://doi.org/10.1016/B978-0-12-813665-2.00011-9>
7. Calvert P. Hydrogels for soft machines. *Adv Mater*. 2009; 21: 743–756. <https://doi.org/10.1002/adma.200800534>
8. Xue J, Xie J, Liu W, Xia Y. Electrospun Nanofibers: New Concepts, Materials, and Applications. *Acc Chem Res*. 2017; 50: 1976–1987. <https://doi.org/10.1021/acs.accounts.7b00218> PMID: 28777535
9. Wang K, Hou W Da, Wang X, Han C, Vuletic I, Su N, et al. Overcoming foreign-body reaction through nanotopography: Biocompatibility and immunoisolation properties of a nanofibrous membrane. *Biomaterials*. 2016; 102: 249–258. <https://doi.org/10.1016/j.biomaterials.2016.06.028> PMID: 27344368
10. Damanik FFR, Spadolini G, Rotmans J, Farè S, Moroni L. Biological activity of human mesenchymal stromal cells on polymeric electrospun scaffolds. *Biomater Sci*. 2019; 7: 1088–1100. <https://doi.org/10.1039/c8bm00693h> PMID: 30633255
11. Alessandrino A, Fregnan F, Biagiotti M, Muratori L, Bassani GA, Ronchi G, et al. SilkBridge™: a novel biomimetic and biocompatible silk-based nerve conduit. *Biomater Sci*. 2019. <https://doi.org/10.1039/C9BM00783K> PMID: 31359013
12. Fu GD, Xu LQ, Yao F, Zhang K, Wang XF, Zhu MF, et al. Smart Nanofibers from Combined Living Radical Polymerization, “Click Chemistry”, and Electrospinning. *ACS Appl Mater Interfaces*. 2009; 1: 239–243. <https://doi.org/10.1021/am800143u> PMID: 20353208
13. Dhand C, Venkatesh M, Barathi VA, Harini S, Bairagi S, Goh Tze Leng E, et al. Bio-inspired crosslinking and matrix-drug interactions for advanced wound dressings with long-term antimicrobial activity. *Biomaterials*. 2017; 138: 153–168. <https://doi.org/10.1016/j.biomaterials.2017.05.043> PMID: 28578293
14. Kim Y-J, Ebara M, Aoyagi T. Temperature-responsive electrospun nanofibers for ‘on-off’ switchable release of dextran. *Sci Technol Adv Mater*. 2012; 13: 064203. <https://doi.org/10.1088/1468-6996/13/6/064203> PMID: 27877530
15. Molnar K, Jozsa B, Barczikai D, Krisch E, Puskas JE, Jedlovsky-Hajdu A. Plasma treatment as an effective tool for crosslinking of electrospun fibers. *J Mol Liq*. 2020; 303: 112628–112636. <https://doi.org/10.1016/j.molliq.2020.112628>
16. Zeng Jun, Hou Haoqing, Joachim H, Wendorff AG. Photo-Induced Solid-State Crosslinking of Electrospun Poly(vinyl alcohol) Fibers. *Macromol Rapid Commun Rapid Commun*. 2005; 26: 1557–1562. <https://doi.org/10.1002/marc.200500545>
17. Theron JP, Knoetze JH, Sanderson RD, Hunter R, Mequanint K, Franz T, et al. Modification, crosslinking and reactive electrospinning of a thermoplastic medical polyurethane for vascular graft applications. *Acta Biomater*. 2010; 6: 2434–47. <https://doi.org/10.1016/j.actbio.2010.01.013> PMID: 20080215
18. Zrinyi M, Gyenes T, Juriga D, Kim J-H. Volume change of double cross-linked poly(aspartic acid) hydrogels induced by cleavage of one of the crosslinks. *Acta Biomater*. 2013; 9: 5122–31. <https://doi.org/10.1016/j.actbio.2012.08.046> PMID: 22975627
19. Thombre SM, Sarwade BD. Synthesis and biodegradability of polyaspartic acid: A critical review. *J Macromol Sci—Pure Appl Chem*. 2005; 42 A: 1299–1315. <https://doi.org/10.1080/10601320500189604>
20. Lim S, Nguyen MP, Choi Y, Kim J, Kim D. Bioadhesive Nanoaggregates Based on Polyaspartamide-g-C18/DOPA for Wound Healing. *Biomacromolecules*. 2017; 18: 28678473. <https://doi.org/10.1021/acs.biomac.7b00584> PMID: 28678473
21. Di Meo C, Cilirzo F, Licciardi M, Scialabba C, Sabia R, Paolino D, et al. Polyaspartamide-Doxorubicin Conjugate as Potential Prodrug for Anticancer Therapy. *Pharm Res*. 2015; 32: 1557–1569. <https://doi.org/10.1007/s11095-014-1557-2> PMID: 25366547

22. Sharma A, Kundu S, Reddy M A, Bajaj A, Srivastava A. Design and Engineering of Disulfide Cross-linked Nanocomplexes of Polyamide Polyelectrolytes: Stability under Biorelevant Conditions and Potent Cellular Internalization of Entrapped Model Peptide. *Macromol Biosci.* 2013; 13: 927–937. <https://doi.org/10.1002/mabi.201300018> PMID: 23696522
23. Craparo EF, Porsio B, Sardo C, Giammona G, Cavallaro G. Pegylated Polyaspartamide-Polylactide-Based Nanoparticles Penetrating Cystic Fibrosis Artificial Mucus. *Biomacromolecules.* 2016; 17: 767–777. <https://doi.org/10.1021/acs.biomac.5b01480> PMID: 26866983
24. Kim M, Shin SW, Lim CW, Kim J, Um SH, Kim D. Polyaspartamide-based graft copolymers encapsulating iron oxide nanoparticles for imaging and fluorescence labelling of immune cells. *Biomater Sci.* 2017. <https://doi.org/10.1039/c6bm00763e> PMID: 27999834
25. Juriga D, Nagy K, Jedlovszky-Hajdú A, Perczel-Kovács K, Chen YM, Varga G, et al. Biodegradation and Osteosarcoma Cell Cultivation on Poly(aspartic acid) Based Hydrogels. *ACS Appl Mater Interfaces.* 2016; 8: 23463–23476. <https://doi.org/10.1021/acsami.6b06489> PMID: 27541725
26. Molnar K, Juriga D, Nagy PM, Sinko K, Jedlovszky-Hajdu A, Zrinyi M. Electrospun poly(aspartic acid) gel scaffolds for artificial extracellular matrix. *Polym Int.* 2014; 63: 1608–1615. <https://doi.org/10.1002/pi.4720>
27. Molnar K, Jedlovszky-Hajdu A, Zrinyi M, Jiang S, Agarwal S. Poly(amino acid)-Based Gel Fibers with pH Responsivity by Coaxial Reactive Electrospinning. *Macromol Rapid Commun.* 2017; 201700147: 1700147–1700151. <https://doi.org/10.1002/marc.201700147> PMID: 28488377
28. Varga Z, Molnár K, Torma V, Zrinyi M. Kinetics of volume change of poly(succinimide) gels during hydrolysis and swelling. *Phys Chem Chem Phys.* 2010; 12: 12670–12675. <https://doi.org/10.1039/c0cp00527d> PMID: 20730186
29. Wang B, Jeon YS, Park HS, Kim YJ, Kim JH. Mussel-mimetic self-healing polyaspartamide derivative gel via boron-catechol interactions. *Express Polym Lett.* 2015; 9: 799–808. <https://doi.org/10.3144/expresspolymlett.2015.75>
30. Sharma A, Srivastava A. Pronounced influence of pH, metal-ion and solvent isotope on the thermoresponse of synthetic amphiphilic polypeptides. *Polym Chem.* 2013; 5119–5128. <https://doi.org/10.1039/c3py00741c>
31. Németh C, Szabó D, Gyarmati B, Gerasimov A, Varfolomeev M, Abdullin T, et al. Effect of side groups on the properties of cationic polyaspartamides. *Eur Polym J.* 2017; 93: 805–814. <https://doi.org/10.1016/j.jpharm.2016.12.007> PMID: 27931785
32. Weyenberg W, Vermeire A, D'Haese E, Vanhaelewyn G, Kestelyn P, Callens F, et al. Effect of different sterilisation methods on the properties of bioadhesive powders and ocular minitablets, and clinical evaluation. *Eur J Pharm Sci.* 2004; 23: 77–87. <https://doi.org/10.1016/j.ejps.2004.05.010> PMID: 15324925
33. Noszticzus Z, Wittmann M, Kály-Kullai K, Beregvári Z, Kiss I, Rosivall L, et al. Chlorine dioxide is a size-selective antimicrobial agent. *PLoS One.* 2013; 8: 1–10. <https://doi.org/10.1371/journal.pone.0079157> PMID: 24223899
34. Pensalfini M, Meneghello S, Lintas V, Bircher K, Ehret AE, Mazza E. The suture retention test, revisited and revised. *J Mech Behav Biomed Mater.* 2018; 77: 711–717. <https://doi.org/10.1016/j.jmbbm.2017.08.021> PMID: 28867371
35. Kumar V, Abbas KA, Aster JC. *Robbins Basic Pathology.* 10th ed. Elsevier Health Sciences; 2017. Available: <https://www.elsevier.com/books/robbins-basic-pathology/kumar/978-0-323-35317-5>
36. Schmitt VH, Planck CN. Histological and Immunohistological Evaluation of the Tissue Response of a New Barrier Material Based on D,L-Polylactide, Trimethylene Carbonate and Caprolactone to Prevent Peritoneal Adhesion Formation. *J Tissue Sci Eng.* 2014;05. <https://doi.org/10.4172/2157-7552.1000138>
37. Krisch E, Messenger L, Gyarmati B, Ravaine V, Szilágyi A. Redox- and pH-Responsive Nanogels Based on Thiolated Poly(aspartic acid). *Macromol Mater Eng.* 2016; 301: 260–266. <https://doi.org/10.1002/mame.201500119>
38. Jones EM, Cochrane CA, Percival SL. The Effect of pH on the Extracellular Matrix and Biofilms. *Adv Wound Care.* 2015; 4: 431–439. <https://doi.org/10.1089/wound.2014.0538> PMID: 26155386
39. Lu W, Ma M, Xu H, Zhang B, Cao X, Guo Y. Gelatin nanofibers prepared by spiral-electrospinning and cross-linked by vapor and liquid-phase glutaraldehyde. *Mater Lett.* 2015; 140: 1–4. <https://doi.org/10.1016/j.matlet.2014.10.146>
40. Jeffries EM, Allen RA, Gao J, Pesce M, Wang Y. Highly elastic and suturable electrospun poly(glycerol sebacate) fibrous scaffolds. *Acta Biomater.* 2015; 18: 30–39. <https://doi.org/10.1016/j.actbio.2015.02.005> PMID: 25686558
41. Zhang C, Wu S, Qin X. Facile fabrication of novel pH-sensitive poly(aspartic acid) hydrogel by crosslinking nanofibers. *Mater Lett.* 2014; 132: 393–396. <https://doi.org/10.1016/j.matlet.2014.06.031>

42. Gyenes T, Torma V, Gyarmati B, Zrínyi M. Synthesis and swelling properties of novel pH-sensitive poly (aspartic acid) gels. *Acta Biomater.* 2008; 4: 733–44. <https://doi.org/10.1016/j.actbio.2007.12.004> PMID: 18280800
43. Guimarães CF, Gasperini L, Marques AP, Reis RL. The stiffness of living tissues and its implications for tissue engineering. *Nat Rev Mater.* 2020; 5: 351–370. <https://doi.org/10.1038/s41578-019-0169-1>
44. Colley H, McArthur SL, Stolzing A, Scutt A. Culture on fibrin matrices maintains the colony-forming capacity and osteoblastic differentiation of mesenchymal stem cells. *Biomed Mater.* 2012; 7: 045015. <https://doi.org/10.1088/1748-6041/7/4/045015> PMID: 22689305
45. Todros S, Pavan PG, Pachera P, Natali AN. Synthetic surgical meshes used in abdominal wall surgery: Part II-Biomechanical aspects. *J Biomed Mater Res Part B Appl Biomater.* 2017; 105: 892–903. <https://doi.org/10.1002/jbm.b.33584> PMID: 26687728
46. Daniell H, Anderson JM, Rodriguez A, Chang DT. Foreign Body Reaction to Biomaterials. *Semin Immunol.* 2008; 20: 86–100. <https://doi.org/10.1016/j.smim.2007.11.004> PMID: 18162407
47. Jones KS. Effects of biomaterial-induced inflammation on fibrosis and rejection. *Semin Immunol.* 2008; 20: 130–136. <https://doi.org/10.1016/j.smim.2007.11.005> PMID: 18191409
48. Chandorkar Y, K R, Basu B. The Foreign Body Response Demystified. *ACS Biomater Sci Eng.* 2019; 5: 19–44. <https://doi.org/10.1021/acsbiomaterials.8b00252> PMID: 33405858
49. Kim J, Nafiujjaman M, Nurunnabi M, Lim S, Lee Y-K, Park H-K. Effects of polymer-coated boron nitrides with increased hemorheological compatibility on human erythrocytes and blood coagulation. *Clin Hemorheol Microcirc.* 2018; 1–16. <https://doi.org/10.3233/CH-170307> PMID: 29710679
50. De Almeida HL, Coelho Bicca EDB, De Andrade MM, Andrade Neto PDR. Scanning electron microscopy of granuloma annulare. *An Bras Dermatol.* 2018; 93: 740–742. <https://doi.org/10.1590/abd1806-4841.20187409> PMID: 30156630



Ultrasound induced, easy-to-store porous poly(amino acid) based electrospun scaffolds



Rita Pázmány^a, Krisztina S. Nagy^a, Ákos Zsembery^b, Angela Jedlovsky-Hajdu^{a,*}

^aLaboratory of Nanochemistry, Department of Biophysics and Radiation Biology, Semmelweis University, Budapest, Hungary

^bDepartment of Oral Biology, Semmelweis University, Budapest, Hungary

ARTICLE INFO

Article history:

Received 24 February 2022

Revised 1 April 2022

Accepted 22 April 2022

Available online 28 April 2022

Keywords:

Tissue engineering

Ultrasonication

3D scaffold

Electrospinning

Amino acid based polymer

Polysuccinimide

ABSTRACT

The aim of tissue engineering is to develop methods to restore, maintain or improve tissue functions. To imitate the fibrous structure of the native extracellular matrix, the electrospinning technique is widely used. However, the dense packing of fibers results in small pores and hereby the inhibition of cellular penetration.

In this study, we used biocompatible and biodegradable poly(aspartic acid) based fibrous hydrogel scaffolds to enhance the cell infiltration using ultrasonication (US). The US can enlarge the space between the fibers in the scaffold and create a 3D structure based on the thickness increase of the samples. To prevent the scaffolds from degradation and create an easy-to-store sample beyond the US treatment, a freeze-drying process was also introduced in this work. After all these treatments, the scaffold's specific load capacity was $0.11 \pm 0.01 \text{ Nm}^2/\text{g}$ which did not change after a rehydration cycle and the elongation break became almost two times higher than before the US treatment. The cytotoxicity results demonstrated that the cellular viability did not show any significant decrease compared to the control groups for none of the samples. The cellular penetration was visualized by multiphoton microscopy.

In summary, we were able to overcome the major limitation of conventional electrospun scaffolds regarding their application in tissue engineering. We also improved the storing conditions of fibrous hydrogel scaffolds and extend their shelf life without degradation.

© 2022 The Authors. Published by Elsevier B.V. This is an open access article under the CC BY license (<http://creativecommons.org/licenses/by/4.0/>).

1. Introduction

Tissue engineering is an interdisciplinary field that applies the principles of engineering and life sciences to develop methods to restore, maintain or improve tissue functions [1]. Most techniques use scaffolds to mimic the native extracellular matrix (ECM) by providing mechanical support for the cells that are intended to replace the injured or diseased tissue [2]. The ECM has a three-dimensional nanofibrillar supramolecular structure and contains a great amount of water. Therefore, it behaves similarly to a gel-like structure and allows not only oxygen and nutrient delivery but waste removal as well.

To imitate the fibrous structure of the native ECM, the electrospinning technique is widely used [3]. During this process, a non-woven mat can be produced consisting of polymer fibers with a diameter on nanometer- or micrometer scale. Plenty of publications have recently appeared in the field of nanotechnology and tissue engineering regarding electrospun fibrous structures using biopolymers such as collagen [4] and gelatin [5], or synthetic poly-

mers such as polycaprolactone [6], polyvinylpyrrolidone [7] or synthetic biopolymers such as poly-L-lactic acid [8], and polyamino acids [9] separately, or in combination [10].

A primary requirement for any type of successful implant is biocompatibility, indicating that neither the material nor its degradation products have cytotoxic effects and generate immunological overreaction [11]. Biopolymers due to their biomimetic structure are biologically suitable, biocompatible, and non-toxic materials [12]. However, the application of biopolymers is restricted by their uncontrollable mechanical strength and rate of degradation, as well as their possible microbial contamination (difficulties in disinfection) [13]. The synthetic polymers have low bioactivity and lack of cell adhesion sites. However, their physical and chemical properties can be much better manipulated compared to the biopolymers [14]. The biocompatibility of synthetic biopolymers like poly(amino acids) is attributable to their structure that is very similar to naturally occurring proteins. In addition, they also possess the advantages of all synthetic polymers like low batch-to-batch variability and controllable properties of strength and rate of degradation [15]. Degradability is also an important factor of potential implants while depending on the intended application

* Corresponding author at: Nagyvárad square 4, 1089 Budapest, Hungary.

E-mail address: hajdu.angela@med.semmelweis-univ.hu (A. Jedlovsky-Hajdu).

purpose, the scaffolding materials should be biodegradable or nondegradable.

A further crucial requirement to fulfil is the porous structure of the artificial scaffolds. The adequate porosity of the scaffold enables the penetration of the cells, and the sufficient diffusion of nutrients and metabolic waste products [16]. Appropriate pore size for supporting colonization is in the range of 100–150 μm regarding most cell types, while pores with a diameter larger than 300 μm cannot be colonized completely [17,18]. However, electrospinning yields densely deposited mesh of randomly arrayed fibers resulting in low porosity and small sized pores, which restricts their use in biomedical applications. To enhance the cellular infiltration of the scaffold, the scientists had to balance between the desired mechanical strength and the increasing porosity, since these two properties seem to be inversely proportional [19]. To improve the porosity of the electrospun scaffolds, researchers developed various methods. In several approaches, the packing density is decreased due to the application of 3D printed scaffolds covered with electrospun fibers [20], special collectors [21], co-electrospinning techniques [22], emulsion electrospinning [23], or post-production processes such as gas foaming [24] and ultrasonication [25–27].

As scaffolding materials, hydrophilic polymers that can form hydrogels through crosslinks, show increasing popularity, as they have been found to be useable in many biomedical applications. Due to their high water content, their mechanical properties are similar to that of the ECM and soft tissues. Consequently, hydrogels are considered potential materials for tissue engineering [28].

However, besides the advantages of hydrogels as scaffolds, they also introduce challenges concerning long-term preservation. Due to their high water content, they are exposed to microbial spoilage [29]. Typically, tissue engineering products that are approved by the FDA (United States Food and Drug Administration) are preserved by cryopreservation at $-80\text{ }^{\circ}\text{C}$ for long term (Apligraf[®] [30], Dermagraft[®] [31]), but the transport of cryopreserved substances are expensive and challenging [32]. Another possible solution is drying the scaffolds, which reduces the water content to a minimal level where the deteriorative chemical reactions and the proliferation of bacteria are decreased or totally inhibited [29], then rehydrating them before use. Freeze-drying is a gentle technique, that is often applied in the case of heat-sensitive materials. However, both the drying [32] and the rehydrating process can affect the mechanical properties, although these effects are not revealed yet. A scaffold that is easy-to-store and transport would be a huge step towards an off-the-shelf product for tissue regeneration.

This study aimed to overcome one of the major limitations regarding the application of conventional electrospun scaffolds, namely the dense packing of fibers, that results in small pores and hereby the inhibition of cellular penetration. The other goal was to improve the storing conditions of fibrous hydrogels and extend their shelf life without degradation. To create a hydrogel scaffolding material, we used the precursor of polyaspartic acid (PASP), i.e. polysuccinimide (PSI) to produce electrospun fibers. The polymer chains were crosslinked with 1,4-Diaminobutane and after hydrolyzation, a fibrous hydrogel network was formed (PASP/DAB). We investigated the influence of ultrasonication on the chemical, mechanical, and toxicological properties, as well as the permeability of PASP/DAB scaffolds for cells. Freeze-drying as an alternative storing condition and its influence on the mechanical properties were also examined.

2. Experimental section

2.1. List of materials

L-aspartic acid (99%), phosphoric acid ($\geq 99.0\%$), 1,4-Diaminobutane (DAB, 99%), imidazole ($\geq 99.5\%$), paraformaldehyde

(PFA, 95%), and phosphate buffered saline (PBS) tablets were purchased from Sigma Aldrich (USA). N, N-dimethylformamide (DMF, $\geq 99.5\%$), and anhydrous ethanol (94–98%) were obtained from Reanal (Hungary). Citric acid monohydrate ($\geq 99.9\%$) and sodium-chloride (99.9%) were bought from VWR (USA). Minimum Essential Medium Eagle (M2279), Minimum Essential Medium without phenol red (51200–046), heat-inactivated Fetal Bovine Serum (FBS), penicillin (10,000 U/ml)-streptomycin (10,000 $\mu\text{g}/\text{ml}$), L-glutamine (200 mM), non-essential amino acids solution (NEAA), sterile phosphate buffered saline (PBS) solution, and Vybrant DiD fluorescent vital dye were purchased from Thermo Fisher Scientific (Gibco, Invitrogen, USA). The WST-1 cell proliferation reagent was obtained from Roche (Switzerland). Ultrapure water was provided by the Human Corporation ZeneerPower I Water Purification System (Republic of Korea). All chemicals were used without further purification.

2.2. Synthesis of Polysuccinimide (PSI)

PSI was synthesized through thermal polycondensation of L-aspartic acid in the presence of phosphoric acid as a catalyst at $180\text{ }^{\circ}\text{C}$ under vacuum using a previously described protocol [33].

Briefly, L-aspartic acid and crystalline phosphoric acid were mixed at a 1:1 mass ratio in a pear-shaped flask without any solvent. The mixture was gradually heated up to $180\text{ }^{\circ}\text{C}$, while the pressure was gradually decreased to 5 mbar using a rotary vacuum evaporator system (130 rpm) (RV10, digital rotary evaporator, IKA, Germany). The duration of the synthesis was 8 h. After the product reached room temperature, it was dissolved in dimethylformamide (DMF), then the solution was poured into ultrapure water and the precipitate was filtered and washed until the pH of the supernatant became neutral. After the final filtering, the PSI was oven-dried at $40\text{ }^{\circ}\text{C}$ for 2 days resulting in a white powder.

Based on the previous work of our research group, the viscosity-average molar mass of PSI is $28500 \pm 3000\text{ g/mol}$ calculated by Kuhn-Mark-Houwink equation [33]. To determine the density of the PSI, prior to using a pycnometer with anhydrous ethanol, a hydraulic press (EZ-Tools Hungary) was utilized to compress the pellets of the polymer powder.

2.3. Fabrication of PSI nanofibers by electrospinning

To fabricate PSI-based electrospun nanofibrous scaffolds, PSI was dissolved in DMF to produce a 25 w/w% solution (Fig. 1). The polymer solution was loaded into a 5 mL syringe (Henke Sass Wolf) fitted with a metal blunt-ended 18G needle and it was electrospun directly on an aluminum foil-covered drum collector (10 rpm; diameter = 10 cm) of the electrospinning system with a 20 cm needle tip-to-collector distance. A syringe pump (KDS100, KD Scientific, USA) was used to deliver the polymer solution to the needle tip at a constant feed rate of 1.0 mL/h. Electrospinning was conducted below 40 % humidity level, at the temperature of $22\text{--}26\text{ }^{\circ}\text{C}$ for 4 h using a high-voltage DC power supply (73030P series, Genvolt, UK) at 12 kV. For the subsequent measurements and modifications, the resultant nanofibrous scaffold sheet was cut into adequate forms (circular: diameter 6 mm or 16 mm, prepared by commercially available hole punchers; rectangular: $2 \times 2.5\text{ cm}$, the longer side of the rectangle is parallel with the axis of rotation, prepared by a pair of scissors).

2.4. Post-electrospinning processing

The schematic representation of the full process can be found in Fig. 1 and the details are listed below. The abbreviations of the samples and the explanations of commonly used features can be found in Table 1.

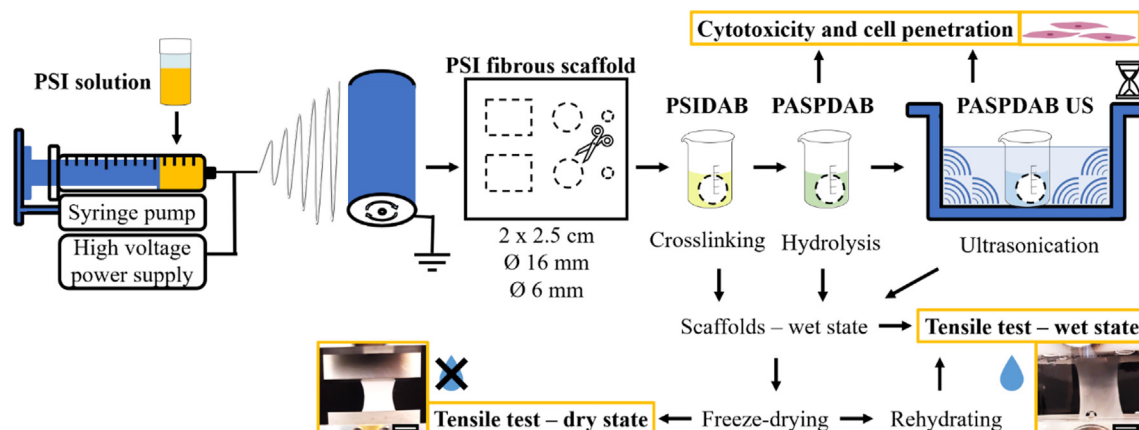


Fig. 1. Schematic representation of the preparation and investigation of different scaffolds. The scale bars indicate 1 cm.

2.4.1. Crosslinking

The polymer chains were chemically crosslinked after the electrospinning process by wet chemistry. The crosslinking was performed by immersing each scaffold in 0.5 M DAB in anhydrous ethanol for 3 h, the same way as it was published previously [34]. After immersion, the scaffolds were repeatedly washed with ultrapure water till neutral pH. A sample of each batch of the resultant scaffolds (PSIDAB) was subjected to a dissolution test in DMF to prove the existence of crosslinks.

2.4.2. Hydrolysis

The hydrolysis of PSIDAB was conducted overnight in a mild alkali medium, in a water-based imidazole buffer at pH 8, where the ionic strength was 250 mM [35]. For 1 L of imidazole buffer (pH = 8) 12.988 g imidazole, 1.728 g citric acid monohydrate and 11.466 g sodium-chloride was dissolved in ultrapure water. After the hydrolysis, the resultant hydrogel samples (PASPDAB) were washed with ultrapure water to remove the remaining salts.

2.4.3. Ultrasonication

The PASPDAB samples were immersed into ultrapure water in a glass sample container at room temperature and ultrasonicated using a USC900THD ultrasonicator (VWR, Germany) with a power of 200 W. The duration of the treatment was in the range of 1 min to 120 min. For further characterization, PASPDAB scaffolds subjected to 60 min ultrasonication treatment were chosen.

2.4.4. Freeze-drying

The fibrous scaffolds were freeze-dried before some investigations. Before freeze-drying, the samples were washed thoroughly with ultrapure water, then were frozen at $-20\text{ }^{\circ}\text{C}$ covered with ultrapure water. The freeze-drying was carried out using a Christ Alpha 1-4 LSC freeze-dryer (Germany). The thickness of the ultrasonicated samples was measured after freeze-drying on calibrated images using the ImageJ program (Open Source Software). The PASPDAB samples went under mechanical investigation after

Table 1

List of abbreviations and explanations of commonly used features.

PSI	Polysuccinimide
PSIDAB	Polysuccinimide crosslinked with 1,4-Diaminobutane
PASPDAB	Poly(aspartic acid) crosslinked with 1,4-Diaminobutane
PASPDAB US	Poly(aspartic acid) crosslinked with 1,4-Diaminobutane – ultrasonicated for 1 h
fresh	the samples were investigated immediately after preparation
rehydrated	the samples were investigated after freeze-drying and hydrating

freeze-drying and followed by hydrating, these samples are hereafter referred to as “rehydrated”.

2.5. Attenuated total Reflectance Fourier Transform Infrared (ATR-FTIR) spectroscopy

To characterize the chemical structure of the samples, Attenuated Total Reflectance Fourier Transform Infrared spectroscopy (ATR-FTIR) was carried out using a JASCO 4700 (type A) FT/IR spectrophotometer equipped with a diamond ATR head. Samples were clamped directly against the diamond with consistent pressure. Infrared spectra were collected in the wavenumber range of $4000 - 400\text{ cm}^{-1}$ at a spectral resolution of 2 cm^{-1} with 126 total numbers of scans, using H_2O , CO_2 , and ATR head subtraction. The background spectra were measured using clean and dry diamond crystal. PSI powder samples were examined oven-dried after synthesis. Electrospun PSI was measured dry, directly after electrospinning. The derivatives of PSI were examined after being washed with ultrapure water and freeze-dried for 18 h. The effect of the sterilization with UV light exposition (1 h) on the chemical structure of PASPDAB was also investigated.

2.6. Scanning electron microscopy (SEM)

Morphological investigations of the fibrous structure of the samples were carried out using a JSM 6380LA scanning electron microscope (JEOL, Japan). PSIDAB, PASPDAB, PASPDAB US samples were washed with ultrapure water and freeze-dried for 18 h before the examination, while PSI required no further treatment. Samples were fixed on an adaptor with a conductive sticker then they were sputter-coated with gold in 20–30 nm thickness using a JFC-1200 Sputter Coating System (JEOL, Japan). During the investigation of the samples by SEM, the applied accelerating voltage was 10 kV. For fiber diameter distribution analysis, 100 individual fibers were measured at 5000x magnification using the ImageJ program (Open Source Software). Shapiro-Wilk test for normality [36] and the following one-way ANOVA (Welch's correction) were performed using the GraphPad Prism 8.0.1 software (GraphPad Inc., USA).

2.7. Mechanical characterization

The mechanical properties of the samples were measured using a uniaxial mechanical testing machine (4952, Instron, USA). For this purpose, rectangular testing samples ($2\text{ cm} \times 2.5\text{ cm}$) were cut from each scaffold ($n = 5$). PSI scaffolds and freeze-dried samples were measured in a dry state at room temperature, below 30% humidity level. PSIDAB and PASPDAB samples were measured under physio-

logical saline solution (150 mM, 25 °C) immediately after the modification, or after washing with ultrapure water, freeze-drying, and rehydrating in saline solution. The specimens were assessed until rupture at a crosshead speed of 1 mm/min [5 37].

From the recorded data, the extension and the regarding load were measured. The specific load capacity (maximal sustained load [N] divided by the area density [g/m²], Equation (1).) and the elongation were calculated (Equation (2)).

$$\text{Specific Load Capacity} \left[\frac{\text{Nm}^2}{\text{g}} \right] = \frac{\text{Maximal Sustained Load [N]}}{\text{Area Density} \left[\frac{\text{g}}{\text{m}^2} \right]} \quad (1)$$

$$\text{Elongation} [\%] = \frac{\text{Deformation [mm]}}{\text{Initial length [mm]}} \cdot 100 \% \quad (2)$$

For the data analysis, one-way ANOVA analysis was performed on the Specific Load Capacities and the Elongation at breakpoint values using the GraphPad Prism 8.0.1 software (GraphPad Inc., USA).

2.8. In vitro cell studies

2.8.1. Cell culture

A human skin fibroblast cell line, 155BR (ECACC 90011809) was cultured as a subconfluent monolayer under standard conditions (37 °C and 5% CO₂) in humidified atmosphere in Minimum Essential Medium supplemented with 15% fetal bovine serum, 1% non-essential amino acids, 2 mM L-glutamine, 1% non-essential amino acids, 100 IU/ml penicillin and 100 µg/ml streptomycin.

2.8.2. Cytotoxicity

Cytotoxicity tests were carried out as described in our previous studies [38,9], with slight modifications. Circular samples of PASP-DAB and PASP-DAB US with a diameter of 6 mm ($m = 0.81 \pm 0.07$ mg) were cut from each scaffold. The sterility of the test samples was ensured by 60 min of UV light exposition. The *in vitro* cytotoxicity test was performed applying the extracts of the test samples with completed cell culture media as an extraction vehicle. In the case of each sample, the extraction was carried out in a 48-well-plate in 500 µl medium at 37 °C for 24 h.

The cells were seeded into 96-well plates at a concentration of 3200 cells/cm² in 100 µl ($n = 5$ for each sample) and maintained at 37 °C for 24 h to provide the possibility for attachment to the surface and formation of a semi-confluent monolayer. After 24 h incubation, the culture medium was aspirated from the cells. The medium was replaced with 200 µl of extract (without dilution), while in the case of control, the replacing solution was fresh culture medium. The blank wells did not contain cells.

After 24 h and 72 h treatments, the cells were examined to identify morphological alterations using a phase-contrast microscope (Nikon Eclipse TS100, Nikon, Japan) equipped with a CCD camera (COHU, USA). The WST-1 cell proliferation reagent was used for the colorimetric quantification of cell viability in each well before treatment and after 24 or 72 h treatment. The reagent was diluted with uncompleted MEM solution without phenol red at a ratio of 1:20. After washing away the non-adherent and loosely attached cells with PBS, 200 µl of the diluted WST-1 solution was added to each well and the plate was incubated at 37 °C for 4 h. The absorbance of the supernatant was measured at 450 nm with a reference wavelength of 655 nm using a microplate reader (Model 3550, Bio-Rad Laboratories, Japan).

For the data analysis, one-way ANOVA analysis (Welch's correction) was performed on the cell viability values using the GraphPad Prism 8.0.1 software (GraphPad Inc., USA).

2.8.3. Multiphoton microscopy

To visualize the 155BR cells infiltrating the fibrous membranes, they were labelled with a fluorescent vital dye (Vybrant DiD) before seeding (according to the manufacturer's suggested protocol). PASP-DAB and PASP-DAB US membrane disks of 16 mm in diameter ($m = 4.75 \pm 0.86$ mg) were prepared and freeze-dried. After the sterilization using UV light, the samples were immersed in the completed cell culture medium for 2 h, then placed into 6-well-plates, and 40 000 cells were seeded onto each disk. The same amount of control cells was seeded on a cover glass. After 24 and 72 h, the samples were fixed by soaking in 4% paraformaldehyde solution (in PBS) for 2 h at room temperature with subsequent washing with PBS. The samples were stored in PBS at 4°C until investigation under a multiphoton microscope (Femto2D, Femtonics, Hungary) applying a 10x objective and 800 nm wavelength to excite the photoactive dye. The size of the images was 1.6 µm × 1.6 µm and they were taken by the MES 4.4v program. The low red channel (600–700 nm) was used to detect the red fluorescence of the cells due to the Vybrant DiD vital staining while the low green channel (490–560 nm) was used to detect the autofluorescence of the PASP-DAB membranes [9]. After image capturing, the ImageJ program was used for further modifications.

3. Results and discussion

3.1. Preparation of scaffolds

The synthesis of PSI resulted in a dry white powder with a density of 1.31 ± 0.02 g/cm³. After solvent preparation, electrospinning was performed. The obtained white fibrous scaffold was cut into adequate forms, crosslinked, and hydrolyzed as described in details in our previous article [9] and also in Fig. 1. After creating cross-links between the polymer chains (PSIDAB) by wet chemistry, and hydrolysis of the PSI to PASP at pH 8 buffer, the samples were freeze-dried to get back the dry format (PASP-DAB). PASP is a versatile polymer, that can be modified through its amino-reactive anhydride PSI, under mild conditions [39]. The biocompatibility [40] and biodegradability [41] of this polymer are arising from the peptide-bonds in the backbone, creating a protein-like structure. PASP and its derivatives offer various applications in biomedical areas like drug delivery [42], surface coating [43], and scaffolding [44]. As we can see in Figure S1 (in Supplementary information), the dry scaffolds remained white after the PSI-PASP conversion, and as they become wet their size and transparency slightly increased. The PASP-DAB scaffold itself has a flat 2D expansion, which is not the ideal shape for tissue engineering [45].

To enhance cell migration and expand the meshes in the 3rd dimension and hereby generate tissues instead of a cell layer, ultrasonication was used. As shown in Fig. 2, the cross-sectional thickness of PASP-DAB US scaffolds was increasing during the ultrasonication process. Already after 5 min, a significant expansion is observable ($148 \pm 11\%$) on the freeze-dried samples. The maximum thickness of the PASP-DAB US scaffolds was increased by more than 300% compared to those of a PASP-DAB scaffold and this change was saturated after 1 h ($389 \pm 31\%$). These thicker scaffolds show reduced fiber density and increased porosity. The shape of the disk-formed scaffolds also changed slightly. Their diameter decreased moderately, and instead of a cylinder, the scaffolds took the shape of a pillow, staying thinner near the edges, where the hole puncher had cut them. Since the thickness did not increase significantly after 60 min of ultrasonication, the scaffolds were chosen to be subjected to this duration of treatment in further experiments.

Lee *et al.* were the first at physically manipulating PLLA (poly-L-lactic acid) nanofibrous membranes by exposing them to ultrason-

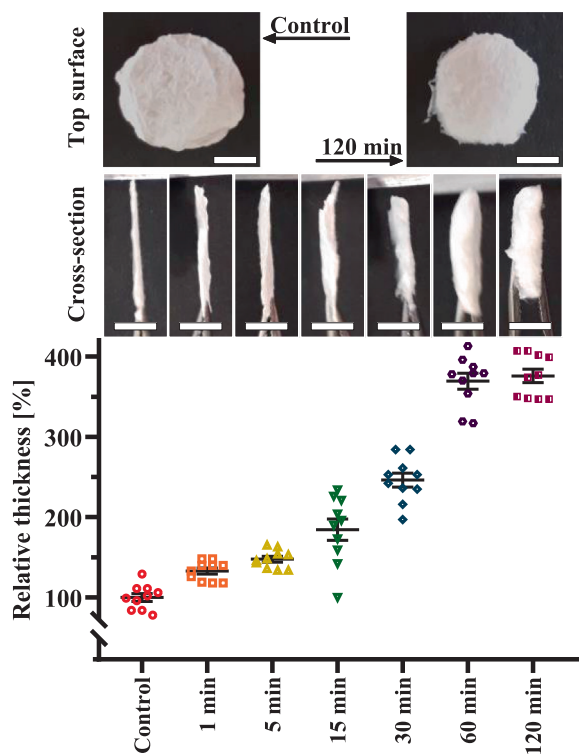


Fig. 2. The cross-sectional thickness of PASPDAB scaffolds as a function of ultrasonication time. The scale bars are 5 mm.

ication [25]. They explored that varying the time-span and energy of ultrasonication, the pore size, and the porosity could be adjusted. In their further work, chitosan and chitin were used for the same purpose and they found that this process is material-dependent [26,27]. In their studies, the maximal thickness was reached by 5 min ultrasonication time (150 W) in the case of PLLA fibers, while there was no significant effect observed after 1 min (225 W) exposition in the case of chitin and chitosan. The average thickness of the samples was increased to a varying extent depending on the type of the used polymer. In the case of PLLA, chitin, and chitosan, the maximal increase in the thickness was 500 %, 2200 %, and 400 % respectively. Comparing our results to these older studies, it must be pointed out that PASPDAB nanofibrous membranes needed more treatment time to reach their expansion plateau after 1 h (200 W) of ultrasonication. The maximal relative thickness of the PASPDAB US membranes was below 400 %. A possible explanation of this phenomenon is the existence of crosslinks between the polymer chains that are also able to crosslink the fibers. Moreover, the strong intermolecular hydrogen bonds are also likely to have an important role in creating a densely packed structure.

According to the assumption of Lee *et al.*, the growth of thickness due to ultrasonication is attributed to vibrational energy that allows water to enter inside the membranes and mechanically agitate to grow the pores between the fibers [25]. Ma *et al.* explained this phenomenon with ultrasonic cavitation [46]. It means that in aqueous media, ultrasonication induces the formation of gas bubbles inside the membrane that grow and collapse. A large number of gas bubbles can loosen the dense structure of the membrane while inducing volume expansion.

The increase in membrane thickness indicates the decrease of fiber density and a loosened structure with larger pores, which can enable the cell migration inside the scaffold. It is possible that the ultrasonication has direct or indirect impact on the chemical, morphological or mechanical properties. These crucial properties need to be examined before *in vitro* studies will be done.

3.2. Chemical and morphological characterization

3.2.1. ATR-FTIR analysis

After the different chemical treatments mentioned above and the US treatment of the samples, the chemical structure of the meshes was determined using ATR-FTIR spectrometry (Section 1.2 in SI). The obtained spectra (Figure S2) are in accordance with our previous works [9,33] and with the results of other research groups [47,48] as well. The detailed analysis of the spectra can be seen in the supplementary information (Figure S2). These results confirmed that the PSI was successfully synthesized and modified. The effects of the further processes like ultrasonication and sterilization with UV light exposition on the chemical structure was also investigated. Importantly, we observed no significant changes following the aforementioned treatments.

3.2.2. Scanning electron microscopy

The morphology of the electrospun fibers at different modification steps were observed applying SEM (Fig. 3 a-d). The electrospinning of PSI resulted in a non-woven mat with an average fiber diameter of around 590 ± 124 nm. These fibers show a smooth surface and bead-free structure as was shown previously [34] (Fig. 3 a). The further images show that the scaffolds kept their fibrous structure during either the chemical processing (Fig. 3 b and c) or the ultrasonication (Fig. 3 d). Based on the SEM micrographs, after hydrolysis, the fibers tend to run parallel and adhere together in groups.

All our data followed a normal distribution based on the Shapiro-Wilk normality test. The statistical analysis showed that the average fiber diameter (presented as means \pm standard deviation) after crosslinking (resulting PSIDAB) significantly decreased (486 ± 86 nm), and after the hydrolysis (resulting PASPDAB) significantly increased (1106 ± 113 nm) compared to the initial values (PSI, 590 ± 124 nm; $p < 0.05$). The ultrasonication process has no significant effect on the average fiber diameter (PASPDAB US, 1155 ± 151 nm).

The changes in fiber diameter are attributed to the chemical reactions that occurred inside the fibers. It is known that the increased crosslinking degree causes decreased swelling ratio of gels [49]. In the case of fibrous meshes (PSI – PSIDAB), this effect resulted in a significant decrease of the fiber diameter [9,34]. After hydrolyzation, hydrogels are formed, which tend to take up water, and swell [50], which is discernible in the increased fiber diameters [9]. Ultrasonication had no significant impact on fiber thickness, which means that the volume of the scaffolds increased due to the increased porosity. The same phenomenon was observed by Jung *et al.* [27] using chitin and Lee *et al.* [25] in the case of PLLA. In our previous work, we already observed the fusion of some of the PASPDAB fibers at the same conditions without any optimization [9]. In this study, we recognized a cord-like structure consisting of 5 to 15 fibers that run parallel and adhered together.

Although the porous structure of the PASPDAB samples is already striking before the ultrasonication process on the SEM images (Fig. 3 e and f), the size and shape of the pores became distorted after ultrasonication, but the honeycomb-like structure was retained. The PASPDAB samples contain a dense layer of fibers on both sides of the membrane, which could hinder cell penetration. Based on the SEM micrographs, the surface of the PASPDAB membranes is dense, two-dimensional. In contrast to this, the surface of the ultrasonicated samples is porous and fluffy (Figure S3).

Sawawi *et al.* reported an interesting phenomenon that ultrasonication can be used to scission electrospun membranes into short fibers [51]. They have found, that brittle electrospun polymers such as poly(styrene) and poly(methyl methacrylate) can be easily broken by the bubble cavitation. In contrast, ultrasonication has less effect on ductile polymers like poly(acrylonitrile) or

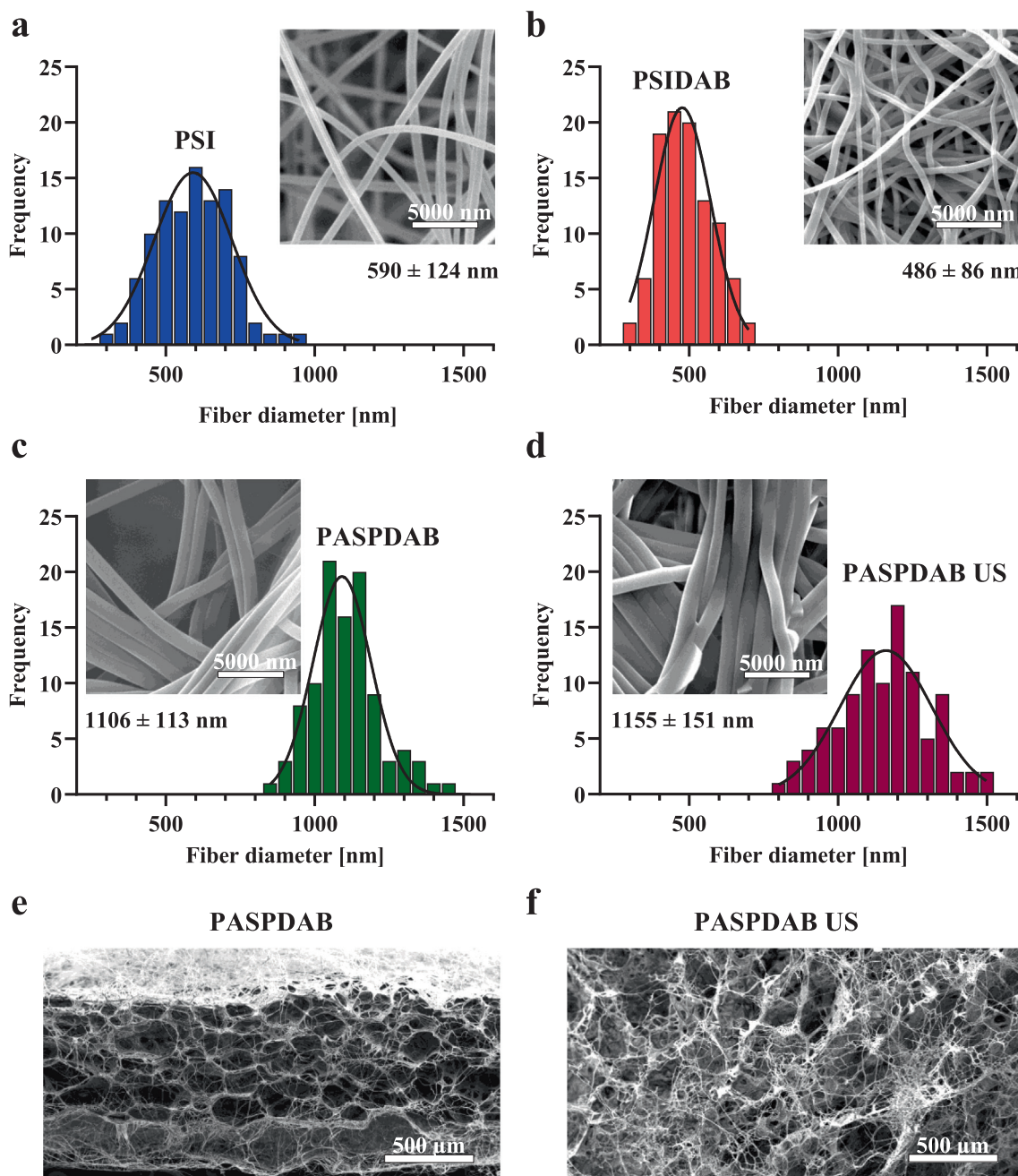


Fig. 3. SEM micrographs and fiber size distribution of PSI (a), PSIDAB (b), PASPDAB (c), and ultrasonicated PASPDAB (d). The fiber diameters were presented as the means \pm standard deviations. SEM micrographs showing the cross-section of the PASPDAB (e) and ultrasonicated PASPDAB (f) meshes.

PLLA. While investigating the PASPDAB US fibers by SEM, we have not found a significant number of broken fibers (Figure S4).

3.3. Physical characterization

3.3.1. Mechanical analysis

The mechanical properties of scaffolds for tissue engineering are crucial, as the tissue healing should not be limited by mechanical failure of the construct [52]. Mechanical strength and ductility of the scaffolds in dry and wet states were measured using a uniaxial mechanical testing machine (Figure S5). In the case of wet state samples (PSIDAB, PASPDAB, PASPDAB US), the scaffolds were measured immediately after production (fresh) or freeze-dried and hydrated (rehydrated) to investigate the effect of freeze-drying on the mechanical properties.

The thickness of electrospun PSI scaffolds and their derivatives is hardly measurable, which makes the accepted practice of calculating tensile stress with the cross-sectional area unreliable. To compare the mechanical strength of the scaffolds, maximum load capacity was used, that is the quotient of the maximal sustained load [N] and the grammage [g/m^2] [53].

Regarding the specific load capacity values of the dry state scaffolds (Fig. 4 a), it is observable that there is a significant difference between the PSI ($0.08 \pm 0.01 \text{ Nm}^2/\text{g}$) and PSIDAB ($0.24 \pm 0.02 \text{ Nm}^2/\text{g}$). This difference can be attributed to the presence of crosslinks, which make the intermolecular bonds stronger. Although the hydrolysis has not changed the mechanical strength of the samples (PASPDAB $0.23 \pm 0.03 \text{ Nm}^2/\text{g}$), ultrasonication has decreased it significantly (PASPDAB US $0.11 \pm 0.01 \text{ Nm}^2/\text{g}$). This loss of mechanical strength could be the consequence of the loosened structure

caused by ultrasonication weakening the interactions between the fibers (Fig. 3 e and f)

Concerning the specific load capacity of the wet state scaffolds (Fig. 4 b - PSIDAB, PASPDAB, PASPDAB US), they were lower by an order of magnitude compared to the dry samples (Fig. 4 a, PSI, PSIDAB, PASPDAB). The effect of ultrasonication on wet samples was not as obvious as at the dry ones and did not show a clear tendency of decreasing the specific load capacity. The only significant difference was observable in the case of rehydrated PASPDAB ($0.021 \pm 0.003 \text{ Nm}^2/\text{g}$) and the rehydrated PASPDAB US ($0.014 \pm 0.004 \text{ Nm}^2/\text{g}$). The effect of freeze-drying and rehydrating on the scaffolds was also investigated, and neither the PASPDAB nor the PASPDAB US showed a significant difference between the freshly prepared and the freeze-dried - rehydrated samples.

Investigating the elongation at breakpoint values of the dry samples (Fig. 4 c and Figure S5), the PSI ($16 \pm 3\%$), PSIDAB ($7 \pm 3\%$), and the PASPDAB ($35 \pm 5\%$) showed similar characters. After ultrasonication, the elongation, increased significantly by

the time point of rupture (PASPDAB US $146 \pm 8\%$). It means that the scaffold is ductile, and it can increase its length about to 2,5x without fraction as predicted from the SEM images (Fig. 3 e and f) where the fibers moved more to the center of the pores, thus becoming more flexible.

Regarding the elongation of the wet scaffolds (Fig. 4 d and Figure S5), the same phenomenon is observable as by the dry samples. The PSIDAB ($61.1 \pm 9\%$), PASPDAB fresh ($73 \pm 8\%$), and PASPDAB rehydrated ($75 \pm 7\%$) showed similar characteristics, and after ultrasonication, the fraction happened significantly later, only at $177 \pm 18\%$ (PASPDAB US fresh) and $181 \pm 13\%$ (PASPDAB US rehydrated). It is also noticeable, that the freeze-drying and rehydrating has no effect on the elongation at breakpoint values.

The reinforcing effect of the crosslinking on the mechanical strength of bulk gels [50] and fibrous materials [54] is already widely investigated in the literature. In our previous work, we observed an inconsistent effect of crosslinking on dry PSI and PSIDAB sutured membranes during an *in vivo* experiment [9]. How-

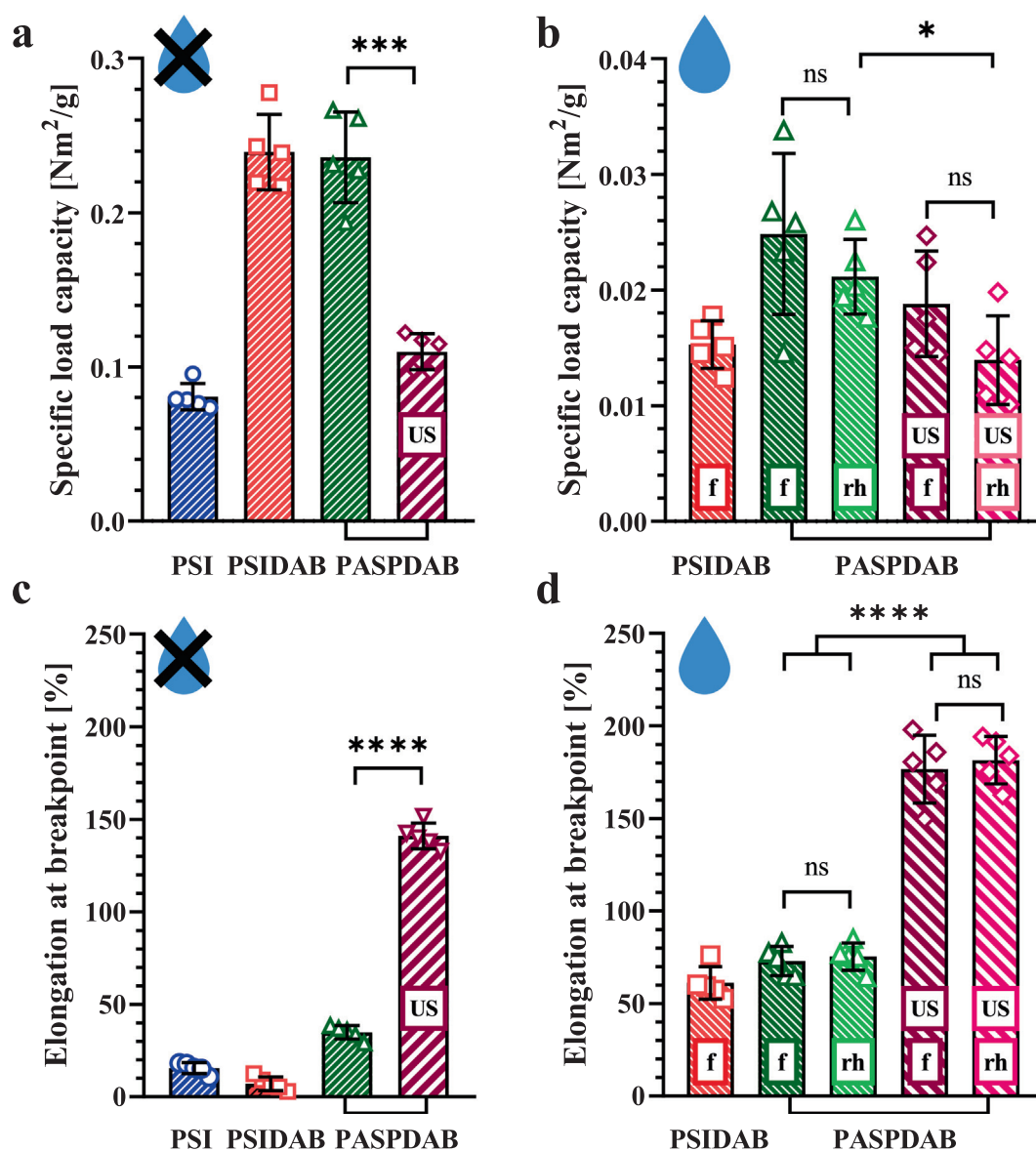


Fig. 4. Specific load capacity (a, b) and elongation at breakpoint values (c, d) of dry (a, c) and wet (b, d) samples measured by a tensile test. On the graph, US marks the ultrasonicated sample, f and rh indicate freshly prepared, and freeze-dried - rehydrated samples respectively. The presented data show the average of 5 independent measurements. The error bars correspond to the standard deviation. The "" indicates that statistical significance exists between the two groups (one-way ANOVA, * $p < 0.05$; **** $p < 0.0001$).

ever, in the case of surgical sutures, the increased rigidity of the membranes is pivotal, and the different electrospinning setup is also modifying the properties of the samples. The ultrasonication treatment significantly decreased the mechanical strength of the dry state samples (Fig. 4 a), which is in good agreement with the results of other research groups[25,26,55]. To the best of our knowledge, wet and ultrasonicated samples were examined only by Gu *et al.*[26] so far, and they found a considerable decrease in tensile strength. However, in our case, this tendency was not unequivocal, the only significant difference was found between the fresh PASPDA and the rehydrated PASPDA UH (Fig. 4 b).

The ductility of ultrasonicated samples was investigated by Lee *et al.*[25] and Gu *et al.*[26], but they found contrary results. Regarding elongation at break, Lee *et al.*[25] observed an almost 7-fold increase after ultrasonication in a dry state using PLLA. In contrast, Gu *et al.*[26] found no significant increase using neutralized chitosan neither in dry nor in the wet state. Since the elongation after ultrasonication (Fig. 4 c and d, PASPDA – PASPDA US) become four times greater in the dry state and three times greater in the wet state, our results are in agreement with Lee *et al.*[25]. The water retention capacity of the membranes was also investigated (Figure S6). We found no significant difference between PASPDA and PASPDA US in this parameter, which means ultrasonication treatment has not influenced the water uptake and retention of the samples.

Our other goal was to improve the storing conditions of fibrous hydrogels to extend their shelf life. Investigating the standard storage of the samples for 4 months in PBS, we found that the hydrogel membranes underwent significant degradation and had structural damage (Figure S7 and S8). To prevent the scaffold from degradation, freeze-drying was investigated as an alternative storing condition.

To the best of our knowledge, there was no other research group investigating the effect of freeze-drying and rehydrating on the mechanical properties of wet electrospun samples (Fig. 4 b and d). Our results indicate that the PASPDA and PASPDA US samples can be stored in the freeze-dried state without losing mechanical strength after rehydration. In the dry state, the scaffolds are easy to transport and store, in addition, they have a longer shelf life. Improving the storing conditions of these scaffolds is a huge step towards making these grafts an off-the-shelf product.

3.4. *In vitro* experiments

3.4.1. Cytotoxicity test

The following *in vitro* experiments were carried out on the PASPDA and PASPDA US samples. According to our previous

work [9], the PSI based scaffolds undergo hydrolysis in cell culture media and shift the pH into the acidic range, therefore PSI and PSI-DAB are not suitable for supporting cell growth. Cytotoxicity studies were conducted on a human skin fibroblast cell line (155BR) to investigate any potential cytotoxic effect, hereby the opportunity of future application of the PASPDA or the PASPDA US as scaffolds.

Phase-contrast microscopical images of the fibroblasts after 24 and 72 h can be seen in Fig. 5. After 24 h, the morphology of the treated cells was similar to the control, and there was no difference observable in the confluence level. After 72 h, the cells formed almost a confluent monolayer in each case indicating that the fibrous meshes did not influence negatively the cell growth. The cells showed their normal fibroblast morphology, no sign of apoptosis was observed.

The cytotoxicity results (Fig. 5) demonstrated that the cell viability in the treated groups (PASPDA, PASPDA US) did not show any significant decrease compared to the control groups. In the first 24 h, the cell viability doubled in each group (control: $209 \pm 24\%$; PASPDA: $205 \pm 16\%$; PASPDA US: $201 \pm 31\%$). These results are in concordance with a previous report where these cells showed a doubling time around 32 h [56]. After 72 h, the viability values increased further, reaching $342 \pm 31\%$ in the control group, $362 \pm 46\%$ in the case of PASPDA, and $347 \pm 15\%$ regarding PASPDA US.

Our results are in agreement with previous studies, where cytotoxicity of PASPDA bulk hydrogels [41] or PASPDA fibrous hydrogels [9] were investigated. Our data indicate that the ultrasonication process does not affect the cytotoxicity of PASPDA membranes.

3.4.2. Cell penetration

After staining the cells by fluorescent labelling, the cells were visualized by applying multiphoton microscopy. After 24 h, the control cells attached to the glass coverslip and showed normal morphology (Fig. 6), and their number notably increased by 72 h. However, on the PASPDA and PASPDA US scaffolds, the cells could be found at a significantly lower density, and these cells did not show a widespread morphology. Such decrease in density can be explained by the loose attachment of the cells to the scaffolds, hereby they could be washed away by the subsequent washing steps of the fixation [9].

Since the surface of the scaffolds was not even, but rather they show fibers on top of the other structure, it cannot be expected to see a spread cell morphology like on tissue culture plates. Fibro-

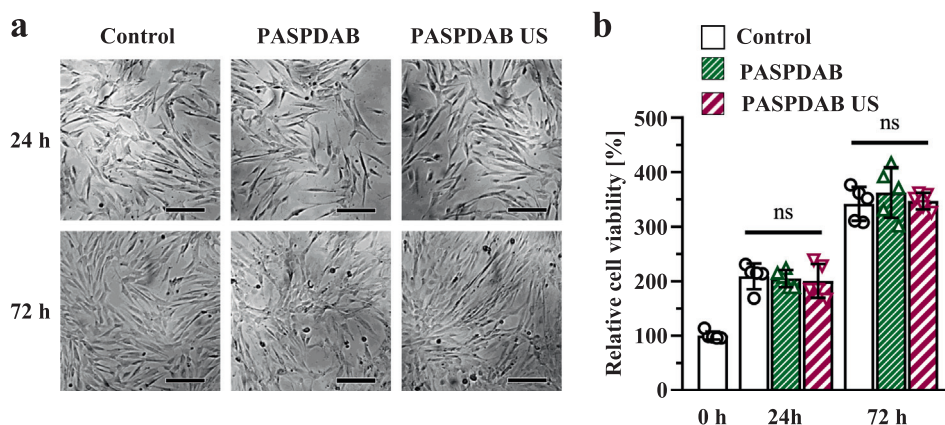


Fig. 5. Phase-contrast microscopical images of 155BR cells (a) without treatment (control), treated with PASPDA or ultrasonicated PASPDA scaffolds after 24 and 72 h. The scale bars indicate 100 μm . The *in vitro* cytotoxicity results (b) of PASPDA and ultrasonicated PASPDA scaffolds after 24 and 72 h ($n = 5$). The "ns" indicates the lack of statistical significance between the two groups (one-way ANOVA, p greater than 0.05).

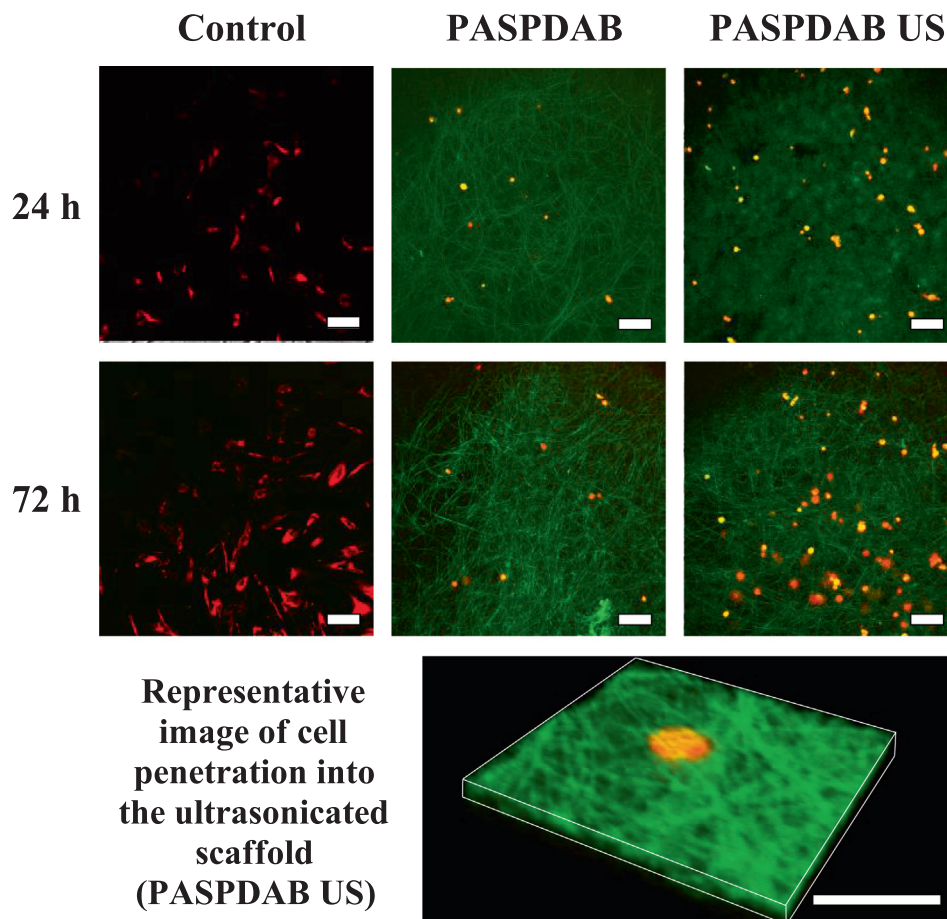


Fig. 6. Multiphoton images of Vybrant DiI-labelled 155BR cells seeded on the surface of a glass coverslip (control) or PASPDAB or ultrasonicated PASPDAB fibrous scaffolds after 24 and 72 h. The cells show red fluorescence due to the Vybrant DiI staining, while the green color indicates the autofluorescence of the PASPDAB scaffolds. The scale bars indicate 200 μm .

lasts seeded on the top of PASPDAB scaffolds showed poor penetration to the centre of the scaffold. The cells adhered to the surface of the membrane, but they were not able to penetrate through the densely packed electrospun fibers. In contrast, the density of the cells in the case of the PASPDAB US seems to be higher, supposedly due to the penetration, which prevented the cells (stuck between the fibers) from washing out.

As shown in Fig. 6, the cells were able to migrate inside the PASPDAB US membranes, therefore the pore sizes are suitable for cellular penetration. These results are in accordance with the previous findings on ultrasonicated electrospun membranes [25,27,57].

4. Conclusion

Electrospinning is commonly used in the biomedical field for creating scaffolds. However, it yields the densely deposited structure of randomly arrayed fibers resulting in low porosity, which restricts their use in biomedical applications. To enhance the cellular infiltration of the scaffold, in this research we used ultrasonication treatment on poly(aspartic acid) (PASP) based fibrous hydrogels. After the chemical crosslinking of the hydrogels with 1,4-Diaminobutane (DAB), our data indicate that the ultrasonication treatment affected the mechanical properties of the scaffolds. The greatly loosened structure weakened the interactions between the fibers in the electrospun scaffold causing a decreased specific load capacity (in the case of dry samples: by 50%, wet samples:

by 40%) and an increased elongation (dry samples: by 300%, wet samples: by 100%). For crosslinked hydrogel samples, the freeze-drying method was used. Since there was no significant effect of freeze-drying on the mechanical properties (mechanical strength and ductility), it can be used as an alternative storage condition, increasing the shelf life, and decreasing the probability of microbiological damage of the hydrogel scaffolds. Based on our *in vitro* investigations, the ultrasonication process does not affect the cytotoxicity of PASPDAB membranes using human skin fibroblast cell line. The two-photon microscopical images show that the cells were able to migrate inside the ultrasonicated PASPDAB membranes therefore the pore sizes are suitable for cellular penetration.

Due to the increased cellular infiltration of the PASPDAB membranes and the alternative dry state storing of the hydrogel fibrous membranes, this kind of scaffold could be a huge step towards an off-the-shelf and effective product for tissue regeneration.

Declaration of Competing Interest

The authors declare that they have no known competing financial interests or personal relationships that could have appeared to influence the work reported in this paper.

Acknowledgement

This work was supported by the National Research, Development, and Innovation Office (NKFIH FK137749). The research was

further financed by the Higher Education Institutional Excellence Program of the Ministry for Innovation and Technology in Hungary, within the framework of the Therapeutic Development thematic program of the Semmelweis University. The authors are especially thanking the SEM images to Ramóna Gottscháll and for the help with the cell studies to Krisztina Tóth.

Appendix A. Supplementary material

Supplementary data to this article can be found online at <https://doi.org/10.1016/j.molliq.2022.119243>.

References

- [1] R.D. Rusk, *SCIENCE: reflections of a Physicist*, by Percy Williams Bridgman. Philosophical Library, Inc., 1950. 392 pp. \$5.00, *The Educational Forum* 15 (1) (1950) 119–120.
- [2] S. Bose, M. Roy, A. Bandyopadhyay, Recent advances in bone tissue engineering scaffolds, *Trends Biotechnol.* 30 (10) (2012) 546–554, <https://doi.org/10.1016/j.tibtech.2012.07.005>.
- [3] R. Bucci, E. Georgilias, A.M. Bittner, M.L. Gelmi, F. Clerici, Peptide-based electrospun fibers: current status and emerging developments, *Nanomaterials*. 11 (2021) 1–22, <https://doi.org/10.3390/nano11051262>.
- [4] K.H. Sizeland, K.A. Hofman, I.C. Hallett, D.E. Martin, J. Potgieter, N.M. Kirby, A. Hawley, S.T. Mudie, T.M. Ryan, R.G. Haverkamp, M.H. Cumming, Nanostructure of electrospun collagen: do electrospun collagen fibers form native structures?, *Materialia* 3 (2018) 90–96, <https://doi.org/10.1016/j.mtlia.2018.10.001>.
- [5] S. Asadpour, S. Kargozar, L. Moradi, A. Ai, H. Nosrati, J. Ai, Natural biomacromolecule based composite scaffolds from silk fibroin, gelatin and chitosan toward tissue engineering applications, *Int. J. Biol. Macromol.* 154 (2020) 1285–1294, <https://doi.org/10.1016/j.ijbiomac.2019.11.003>.
- [6] P. Ginestra, E. Ceretti, A. Fiorentino, Electrospinning of Poly-caprolactone for Scaffold Manufacturing: experimental Investigation on the Process Parameters Influence, *Procedia CIRP*. 49 (2016) 8–13, <https://doi.org/10.1016/j.procir.2015.07.020>.
- [7] Utkarsh, H. Hegab, M. Tariq, N.A. Syed, G. Rizvi, R. Pop-Iliev, Pop-Iliev, Towards Analysis and Optimization of Electrospun PVP (Polyvinylpyrrolidone) Nanofibers, *Adv. Polym. Technol.* 2020 (2020) 1–9, <https://doi.org/10.1155/2020/4090747>.
- [8] M. Alessandri, G. Lizzo, C. Gualandi, C. Mangano, A. Giuliani, M.L. Focarete, L. Calzà, Influence of biological matrix and artificial electrospun scaffolds on proliferation, differentiation and trophic factor synthesis of rat embryonic stem cells, *Matrix Biol.* 33 (2014) 68–76, <https://doi.org/10.1016/j.matbio.2013.08.001>.
- [9] K. Molnar, C. Voniatis, D. Feher, G. Szabo, R. Varga, L. Reiniger, D. Juriga, Z. Kiss, E. Krisch, G. Weber, A. Ferencz, G. Varga, M. Zrinyi, K.S. Nagy, A. Jedlovsky-Hajdu, W. Cui, Poly(amino acid) based fibrous membranes with tuneable in vivo biodegradation, *PLoS One*. 16 (8) (2021) e0254843, <https://doi.org/10.1371/journal.pone.0254843>, <https://doi.org/10.1371/journal.pone.0254843.g001>, <https://doi.org/10.1371/journal.pone.0254843.g002>, <https://doi.org/10.1371/journal.pone.0254843.g003>, <https://doi.org/10.1371/journal.pone.0254843.g004>, <https://doi.org/10.1371/journal.pone.0254843.g005>, <https://doi.org/10.1371/journal.pone.0254843.g006>, <https://doi.org/10.1371/journal.pone.0254843.g007>, <https://doi.org/10.1371/journal.pone.0254843.g008>, <https://doi.org/10.1371/journal.pone.0254843.g009>, <https://doi.org/10.1371/journal.pone.0254843.g010>, <https://doi.org/10.1371/journal.pone.0254843.g011>, <https://doi.org/10.1371/journal.pone.0254843.g012>.
- [10] J. Chen, T. Zhang, W. Hua, P. Li, X. Wang, 3D Porous poly(lactic acid)/regenerated cellulose composite scaffolds based on electrospun nanofibers for biomaterialization, *Colloids Surfaces A Physicochem. Eng. Asp.* 585 (2020) 124048, <https://doi.org/10.1016/j.colsurfa.2019.124048>.
- [11] S. Naahidi, M. Jafari, M. Logan, Y. Wang, Y. Yuan, H. Bae, B. Dixon, P. Chen, Biocompatibility of hydrogel-based scaffolds for tissue engineering applications, *Biotechnol. Adv.* 35 (5) (2017) 530–544, <https://doi.org/10.1016/j.biotechadv.2017.05.006>.
- [12] F. Achatz, R. Kujat, C. Pfeifer, M. Koch, M. Nerlich, P. Angele, J. Zellner, In vitro testing of scaffolds for mesenchymal stem cell-based meniscus tissue engineering—Introducing a new biocompatibility scoring system, *Materials (Basel)*. 9 (4) (2016) 276, <https://doi.org/10.3390/ma9040276>.
- [13] M.S.B. Reddy, D. Ponnamma, R. Choudhary, K.K. Sadasivuni, A comparative review of natural and synthetic biopolymer composite scaffolds, *Polymers (Basel)*. 13 (7) (2021) 1105, <https://doi.org/10.3390/polym13071105>.
- [14] A. Accardo, C. Cirillo, S. Lionnet, C. Vieu, I. Loubinoux, Interfacing cells with microengineered scaffolds for neural tissue reconstruction, *Brain Res. Bull.* 152 (2019) 202–211, <https://doi.org/10.1016/j.brainresbull.2019.07.020>.
- [15] H. Adelnia, H.D.N. Tran, P.J. Little, I. Blakey, H.T. Ta, Poly(aspartic acid) in Biomedical Applications: from Polymerization, Modification, Properties, Degradation, and Biocompatibility to Applications, *ACS Biomater. Sci. Eng.* 7 (6) (2021) 2083–2105, <https://doi.org/10.1021/acsbomaterials.1c00150>.
- [16] S. Yang, K.-F. Leong, Z. Du, C.-K. Chua, The design of scaffolds for use in tissue engineering. Part I. Traditional factors, *Tissue Eng.* 7 (6) (2001) 679–689, <https://doi.org/10.1089/107632701753337645>.
- [17] B.J. Lawrence, S.V. Madhally, Cell colonization in degradable 3D porous matrices, *Cell Adh. Migr.* 2 (1) (2008) 9–16, <https://doi.org/10.4161/cam.2.1.5884>.
- [18] F.J. O'Brien, B.A. Harley, I.V. Yannas, L.J. Gibson, The effect of pore size on cell adhesion in collagen-GAG scaffolds, *Biomaterials*. 26 (4) (2005) 433–441, <https://doi.org/10.1016/j.biomaterials.2004.02.052>.
- [19] K.P. Feltz, E.A.G. Kalaf, C. Chen, R.S. Martin, S.A. Sell, A review of electrospinning manipulation techniques to direct fiber deposition and maximize pore size, *Electrospinning*. 1 (2017) 46–61, <https://doi.org/10.1515/esp-2017-0002>.
- [20] N. Maurmann, D.P. Pereira, D. Burguez, F.D.A. de S Pereira, P. Inforçatti Neto, R. A. Rezende, D. Gamba, J.V.L. da Silva, P. Pranke, Mesenchymal stem cells cultivated on scaffolds formed by 3D printed PCL matrices, coated with PLGA electrospun nanofibers for use in tissue engineering, *Biomed. Phys. Eng. Express*. 3 (4) (2017) 045005, <https://doi.org/10.1088/2057-1976/aa6308>.
- [21] C. Vaquette, J.J. Cooper-White, Increasing electrospun scaffold pore size with tailored collectors for improved cell penetration, *Acta Biomater.* 7 (6) (2011) 2544–2557, <https://doi.org/10.1016/j.actbio.2011.02.036>.
- [22] B.M. Baker, A.O. Gee, R.B. Metter, A.S. Nathan, R.A. Marklein, J.A. Burdick, R.L. Mauck, The potential to improve cell infiltration in composite fiber-aligned electrospun scaffolds by the selective removal of sacrificial fibers, *Biomaterials*. 29 (15) (2008) 2348–2358, <https://doi.org/10.1016/j.biomaterials.2008.01.032>.
- [23] P. Pal, P.K. Srivas, P. Dadhich, B. Das, D. Maulik, S. Dhara, Nano-/Microfibrous Cotton-Wool-Like 3D Scaffold with Core-Shell Architecture by Emulsion Electrospinning for Skin Tissue Regeneration, *ACS Biomater. Sci. Eng.* 3 (12) (2017) 3563–3575, <https://doi.org/10.1021/acsbomaterials.7b00681.1021/acsbomaterials.7b00681.s001>.
- [24] J. Jiang, M.A. Carlson, M.J. Teusink, H. Wang, M.R. MacEwan, J. Xie, Expanding Two-Dimensional Electrospun Nanofiber Membranes in the Third Dimension by a Modified Gas-Foaming Technique, *ACS Biomater. Sci. Eng.* 1 (10) (2015) 991–1001, <https://doi.org/10.1021/acsbomaterials.5b00238>.
- [25] J.B. Lee, S.I. Jeong, M.S. Bae, D.H. Yang, D.N. Heo, C.H. Kim, E. Alsberg, I.K. Kwon, Highly porous electrospun nanofibers enhanced by ultrasonication for improved cellular infiltration, *Tissue Eng. - Part A*. 17 (21–22) (2011) 2695–2702, <https://doi.org/10.1089/ten.tea.2010.0709>.
- [26] B.K. Gu, S.J. Park, M.S. Kim, C.M. Kang, J.-I. Kim, C.-H. Kim, Fabrication of sonicated chitosan nanofiber mat with enlarged porosity for use as hemostatic materials, *Carbohydr. Polym.* 97 (1) (2013) 65–73, <https://doi.org/10.1016/j.carbpol.2013.04.060>.
- [27] S. Jung, B.K. Gu, Y.J. Gin, S.J. Park, I.K. Kwon, C. Kim, Thickness and Pore Size Control of Chitin Nanofibers by Ultra-sonication and Its Biological Effect in vitro, *Biomater. Res.* 16 (2012) 11–18.
- [28] K.T. Nguyen, J.L. West, Photopolymerizable hydrogels for tissue engineering applications, *Biomaterials*. 23 (22) (2002) 4307–4314.
- [29] F. Smaniotto, V. Prosapio, I. Zafeiri, F. Spyropoulos, Freeze drying and rehydration of alginate fluid gels, *Food Hydrocoll.* 99 (2020) 105352, <https://doi.org/10.1016/j.foodhyd.2019.105352>.
- [30] S. Watson, M. Toner, Cryopreservation of harvested skin and cultured skin or cornea equivalents by slow freezing, 1999.
- [31] D. Applegate, J. Kim, Cryopreservation process scaleup for a tissue-engineered, metabolically active, human dermal replacement, *dermagraft*, *Cryobiology*. 37 (1998) 409–410.
- [32] A. Merivaara, J. Zini, E. Koivunotko, S. Valkonen, O. Korhonen, F.M. Fernandes, M. Yliperttula, Preservation of biomaterials and cells by freeze-drying: change of paradigm, *J. Control. Release*. 336 (2021) 480–498, <https://doi.org/10.1016/j.jconrel.2021.06.042>.
- [33] K. Molnar, D. Juriga, P.M. Nagy, K. Sinko, A. Jedlovsky-Hajdu, M. Zrinyi, Electrospun poly(aspartic acid) gel scaffolds for artificial extracellular matrix, *Polym. Int.* 63 (9) (2014) 1608–1615, <https://doi.org/10.1002/pi.4720>.
- [34] K. Molnar, A. Jedlovsky-Hajdu, M. Zrinyi, S. Jiang, S. Agarwal, Poly(amino acid)-Based Gel Fibers with pH Responsivity by Coaxial Reactive Electrospinning, *Macromol. Rapid Commun.* 38 (14) (2017) 1700147, <https://doi.org/10.1002/marc.v38.1410.1002/marc.201700147>.
- [35] Z. Varga, K. Molnár, V. Torma, M. Zrinyi, Kinetics of volume change of poly (succinimide) gels during hydrolysis and swelling, *Phys. Chem. Chem. Phys.* 12 (2010) 12670–12675, <https://doi.org/10.1039/c0cp00527d>.
- [36] A. Ghasemi, S. Zahediasl, Normality tests for statistical analysis: a guide for non-statisticians, *Int. J. Endocrinol. Metab.* 10 (2) (2012) 486–489, <https://doi.org/10.5812/ijem.3505>.
- [37] C. Ao, Y. Niu, X. Zhang, X. He, W. Zhang, C. Lu, Fabrication and characterization of electrospun cellulose/nano-hydroxyapatite nanofibers for bone tissue engineering, *Int. J. Biol. Macromol.* 97 (2017) 568–573, <https://doi.org/10.1016/j.ijbiomac.2016.12.091>.
- [38] K. Molnar, R. Varga, B. Jozsa, D. Barczikai, E. Krisch, K.S. Nagy, G. Varga, A. Jedlovsky-Hajdu, J.E. Puskas, Investigation of the cytotoxicity of electrospun polysuccinimide-based fiber mats, *Polymers (Basel)*. 12 (2020) 1–11, <https://doi.org/10.3390/polym12102324>.
- [39] M.M. Patil, S.S. Rajput, Succinimides: Synthesis, reaction and biological activity, *Int. J. Pharm. Pharm. Sci.* (2014) 8–14.
- [40] D.V. Salakhieva, D.R. Gumerova, R.A. Akhmadishina, M.I. Kamalov, I.S. Nizamov, C. Nemeth, A. Szilágyi, T.I. Abdullin, Anti-Radical and Cytotoxic Activity of Polysuccinimide and Polyaspartic Acid of Different Molecular Weight, *Bionanoscience*. 6 (4) (2016) 348–351, <https://doi.org/10.1007/s12668-016-0230-0>.

- [41] D. Juriga, K. Nagy, A. Jedlovszky-Hajdú, K. Perczel-Kovács, Y.M. Chen, G. Varga, M. Zrínyi, Biodegradation and osteosarcoma cell cultivation on poly(aspartic acid) based hydrogels, *ACS Appl. Mater. Interfaces*. 8 (36) (2016) 23463–23476, <https://doi.org/10.1021/acsami.6b06489>.s001.
- [42] G. Horvát, B. Gyarmati, S. Berkó, P. Szabó-Révész, B.Á. Szilágyi, A. Szilágyi, J. Soós, G. Sandri, M.C. Bonferoni, S. Rossi, F. Ferrari, C. Caramella, E. Csányi, M. Budai-Szucs, Thiolated poly(aspartic acid) as potential in situ gelling, ocular mucoadhesive drug delivery system, *Eur. J. Pharm. Sci.* 67 (2015) 1–11, <https://doi.org/10.1016/j.ejps.2014.10.013>.
- [43] M. Xu, Y. Zhao, M. Feng, Polyaspartamide derivative nanoparticles with tunable surface charge achieve highly efficient cellular uptake and low cytotoxicity, *Langmuir*. 28 (31) (2012) 11310–11318, <https://doi.org/10.1021/la3025028>.
- [44] J.H. An, N.T. Huynh, Y. Sil Jeon, J.-H. Kim, Surface modification using bio-inspired adhesive polymers based on polyaspartamide derivatives, *Polym. Int.* 60 (11) (2011) 1581–1586, <https://doi.org/10.1002/pi.3116>.
- [45] M. Mabrouk, H.H. Beherei, D.B. Das, Recent progress in the fabrication techniques of 3D scaffolds for tissue engineering, *Mater. Sci. Eng. C*. 110 (2020) 110716, <https://doi.org/10.1016/j.msec.2020.110716>.
- [46] F.-F. Ma, D.i. Zhang, T. Huang, N. Zhang, Y. Wang, Ultrasonication-assisted deposition of graphene oxide on electrospun poly(vinylidene fluoride) membrane and the adsorption behavior, *Chem. Eng. J.* 358 (2019) 1065–1073, <https://doi.org/10.1016/j.cej.2018.10.121>.
- [47] S.L. Lim, W.N.H. Tang, C.W. Ooi, E.-S. Chan, B.T. Tey, Rapid swelling and deswelling of semi-interpenetrating network poly(acrylic acid)/poly(aspartic acid) hydrogels prepared by freezing polymerization, *J. Appl. Polym. Sci.* 133 (24) (2016) n/a–n/a, <https://doi.org/10.1002/app.43515>.
- [48] C. Zhang, S. Wu, X. Qin, Facile fabrication of novel pH-sensitive poly(aspartic acid) hydrogel by crosslinking nanofibers, *Mater. Lett.* 132 (2014) 393–396, <https://doi.org/10.1016/j.matlet.2014.06.031>.
- [49] S. Khan, N.M. Ranjha, Effect of degree of cross-linking on swelling and on drug release of low viscous chitosan/poly(vinyl alcohol) hydrogels, *Polym. Bull.* 71 (8) (2014) 2133–2158, <https://doi.org/10.1007/s00289-014-1178-2>.
- [50] E. Krisch, B. Gyarmati, A. Szilágyi, Preparation of pH-responsive poly(Aspartic acid) nanogels in inverse emulsion, *Period. Polytech, Chem. Eng.* 61 (2017) 19–26, <https://doi.org/10.3311/PPCh.9788>.
- [51] M. Sawawi, T.Y. Wang, D.R. Nisbet, G.P. Simon, Scission of electrospun polymer fibres by ultrasonication, *Polymer (Guildf)*. 54 (16) (2013) 4237–4252, <https://doi.org/10.1016/j.polymer.2013.05.060>.
- [52] D.W. Hutmacher, Scaffolds in tissue engineering bone and cartilage, *Biomater. Silver Jubil. Compend.* 21 (2000) 175–189, <https://doi.org/10.1016/B978-008045154-1.50021-6>.
- [53] C. Voniatis, R. Gottscháll, D. Barczikai, G. Szabó, A. Jedlovszky-Hajdu, Enhancing critical features of poly (amino acid) based meshes, *J. Appl. Polym. Sci.* 139 (15) (2022) 51933, <https://doi.org/10.1002/app.v139.1510.1002/app.51933>.
- [54] D. Nataraj, R. Reddy, N. Reddy, Crosslinking electrospun poly (vinyl) alcohol fibers with citric acid to impart aqueous stability for medical applications, *Eur. Polym. J.* 124 (2020) 109484, <https://doi.org/10.1016/j.eurpolymj.2020.109484>.
- [55] M. Aghajanoor, S. Hashemi-Najafabadi, M. Baghaban- Eslaminejad, F. Bagheri, S. Mohammad Mousavi, F. Azam Sayyahpour, Azam Sayyahpour, The effect of increasing the pore size of nanofibrous scaffolds on the osteogenic cell culture using a combination of sacrificial agent electrospinning and ultrasonication, *J. Biomed. Mater. Res. - Part A*. 105 (7) (2017) 1887–1899, <https://doi.org/10.1002/jbm.a.36052>.
- [56] L. Grossman, S.I. Moriwaki, S. Ray, R.E. Tarone, Q. Wei, K.H. Kraemer, Age-associated changes in DNA repair and mutation rates, *Adv. Cell Aging Gerontol.* 4 (2001) 17–30, [https://doi.org/10.1016/S1566-3124\(01\)04025-1](https://doi.org/10.1016/S1566-3124(01)04025-1).
- [57] S.I. Jeong, N.A. Burns, C.A. Bonino, I.K. Kwon, S.A. Khan, E. Alsborg, Improved cell infiltration of highly porous 3D nanofibrous scaffolds formed by combined fiber-fiber charge repulsions and ultra-sonication, *J. Mater. Chem. B*. 2 (46) (2014) 8116–8122.